STUDY ON INTEGRATED ELECTROKINETICS-ADSORPTION REMEDIATION TECHNIQUE FOR SIMULTANEOUS REMOVAL OF HEAVY METALS AND ORGANICS FROM SALINE-SODIC SOIL: EFFECTS OF OPERATING PARAMETERS

BY

SALIHU LUKMAN

A Dissertation Presented to the

DEANSHIP OF GRADUATE STUDIES

KING FAHD UNIVERSITY OF PETROLEUM & MINERALS

DHAHRAN, SAUDI ARABIA

In Partial Fulfillment of the

Requirements for the Degree of

DOCTOR OF PHILOSOPHY

In

CIVIL ENGINEERING

NOVEMBER 2013

KING FAHD UNIVERSITY OF PETROLEUM & MINERALS

DHAHRAN- 31261, SAUDI ARABIA

DEANSHIP OF GRADUATE STUDIES

This thesis, written by **Salihu Lukman** under the direction his thesis advisor and approved by his thesis committee, has been presented and accepted by the Dean of Graduate Studies, in partial fulfillment of the requirements for the degree of **DOCTOR OF PHILOSOPHY IN CIVIL ENGINEERING.**

Dr. Alaadin Bukhari
(Advisor)

26 NOV 2013

Prof. Nedal T. Ratrout
Department Chairman

Prof. Muhammad H. Al-Malack
(Co-Advisor)

Prof. Salam A. Zummo
Dean of Graduate Studies

Prof. Mohammed S.
Al-Suwaiyan
(Member)

2/12/13

Date

Dr. Muhammad S. Vohra
(Member)

Prof. Sleem U. Rahman
(Member)

This dissertation is dedicated to the loving memory of my late parents

ACKNOWLEDGMENTS

All best thanks and praises are always due to Almighty Allah (glorified and exalted is He) alone, who smoothened my path towards achieving this milestone. May peace and blessings of Allah be upon His beloved servant, His last messenger and the seal of the prophet-hood, Prophet Muhammad (may the peace and blessings of Allah be upon him), his house-hold, companions and those that follow their unique and most guided foot-steps till the day of resurrection.

Life is beautiful when we have people around us, people that make walking through challenges interesting. Space will not permit me to enumerate the people in my life who made this task possible, by Allah's will. Allah, the almighty knows you all. May He reward you beyond measure.

To my parents, my pillars – you raised me to be what I am. May Allah (SWA) accept this as charity from you and send light to your graves. To my family, my support – you bore with me through those sleepless nights and never-ending deadlines and schedules. Thank you for making home a holiday resort. May Allah (SWA) join us together in the loftiest part of paradise. My doc, my better half, you gave me strength knowing that there is always a shoulder to cry on when times are tough. Your linguistic skills were invaluable. Thank you for reasons too numerous to mention. To my boy and my little angel, Muhammad and Halima - your thoughts have always preoccupied my heart and brought a smile to daddy's face. To my little Maryam, my lovely one – the thought of coming home

to meet you always gladdened daddy's heart. To Khadijah, a timely gift – the memory of the day you were born will forever be cherished.

To my professors, Bukhari, Al-Malack, Al-Suwaiyan, Vohra and Rahman, my guide – you held the light and shone it, making the journey easy and the challenges surmountable. Thank you for the guidance and for your patience and forbearance. By Allah's will, you made it all possible. To Drs. Essa and Nuhu Mu'azu, your wealth of experience and homely welcome made the journey interesting and the challenges bearable. You are indeed, God-sent.

To Drs. Ismail and Otun, the two somebodies who made me stop feeling like a nobody. You nurtured me and made me strong enough to face the world. To Engr. Idris Nuhu and Dr. Lawal Halliru, you mentored me and offered a hand through those baby steps. To Major Suleiman Lukman, my brother – you taught me to believe in myself and never give up. May Allah (SWA) send light to your grave and admit you into paradise. To Engr. Amin, my course mate – you filled the days with laughter. To Abdullahi Usman, thank you for the technical support. To the Emir of Zazzau, Dr. Shehu Idris and all the good people of the Muslim Refresher Course Program – you believed in me and taught me to stand firm. May Allah (SWA) reward you with Firdaus and ease all your affairs.

I would like to acknowledge the support provided by King Abdul-Aziz City for Science and Technology (KACST) through the Science & Technology Unit at King Fahd University of Petroleum & Minerals (KFUPM) for funding this work through Project No. 11-Env1669-04, as part of the National Science, Technology and Innovation Plan.

TABLE OF CONTENTS

LIST OF TABLES

LIST OF FIGURES

LIST OF ABBREVIATIONS

3FD	:	3 level factorial design
AC	:	Activated Carbon
ANN	:	Artificial Neural Network
ANOVA	:	Analysis of Variance
ASTM	:	American Society of Testing and Materials
BBD	:	Box-Behnken Design
BET	:	Brunauer-Emmet-Teller
CCD	:	Central Composite Design
CEC	:	Cation Exchange Capacity
CI	:	Confidence Interval
DD	:	Doehlert Design
EC	:	Electrical Conductivity
Eh	:	Redox Potential
EK	:	Electrokinetics
EKR	:	Electrokinetic Remediation
EO	:	Electroosmosis
EOV	:	Electroosmotic Volume
ESP	:	Exchangeable Sodium Percentage
GAC	:	Granular Activated Carbon
HEKA	:	Hybrid Electrokinetics-Adsorption
ICP	:	Inductively Coupled Plasma

IEKAR	:	Integrated Electrokinetics-Adsorption Remediation
KACST	:	King Abdulaziz City for Science and Technology
KFUPM	:	King Fahd University of Petroleum and Minerals
KSA	:	Kingdom of Saudi Arabia
MC	:	Multi-Component
OFAT	:	One-Factor-at-a-Time
PZC	:	Point of Zero Charge
RSM	:	Response Surface Methodology
SASO	:	Saudi Arabian Standards Organization
SC	:	Single Component
TCE	:	Trichloroethylene
TPH	:	Total Petroleum Hydrocarbons
USEPA	:	United States Environmental Protection Agency
VIF	:	Variance Inflation Factor

ABSTRACT

Full Name : [Salihu Lukman]

Thesis Title : [Study on Integrated Electrokinetics-Adsorption Remediation Technique for Simultaneous Removal of Heavy Metals and Organics from Saline-Sodic Soil: Effects of Operating Parameters]

Major Field : [Civil Engineering (Environmental Engineering)]

Date of Degree : [November 2013]

In this research, three sets of tests were conducted, to study the potential of remediating saline-sodic soil that was spiked with contaminant mixture (Cr, Cu, Cd, Pb, Zn, Hg, phenol and kerosene) using integrated electrokinetics-adsorption remediation (IEKAR). The soil physico-chemical properties were characterized and then subjected to adsorption and desorption at different pH where multi-component adsorption selectivity sequence was obtained: Cr > Pb > Cu > Cd > Zn. The potential of coupling electrokinetics and adsorption using locally produced granular activated carbon from date palm pits for the remediation of the this soil was investigated. In one of the runs which was operated for 21- day period, remedial efficiency for Zn, Pb, Cu, Cd, Cr, Hg, phenol and kerosene were found to reach 26.8, 55.8, 41.0, 34.4, 75.9, 92.49, 100.0 and 49.8 % respectively. Geochemical modeling and ionic speciation were carried using Visual MINTEQ 3.0. Passage of electric current and variations in the pore fluid chemistry led to soil mineral degradation and alteration via biotransformation. The soil salinity and sodicity, which provided large amount of dissolved salts and minerals in the pore fluid for sustained high electrical conduction, were responsible for the extremely high electric current flow which led to excessive soil heating, high energy and process fluid consumption, high

electroosmotic volume, dissolution and corrosion of anodic electrodes and DC voltage clips and in some cases, higher contaminant remedial efficiency. Fifteen (15) bench-scale experiments were designed using Box-Behnken Design and executed to investigate the migration and distribution of the contaminant mixture using the IEKAR and to understand the operating variables' effects on some key factors and responses. The investigated variables, voltage gradient, initial contaminant concentration and polarity reversal rate were coded and varied at three levels simultaneously to investigate their interaction effects on 41 responses monitored. RSM, incorporated into Design-Expert® 8.0, was used in mathematical modeling, numerical optimization and interpretation of the results. The results obtained suggest that integrating adsorption into electrokinetic technology is a promising solution for soil remediation.

ملخص الرسالة

الاسم الكامل: صالح لقمان

عنوان الرسالة: دراسة على حركي كهربي-الامتزاز المتكاملة علاج تقنية لإزالة في وقت واحد من المعادن الثقيلة والمواد العضوية من التربة المالحة سوديك: آثار معايير التشغيل

التخصص: هندسة مصادر مياه و بيئة

تاريخ الدرجة العلمية: نوفمبر ٢٠١٣م

في هذا البحث ، وأجريت ثلاث مجموعات من الاختبارات، لدراسة إمكانية علاجها التربة المالحة سوديك الذي ارتفعت مع الخليط الملوث (الكروم ، النحاس، الكادميوم ، الرصاص ، الزنك والزئبق و الفينول والكيروسين) باستخدام كهربي المتكاملة - وتميزت الخصائص الفيزيائية والكيميائية للتربة و ثم تعرض ل الامتزاز و المج في درجة . (IEKAR)الامتزاز المعالجة <النحاس <الرصاص <الحموضة مختلفة حيث تم الحصول على تسلسل متعدد العناصر الامتزاز الانتقائية : الكروم إمكانات كهربي اقتران و الامتزاز باستخدام حبيبات الكربون المنشط المنتجة محليا من حفر النخيل لل . الزنك <الكادميوم في واحدة من أشواط التي تم تشغيلها لمدة 21 - فترة يوم والكفاءة العلاجية لل زنك . علاج من تم التحقيق هذه التربة والرصاص ، النحاس، الكادميوم ، الكروم ، تم العثور على الزئبق ، الفينول والكيروسين لتصل إلى 26.8 ، 55.8 ، 41.0 ، أجريت النمذجة الجيوكيميائية و أنواع جديدة الأيونية باستخدام . ٪ على التوالي49.8و 34.4100.0 ، 75.9 ، 92.49 ، مرور التيار الكهربائي والتغيرات في كيمياء السوائل المسام أدى إلى تدهور التربة المعدنية .Visual MINTEQ 3.0 ، التي وفرت كمية كبيرة من الأملاح و المعادن الذائبة في السائل sodicity ملوحة التربة و . والتغيير عبر التحول الأحيائي المسام ل التوصيل الكهربائي عالية ومستدامة ، كانوا مسؤولين عن تدفق التيار الكهربائي مرتفعة للغاية مما أدى إلى التدفئة المفرطة التربة ، والطاقة العالية و استهلاك السوائل العملية ، والكهربائية عالية الحجم ناضح ، وانحلال والتآكل من الأقطاب تم تصميم خمسة عشر (.الكهربائية انوديك ومقاطع العاصمة الجهد ، وفي بعض الحالات ، وارتفاع الكفاءة العلاجية الملوثات 15) تجارب مقاعد البدلاء النطاق باستخدام بوكس بينكين تصميم و تنفيذ للتحقيق في الهجرة و توزيع الخليط الملوث باستخدام تم ترميز المتغيرات التحقيق ، والجهد التدرج .وفهم آثار المتغيرات التشغيل ' على بعض العوامل الرئيسية و الردود IEKAR ، تركيز الملوثات الأولية و معدل انعكاس الاستقطاب و اختلفت على ثلاثة مستويات في وقت واحد للتحقيق في الآثار تفاعلها

، تدمج التصميم الخبراء ® 8.0 ، وكان يستخدم في النمذجة الرياضية ، العددي الأمثل RSM .على 41 استجابات رصدها . وتشير النتائج المتحصل عليها أن دمج التكنولوجيا في الامتزاز كهربي هو الحل واعدة ل معالجة التربة .وتفسير النتائج

CHAPTER 1

INTRODUCTION

The Kingdom of Saudi Arabia has been experiencing massive infrastructural development and rapid proliferating industrialization and manufacturing processes in the recent decades. Presently, within the Kingdom, there exist more than ten huge refinery plants with hundreds of petrochemical and other manufacturing plants. Many more are under construction. One of the major environmental consequences of these progressive achievements is the improper release of elevated amounts of variety of organic and inorganic pollutants into the environment. These pollutants could enter the environment directly as a result of accidents, spills during transportation, and leakage from waste disposal sites, storage sites and industrial facilities etc, thereby contaminating the environment. For instance, presently, diesel soil contamination on gas stations or refinery plants is a worldwide environmental problem. A study of storage tank accidents [1] revealed 242 accidents occurred in industrial facilities over 43 years (1960 - 2003). Government, industry and the public are well aware and recognize the potential dangers that complex chemical mixtures such as total petroleum hydrocarbons (TPH), phenols, heavy metals, radionuclides and pesticides pose to human health and the environment. Some of the pollutants can be degraded easily within the soil by indigenous microorganisms. Because of the fact that there are recalcitrant and bio-inhibitor contaminants, cost-effective remediation technologies must be developed to remove all

the different types of pollutants from the soil to effectively solve problems associated with contaminated sites in order to ensure a sustainable environment.

A novel in situ treatment technology for remediation of low permeability or heterogeneous soils containing low permeability zones has been developed in the last two decades. The approach, called Lasagna^{TM} process, involves synergistic coupling of electrokinetics and adsorption [2]. Owing to the uniqueness of electrokinetics in the remediation of low permeability soils, the technology has received much attention in the past decades [3-11]. The technology is called Lasagna^{TM} due to its layered appearance of electrodes and treatment zones as shown in Figure 1. It may have horizontal or vertical configuration. The original intent was to use hydrofracturing in the installation of the electrodes and treatment zones horizontally in a layered manner like Lasagna, but vertical emplacements have been found to be more practical [12-16].

In situ treatment technologies for contaminated soils and groundwater has been the subject of a great deal of research in the last three decades owing to their attendant advantages; potential lower cost, less environmental disruption and reduction in worker exposure to hazardous materials [13]. Particularly, electrokinetic remediation has been found to have an edge over all other promising in situ treatments such as bioremediation, vapor extraction and pump-and-treat when applied to low permeability soils. These low permeability soils are present at many contaminated sites [13]. Of the several electrokinetic remediation techniques, Lasagna process has been found to yield the best removal efficiency of organic contaminants from soils [17].

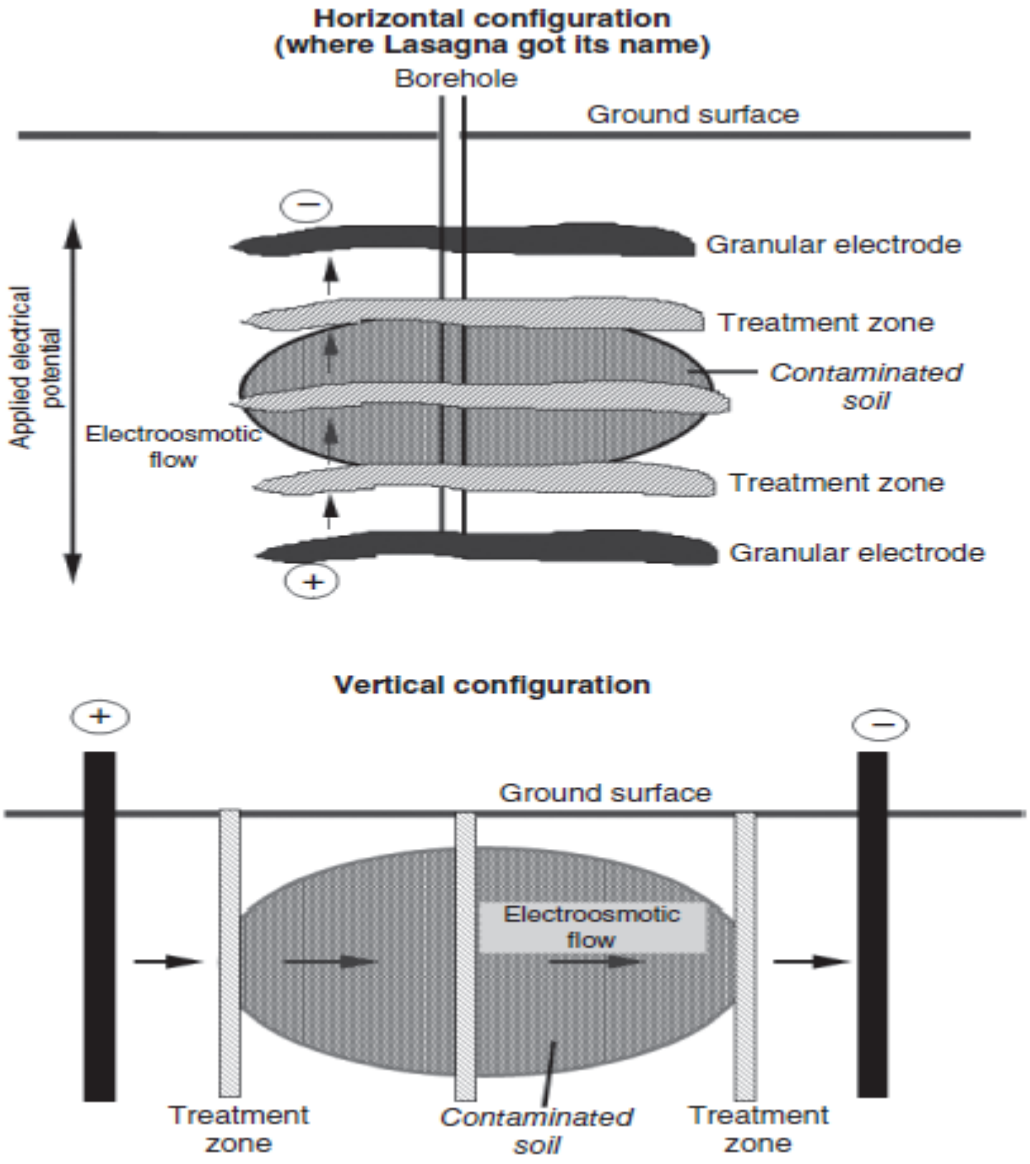

Figure 1 Typical horizontal and vertical configurations of the Lasagna™ process [12]

The general concept of the Lasagna process is the transportation of contaminants from contaminated soil section into treatment zones using major electrokinetic transport mechanisms (i.e. electroosmosis or electromigration). Once at the treatment zones, the contaminants may be removed from the pore water by sorption, degradation or immobilization depending on treatment zone design [2, 13-15].

Pore-water movement under electroosmosis offers unique advantages in the overall treatment of the contaminated soil. These include uniform water flow through low permeability and heterogeneous soil and control of flow direction under very low power consumption [13].

1.1 Problem Definition and Justification

In situ remediation technologies are faced with significant technical challenges when the contaminated soil is of low permeability. Popular traditional technologies such as vapor extraction and pump-and-treat are rendered ineffective due to the difficulty encountered in accessing the contaminants and delivering treatment reagents. In addition, these treatment technologies cannot be applied in settings where the soil contains mixed contaminants such as petroleum hydrocarbons, heavy metals and radionuclides. Conceptually, the Lasagna process has the potential to treat mixed contaminants in situ [16].

It has been observed that contaminated soils do not contain single contaminants but usually several pollutants appear in the soil as mixed components. In reality, soil polluted with organic contaminants often contains other contaminants such as heavy metals. The implication of the presence of the different nature of the two contaminant groups is that there may be synergistic or antagonistic effects on their respective removal using electrokinetic remediation technique [18-21]. Reddy [22] posited that presence of mixed contaminants will retard individual contaminant migration and removal. Also, as organic pollutants are removed by electroosmotic flow and heavy metals by electromigration, the solubility as well as hydrophobicity disparities between the organic pollutants and heavy metals indicates the complexity of electrokinetic remediation of soils polluted with mixed

contaminants. To date, several studies have been conducted using electrokinetics for mixed contamination [19, 23-33]. However, to the best found knowledge, only one study was conducted using Lasagna process for the remediation of contaminant mixture [34] despite its added advantages over electrokinetics only. More studies need to be carried out to better understand the behavior of different contaminant mixture using the Lasagna process.

Saline-sodic soils (usually found in arid and semiarid regions) possess high electrical conductivity (4 dS/m) which prevents the application of appropriate voltage gradient in an electrokinetic study owing to current limitations. In addition, these soils are associated with high pH > 8.2, dominated by 2:1 type clay minerals and exchangeable sodium percentage at levels greater than 15. These properties make saline-sodic soils to be high acid buffering, alkaline and very difficult to remediate if contaminated with heavy metals due to precipitation of heavy metals in alkaline environment. These extreme soil characteristics pose great difficulty in having such soils remediated from mixed contaminants using electrokinetic-based technique. Despite these challenges posed by saline-sodic soils, there is the need to investigate possible remediation of such soils using the integrated electrokinetics-adsorption technique given its promise in remediating low permeability soils. The usual voltage gradient of 1 V/cm for bench-scale studies when applied to such soils could lead to high electric current flow. This in turn could lead to excessive soil heating, reduction in the soil moisture content, high energy and process fluid consumption, high electroosmotic flow rate, and in some cases, higher percentage removal of contaminants [12, 35, 36].

Lasagna process uses activated carbon as the sorbent material to improve the removal of contaminants from contaminated soil [13, 37, 38]. However, commercially available activated carbon is expensive, which may limit its use in field-scale remediation. Therefore, from economic point of view and for cost-effectiveness, the need to develop low-cost, easily available adsorbents cannot be overemphasized. In that regard, use of granular activated carbon (GAC) locally produced from date palm pits was proposed herein. Thousands of date palm trees are currently grown in the Kingdom of Saudi Arabia (KSA) and several parts of such plantation go as wastes, thereby generating huge volume of solid wastes annually. The potential application of using activated carbons produced locally from date pits and branches as adsorbents for removal of water pollutants have been tested for removal of phenol, O-Cresol and methylene blue in previous studies conducted at King Fahd University of Petroleum and Minerals (KFUPM) under King Abdulaziz City for Science and Technology (KACST) sponsored project [39-43]. The integrated electrokinetic-adsorption technique using granular activated carbon produced locally from date palm pits proposed in this study is expected to improve efficiency of removing contaminants in contaminated soils by overcoming the dwindling effectiveness usually encountered when electrokinetic technique is employed alone. Moreover, the proposed integrated approach will serve as an avenue to support a sound solid waste management practice via utilization of date palm pits. Due to relevance of adopting cost-effective environmental management strategies particularly via locally developed innovative solutions, it is anticipated that research of this kind will successfully enhance and support meeting the imminent challenges facing the ongoing massive industrial development. Hence, the significance of application of the proposed remediation

technology at sites that undergo environmental deterioration due to soil contaminated with mixed pollutants cannot be overemphasized owing to localization of the solution and high expectation of the decontamination efficiency as reported by Huang *et al.*[17].

Modeling of environmental phenomenon using Response Surface Methodology (RSM) has been widely reported, but its application in electrokinetics is very rare, let alone the Lasagna process. The main aim of RSM is the determination of optimal operational conditions of a particular process by determining a region that meets the operating specifications thereby reducing the number of costly experimental trials needed for the evaluation of multiple parameters and their interactions [44, 45]. Variables investigated and optimized so far using RSM in electrokinetic remediation include initial ion concentration, voltage gradient, treatment time [46] and optimization of different combinations of enhancement reagents [47]. Other variables that affect contaminant removal efficiency in the Lasagna process include polarity reversal rate, pulse application of DC voltage gradient and pH of process fluids. Investigation of these variables in the Lasagna process will in no small measure, optimize the removal efficiency of contaminants. From the best found knowledge, RSM has never been applied to optimize and model the Lasagna process.

1.2 Research Objectives and Scope

The main aim of the research is to design, test and evaluate proposed innovative technique that combines electrokinetics and adsorption using locally produced activated carbon from date palm pits for remediation of saline-sodic soil contaminated with mixture of toxic pollutants comprising of petroleum byproduct (kerosene), organic

compound (phenol) and heavy metals (Cr, Cu, Cd, Zn, Pb and Hg). Hence, the specific objectives to be achieved in this study are:

a) Use batch adsorption to investigate the adsorption and desorption behaviors in addition to selectivity sequences of Cd, Cr, Cu, Pb and Zn ions onto the clay minerals in single and multi-component scenarios and at different pH values.
b) Investigate the potential of coupling electrokinetics and adsorption using locally produced granular activated carbon from date palm pits for the remediation of saline-sodic soil spiked with Cr, Cd, Cu, Zn, Pb, Hg, phenol and kerosene.
c) Investigate ionic speciation, migration and distribution of the heavy metal contaminant mixture (using Visual MINTEQ 3.0) to provide clear understanding of how the operating variables affect the geochemical processes and responses.
d) Vary voltage gradient, initial contaminant concentration and polarity reversal rate according to statistical experimental design using the Box-Behnken Design (BBD) to study the interaction effects of these factors on the contaminant remedial efficiencies and other responses such as soil pH, electrical conductivity and processing fluid refill or replacement rate.
e) Develop mathematical response surface predictive models and numerical optimization scenarios using RSM incorporated into the Design Expert® 8.0 software for the determination of optimal remediation efficiency that minimizes input requirements and conditioning such as voltage gradient, energy consumption and processing fluids.

1.3 Scope of the Research

The study will be limited to the bench-scale only. Data obtained from the bench-scale investigations may be used for pilot-scale implementation using the optimal factor levels. The bench-scale study will utilize continuous and uniform electric field created between graphite electrodes. No surfactant, complexing or chelating agent will be used apart from processing fluids for electrolyte conditioning. Mathematical models to be developed herein are limited to the derived results obtained from the saline-sodic soil, hence, generalization and use of the model for different soil types and different operating conditions outside those investigated may lead to incorrect estimation of the responses.

1.4 Uniqueness of the Research

To the best knowledge of the author, the following important aspects of the Lasagna process have not been addressed or investigated in previous research studies:

a) Remediation of soil contaminated by a combination of multiple heavy metals, petroleum hydrocarbons and organic pollutants.

b) This is the first study that attempts the treatment of contaminated saline-sodic soil using electrokinetic remediation. High salinity and sodicity soils possess high electrical conductivity which prevents the application of appropriate voltage gradient owing to current limitations.

c) This is the first research that uses BBD for experimental design of electrokinetic remediation - two previous investigators used central composite design (CCD) and optimal design. Hence, it will be the third research that utilizes RSM for electrokinetic remediation.

The above issues will be addressed in this study to provide important research findings that may go a long way in enhancing field applications of the Lasagna technology for the remediation of saline-sodic soils.

1.5 Organization of the Dissertation

This dissertation has been subdivided into eleven (11) chapters. These chapters try to address the stated objectives of the research, with each, addressing a particular problem. The highlight of each chapter is briefly provided below:

- Chapter 1 contains the problem definition, research objectives, scope, uniqueness and organization of the dissertation.
- Chapter 2 contains review of relevant literature
- Chapter 3 contains detailed experimental and mathematical methodology
- Chapter 4 presents the results of the adsorption and desorption experiments.
- Chapter 5 presents the results of the preliminary electrokinetics and integrated electrokinetics-adsorption experiments.
- Chapter 6 delves more into the geochemical modeling and migration of trivalent Cr.
- Chapter 7 demonstrates the application of the mathematical modeling and numerical optimization concepts to the remediation of saline-sodic soils contaminated with mixed pollutants where Cd was chosen as a model contaminant.
- Chapter 8 discusses the application of the Box-Behnken Design for mathematical modeling and optimization of Hg remedial efficiency.

- Chapter 9 models the effects of the investigated factors on the soil electrical conductivity.
- Chapter 10 discusses how the processing fluids refill or replacement rate affects the geochemical processes
- Chapter 11 contains the overall summary, conclusions and recommendations.

CHAPTER 2

LITERATURE REVIEW

2.1 Lasagna Process: From Inception to Date

2.1.1 Historical Background

In early 1992, a discussion took place between the then Monsanto chief executive officer (CEO) and administrator of the United States Environmental Protection Agency (EPA) which ultimately led to the invention of the Lasagna process. They discussed about lack of effective technology to clean up soils contaminated with hazardous wastes. The outcome was an open meeting in Washington in June 1992 which included representatives from industry, academia, government and public interest groups. Enthusiastic responses obtained from this meeting encouraged EPA to initiate a program dubbed Remediation Technology Development Forum (RTDF) tasked with the responsibility of getting common interest groups to develop innovative and cooperative technologies in the environmental area. In January 1993, Monsanto proposed to the RTDF that an effort be put in place for the advancement of a novel method which will deal particularly with remediating low permeability soils (such as clay or silt) which are very difficult to clean up [15]. Later that year, Philip H. Brodsky and Sa V. Ho of Monsanto filed the first Lasagna^{TM} U.S. patent followed by a second one in 1993 all published in 1995 [48, 49]. Other collaborators were invited by Monsanto for successful development of the multi-component technology which requires different skills and experience that were not available within Monsanto alone. Industrial consortia consisted

of Monsanto, General Electric (GE) and DuPont partnered with EPA and U.S. department of energy (DOE) to bring the Lasagna technology development to fruition. The responsibility of each of these segments towards implementing the novel integrated in situ remediation technology is depicted in Figure 2.

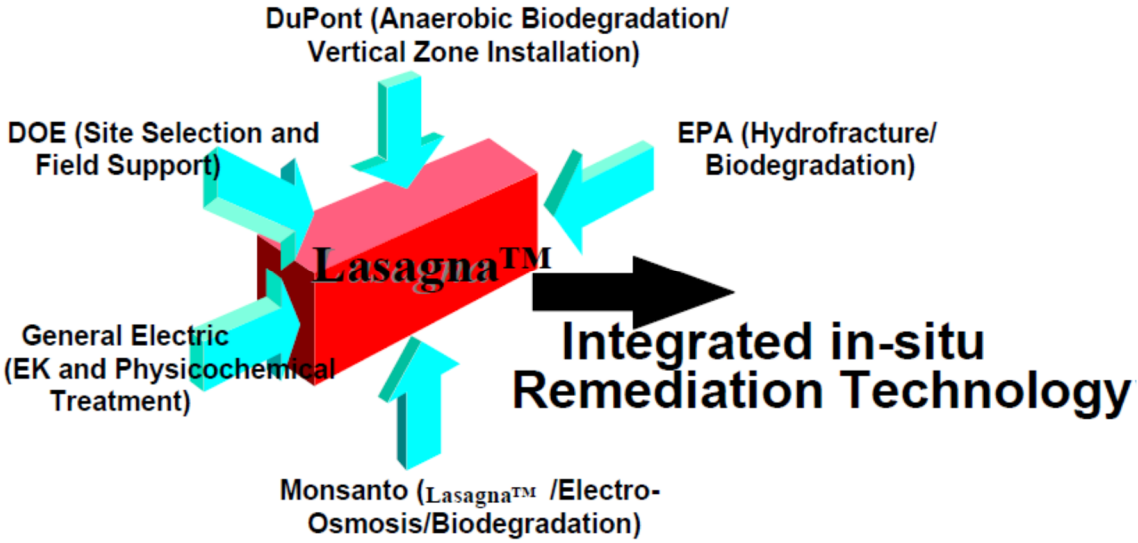

Figure 2 Integrated segments behind the integrated electrokinetics-adsorption technology [50]

In the Lasagna process, contaminated soil is remediated by creating at least one liquid permeable zone within a contaminated soil region and turning it into treatment zone. Appropriate materials (sorbents, catalytic agents, microbes, oxidants, buffers) are then introduced into the treatment zone. An electrode is placed at the first end of the contaminated soil region and another of opposite charge is placed at the opposite end of the contaminated soil region. A direct electric current is then transmitted through the contaminated soil region between the two electrodes. This causes movement of water and dissolved organic and inorganic materials in subsurface soils from one electrode (anode) to the other (cathode) under electroosmosis as a result of current movement from anode

to cathode. In 1802 electroosmosis was first observed, detailed study of the mechanism was done by Reuss [51] in his classic experiment reported by Abramson [52]. The electric transport of dissolved contaminants and pore fluid in soils induced by an applied DC voltage is termed electrokinetics. It is made up of transport of pore fluid via electroosmosis (EO) and transport of ions or charged species via electromigration [2, 12-15, 17, 53, 54]. Numerous applications of electroosmosis in soil consolidation to increase its shear strength has been reported elsewhere [54]. First application of electrokinetics took place in India in the 1930s. It was used to remove excess salts from alkali soils in order to restore it to arable condition [55].

Electroosmosis has been found to be most efficient for moving water through low permeability soils. These soils are highly resistant to hydraulic flow and prone to chanelling. These drawbacks make it very difficult to be remediated effectively using other remediation technologies [15].

2.1.2 Implementation of the Lasagna Process at Different Scales

Following its invention in 1993, extensive studies started in 1994 in bench-scale [13], then scaled up in a pilot-scale under laboratory conditions. Development of temperature models and designs for the field tests followed after successful implementation in the pilot-scale [2]. The first field test called Phase I: Small Field Test was conducted in 1995 at the Paducah gaseous diffusion plant (PGDP) site whose soil was contaminated with trichloroethylene (TCE). Very high TCE removal was accomplished (99 %) even in area of possible dense non-aqueous phase liquid (DNAPL) contamination. The main requirement for the removal of non-polar organic contaminants using electrokinetics is that they need to possess some solubility in pore water. This will enable their movement

within the pore fluid to treatment zones or electrode chambers. Having got proof of concept of the Lasagna process under the small field conditions, a second and larger field test dubbed Phase II was conducted at the site so as to demonstrate the effectiveness of the Lasagna technology for in situ degradation of TCE and to perfect methods for installing the technology in the field. This large field test also achieved high TCE removal ranging from 95 % to over 99 % in the contaminated areas bracketed by the treatment zones [14, 15]. Full-scale remediation using the Lasagna technology was undertaken at two other contaminated sites in the United States [12]. The first one began operation in 1999 and operated for 2 years in Paducah, Kentucky. The second full-scale implementation of the Lasagna technology was started in 2006 at Fond du Lac, Wisconsin. The specific details of all the Lasagna process implementations are presented in Tables 1 and 2. Ma and his co-workers [37, 38] achieved a high Cd removal efficiency of 79.6 % and 93 % using sandy loam and kaolin respectively. They used a new bamboo charcoal activated carbon as the sorbent in two studies (see Table 1). In another related study [34] they investigated the simultaneous removal of 2,4-dichlorophenol and Cd from an artificially spiked natural sandy loam (Table 1). This is the first and only study that investigated mixed contaminants removal using the Lasagna process. It can be seen from Tables 1 and 2 that most of these studies considered polarity reversal. Periodic electrical polarity reversal may be carried out to reverse pore fluid and direction of contaminant transport. This will play a major role in stabilizing the electroosmotic process and ensures multiple passes of the contaminants across the treatment zones [2, 15].

Table 1 Applications of Lasagna process on a bench-scales from inception to date

Treatment zone material	Contaminant	Soil type	Cell dimensions (length x width x depth)	Polarity reversal/ Downtime	Removal efficiency, %	Voltage gradient, (V/cm)/ Current (mA)	Power consumption, kWhr/m^3	Run Time, days	Electroosmotic conductivity, $cm^2V^{-1}\ s^{-1}$ ($x10^{-5}$)	Treatment zone spacing, cm	Reference
AC* + sand, bacteria + AC + sawdust	*p*-nitrophenol	Kaolinite	10 cm ID, 21.6 cm long	Yes/Continuous	90-99	1-7/3 (constant)	10	20	2.5	6	[2, 13]
AC (Bamboo charcoal)	Cd	Sandy loam	24 cm × 10 cm × 8 cm	Yes/Continuous	79.6	1/7 - 27	-	12	-	10	[37]
AC (Bamboo charcoal)	Cd	Kaolin	24 cm × 10 cm × 8 cm	No/Continuous	93	1/3 - 23	-	8	-	10	[38]
AC (Bamboo charcoal)	2,4-dichlorophenol and Cd	Sandy loam	24 cm × 10 cm × 10 cm	Yes/Continuous	75.97 (Cd); 54.92 (2,4-dichlorophenol)	1/Variable	121.91 - 128.48	10.5	-	16	[34]

*Activated carbon; **Granular activated carbon

Table 2 Applications of Lasagna process on a pilot- and field-scales from inception to date

Treatment zone material	Contaminant	Soil type	Site dimensions (length x width x depth)	Polarity reversal/ Downtime	Removal efficiency, %	Voltage gradient, (V/cm)/ Current (A)	Power consumption, kwh/m^3	Run time, month	Electroosmotic conductivity, $cm^2V^{-1}\ s^{-1}$ ($x\ 10^{-5}$)	Treatment zone spacing, cm	Reference
AC + sand	*p*-nitrophenol	Kaolin/Kaolinite/clay loam	1.22 m x 0.61 m x 0.61 m	Yes/Continuous	98	1 (Constant) /96.2 (based on current density)	51	3	0.56 - 1.7	35.56	[2]
GAC[1]	TCE[2]	Clay loam	4.6 m × 3 m × 4.6 m	Yes/Continuous	99	0.35 - 0.45/40 (Constant)	-	4	1.2	60	[53]
Iron filings + kaolin	TCE	Clay loam	6.4 m × 9.2 m × 13.7 m	Yes/3-week	95 - 99	0.23-0.31 (Constant)/ 110-200	-	12	1.2	60 & 150	[14]
Iron filings + kaolin	TCE	Clay loam	27.4 m × 22 m × 13.5 m	No/Pulse mode	99	0.15-0.26 (Constant)/ 500-700	-	24	-	150	[12, 56]
Iron filings + kaolin	TCE	Clay loam	33 m x 24 m x 7.5 m	-	60 (after 1 year)	0.16 (Constant)/ 250-400	-	24	-	150	[12]

[1]Granular activated carbon; [2]Trichloroethylene

From the foregoing reviews, it is noteworthy that only one of the studies has considered simultaneous removal of contaminant mixture. All others have dealt with only a single organic compound or heavy metal. It has already been observed that contaminated soils do not contain single contaminants only, but usually several pollutants appear in the soil in mixed components [18-21]. The need to study the removal of more complex contaminant mixtures using the Lasagna process cannot be overemphasized.

2.2 Lasagna Process and Other Competing Technologies

Technologies that have been identified as potential competitors to the Lasagna process are enhanced vacuum extraction, in situ enhanced soil mixing, conventional electrokinetics, excavation and incineration and pump-and-treat. Site and contaminant characteristics determine the suitability and effectiveness of the application of each of these technologies. Table 3 attempts to qualitatively compare each of these technologies in terms of soil type, contaminants, cost, treatment time, further disposal, disruption to site/soil and depth. From Table 3, Lasagna stands apart from all other treatment technologies when treating low permeability soil such as clay or silt which is contaminated with mixed contaminants. It has low cost and it is the only technique that does not need aboveground treatment. More recently [17] different types of electrokinetic remediation technologies have been reviewed in terms of removal of different organic pollutants from different types of soils. As expected, Lasagna furnished the best removal efficiency.

Table 3 Characteristics of the Lasagna process and competing technologies [15]

Characteristics	Technology					
	Lasagna™	Excavation & incineration	Pump & treat	Electrokinetics	Soil vapor extraction	In situ soil mixing
Soil type	Low permeability /heterogeneous soils	All types	Sandy, permeable soils	Low permeability heterogeneous soils	Permeable soils, less effective with clay	All types, more difficult with clay
Contaminants	Organics, metals, mixed contaminants	All types	Soluble organics & metals	Organics & metals	Volatile/ semi-volatile organics	Volatile/ semi-volatile organics
Cost	Low	High to very high	Medium to high	Medium	Low	Medium
Treatment time	1-3 years	A few months to years	> 20 years at most sites	1-3 years	A few months, longer with complications	A few months, longer with complications
Further disposal	No	Yes	Yes	Yes	Yes	Yes
Disruption to site/soil	Minimal	Highly disruptive to both site & soil	Some, from continuous pumping	Some, from aboveground treatment	Some, from aboveground treatment	Highly disruptive to the soil
Depth	In principle, no limit, treatment can be localized to contaminated area	Shallow, cost increasing greatly with depth	No limit, less control as depth increases	In principle no limit, will be more difficult to bring contaminants up as depth increases	More effective shallow	More effective shallow

2.3 Other Important Considerations Affecting the Lasagna Process

Upon application of a DC potential to soil containing water and ions, acid and base are generated at the anode and cathode respectively due to water electrolysis according to the following chemical reactions.

$$2H_2O \longrightarrow O_2 + 4H^+ + 4e^- \quad (2.1)$$

$$4H_2O + 4e^- \longrightarrow H_2 + 4OH^- \quad (2.2)$$

The hydrogen ions produced at the anode decrease the pH near the anode and the generated acid front is carried towards the cathode by electrical migration, diffusion and advection. At the same time, an increase in the hydroxide ion concentration causes an increase in the pH near the cathode. Non-ionic species such as most organic contaminants are transported along with the electroosmotic induced water flow; while contaminants bound to mobile particulate matter can be transported via electrophoresis and metals or charged ions are transported mainly by electromigration [57-59]. The direction and quantity of contaminant movement is influenced by the contaminant concentration solubility and degree of hydrophobicity, soil type and structure, and the mobility of contaminant ions, as well as the interfacial chemistry and the conductivity of the soil pore water [57]. The removal efficiency generally depends on the nature of the contaminants, and soil properties, such as pH, permeability, adsorption capacity, buffering capacity, etc. [60]. Moreover, other interacting mechanisms such as advection that is generated by electroosmotic flow and externally applied hydraulic gradient, diffusion of the acid front to the cathode, and the rate of migration of cations and anions towards the respective electrode also significantly influence the efficiency of the electrokinetic process [61].

The acidic environment created near the anode could deter electroosmotic flow (EOF) if the soil zeta potential falls too low or reverses. Solubilization of inorganic contaminants is enhanced by a low pH environment which speeds up their removal by electromigration and electroosmosis. However, when zeta potential of soil particle surface is reversed due to a low pH environment, EOF may correspondingly be reversed [62-64]. To eliminate the low pH at the anode, steel plates may be used as the anode electrode to promote iron oxidation as the major anodic reaction as against

water oxidation which leads to the formation of acid as demonstrated by equation 2.3 [2, 12]. Oxidation and reduction takes place at the anode and cathode respectively.

$$Fe^{0} \longrightarrow Fe^{2+} + 2e^{-} \qquad (2.3)$$

If the dissolved ion will pose some concerns, then, process fluids (catholyte and anolyte) may be used to neutralize the hydroxyl and hydrogen ions respectively. An extensive review of the methods and strategies for enhancing the performance of electrokinetic remediation has been reported elsewhere [65]. Chemically inert and electrically conducting materials such as graphite, coated titanium or platinum may be used as an anode so as to prevent electrode dissolution with subsequent generation of undesirable corrosion products in an acidic environment. As for the cathode material, any conductive material which resists corrosion in basic environment may be used [66]. Planar electrode configuration has been found to be more effective than cylindrical well-based electrodes. Uniform current distribution, soil resistance and heating are provided by the planar electrodes whereas cylindrical well-based electrodes cause current density restriction and excessive heating in local areas leading to drying of the soil around the electrode well and untimely failure of the electrokinetic system [12].

Passage of electric current through the soil causes soil heating due to thermal effects of Joule heating. Soil heating has not been reported to be an issue of concern for bench-scale experiments [2], however, it is one of the most important parameters to be considered in field applications [2, 12, 14, 53]. Soil temperature determines the voltage gradient to be used. Running at lower voltage gradients has the advantage of reducing the anodic current density and provides a far more stable long-term operation. Usually, 1 V/cm is the appropriate voltage gradient for bench-scale studies

(Table 1). However, for sustained practical field operation, this voltage gradient would heat up soils above 100 ^{0}C within weeks. As such, for Lasagna systems, voltage gradients are limited to around 0.1 - 0.3 V/cm [12, 54]. If high electrical current density is allowed to pass through the soil, large volume of air bubbles would be generated by electrolytic decomposition of water at the electrodes, leading to the impediment of EOF. When these bubbles migrate into the soil, the degree of saturation decreases, consequently affecting the following flow parameters of fluid and chemicals: coefficient of electroosmotic conductivity, hydraulic conductivity, effective diffusion coefficient and effective ionic mobilities of contaminants [54].

2.4 Numerical Modeling of Lasagna Process

Thermal effect was modeled numerically and validated. This model was able to predict the temperature rise in pilot and field experiments successfully [2, 14, 53]. The developed model describes Joule heating and heat transfer by conduction and convection. A computational flow dynamic (CFD) finite element package called FIDAP® was used to execute the model. One-dimensional model which describes the transport of chemical species in the Lasagna process was also developed [67]. The following mechanisms were accounted for in the model: charge transfer in the double layer, pH buffering capacity of the soil together with electroosmosis, ionic migration, electrode reactions, zeta potential dependency of pH and ionic strength, and soil/water chemistry. However, description of all the simultaneous processes occurring during the Lasagna remediation has not been achieved by a single model [54].

2.5 Process Modeling Using Response Surface Methodology

Empirical modeling using Response Surface Methodology (RSM) offers great and numerous advantages which include - large amount of information from a small number of experiments, evaluation of simultaneous interaction effects of the independent parameters on the responses and simultaneous optimization of multiple factors and responses for obtaining optimal conditions [68, 69]. The key success of RSM is uncovering interactions of factors which cannot be achieved using the traditional one-factor-at-a-time (OFAT) optimization approach [70]. Fundamental understanding of the physics and chemistry which governs the process is essential in determining the influential factors to be investigated and their levels or ranges is necessary for successful implementation of RSM for any process modeling and optimization. Basically, there exist four different experimental designs for RSM implementation - 3 level factorial design (3FD), Box-Behnken Design (BBD), central composite design (CCD) and Doehlert design (DD). Bezerra et al. [69] have reviewed each of these design methods. The Box-Behnken Design is obtained by combining two-level factorial designs with incomplete block designs followed by adding a specified number of replicated center points. BBD is preferred when investigating three (3) factors using RSM because it will give enough information for analyzing factor-response interactions from the least experimental runs when compared to 3FD and CCD. For higher number of factors, DD gives fewer experimental runs at variable factor levels. The limitation of DD is that it is irrotatable, hence, it becomes biased in response prediction [69, 70]. Bias should be avoided by all means possible and rotatability is a desirable feature of Response Surface Methodology [71].

CCD was used to investigate the effects of ion concentration, applied potential and treatment time on removal of lead and nickel from sand using electrokinetic

remediation [46]. However, important issues to do with preliminary model evaluation and diagnostics, experimental model validation and optimal conditions generation using optimization were not included. Recently, Bongay and Ngo [47] applied optimal design method for the optimization of concentration of anolyte-catholyte pair that is most significant for the electrokinetic remediation of a Cu-contaminated soil. However, the use of single contaminant and single response for optimization using Desirability function may lead to overestimation of the Desirability values.

2.6 Heavy Metal Analysis - Flame Atomic Absorption Spectrometry and Mercury Analyzer

Flame atomic absorption spectrometry (FLAA) is used for heavy metal quantification if the sample is expected to contain high concentration of the analyte (> 100 ppb) [72]. In this situation, inductively coupled plasma - atomic emission spectrometry (ICP-AES) or inductively coupled plasma - optical emission spectrometry (ICP-OES) may also be used in place of FLAA [73]. FLAA uses direct aspiration technology in which a sample is aspirated and then atomized in a flame using air and acetylene gas. A light beam emanating from a hollow cathode lamp (or electrodeless discharge lamp) is then directed through the flame into a monochromator, and onto a detector which is used to measure the amount of absorbed light by the metal being determined. Presence of free unexcited ground-state atoms in the flame determines the absorption. The amount of light energy absorbed is proportional to the metal concentration in the sample, and the wavelength of the light beam is a characteristic of only that metal [73].

Mercury analyzer is used for the analysis of mercury in solid and aqueous matrixes. EPA Method 7473 [74] describes the procedure for mercury quantification in solids

and solution by thermal decomposition, amalgamation and atomic absorption spectrometry.

2.6 Quantification of Total Petroleum Hydrocarbon in Soils - Kerosene

Total petroleum hydrocarbon (TPH), also called mineral oil, hydrocarbon oil, extractable hydrocarbon or oil and grease is used in evaluating sites contaminated with petroleum hydrocarbons. Alkanes and aromatics are the basic compounds present in all petroleum products. These products are classified based on the carbon range of hydrocarbons they contain. Kerosene which is sometimes referred to as jet fuel or paraffin, falls within the range of diesel range organics (DRO) [75]. It contains 80 - 90 % alkanes, 10 - 20 % aromatics and do not usually contain alkenes [76]. Different carbon range for kerosene has been reported; C_8 - C_{16} [77, 78], C_{10} - C_{16} [79] and C_8 - C_{17} [76] with majority of the constituent compounds falling within the range C_{10} - C_{14} [76]. Kerosene has specific gravity of 0.83 at 15 ^{0}C and boiling point 190 - 260 ^{0}C [77, 78]. There exist numerous methods for the quantification of TPH in soils. All these methods can be classified into specific and non-specific, depending on whether the method provides fingerprint of all the compounds in the petroleum hydrocarbon or not [80]. Specific methods include gas chromatography–mass spectrometry (GC-MS), high performance liquid chromatography–mass spectrometry (HPLC-MS), isotope dilution mass spectrometry (IDMS), nuclear magnetic resonance (NMR), and electrospray ionization–mass spectrometry (ESI-MS) [81-84]. On the other hand, conventional non-specific methods include the following: fieldscreening gas chromatography with flame ionisation detector (GC-FID) or photo-ionisation detector (GC-PID) [85, 86], gravimetric determination and infrared spectrophotometry (IR) including EPA Methods 418.1, 8440, and 9071B, and American Society for Testing and Materials (ASTM) methods 3414 and 3921 [87-91],

turbidimetry [92], ultraviolet and fluorescence spectroscopy [93, 94], thin-layer chromatography (TLC) [95], high performance liquid chromatography (HPLC) [96, 97], size-exclusion chromatography [97], supercritical fluid chromatography (SFC) [98], total organic carbon [99], isotope ratio mass spectrometry [100] and fibre optic infra red sensor [101]. From all these quantification techniques, GC-based methods are the preferred laboratory methods for TPH measurement [102]. This is because they can detect a wide range of hydrocarbons and provide both sensitivity and selectivity. They can also be used for TPH identification and quantification [76]. In the past, IR-based methods were widely used because they are simple, quick and inexpensive. However, worldwide ban on Freon production led to a decrease in their application. Freon is needed for sample extraction and measurement using the IR-based method. Gravimetric-based techniques are useful for oily sludge and wastewaters. These wastes will present analytical difficulties for other more sensitive methods like the GC-based. For in situ field TPH quantification, immunoassay provides good results [76].

GC separates chemical mixtures such as petroleum hydrocarbons into its individual components as the sample travels through a column in the GC. A combination of factors is used to achieve this separation. These factors include boiling point, polarity and differences in affinity among the different compounds in the sample. Compound retention time (RT) is specific, reproducible and characteristic of that compound under given experimental parameters and specified column [103]. Upon elution of the separated compounds from the column, mass spectrometer (MS) detects them by ionizing compounds and scanning for ions of specific mass-to-charge ratios using their fragmentation patterns. Spectrum gives the results of scan of all the mass-to-charge ratios performed in a fraction of a second. It is unique for every compound

apart from isomers, which possess identical spectra. An ion chromatogram is generated by plotting intensity of a single ion over time [76]. Different temperature programs for semi-volatile analysis such as kerosene and phenol have been reported [75, 102, 104-106].

CHAPTER 3

MATERIALS AND METHODS

3.1 Preparation, Production and Characterization of Clay and GAC

Local Saudi Arabian clay from Al-Hassa oasis was used in this study. From the chemical analysis conducted by acid digestion of 1 g of clay sample using 10 mL of concentrated hydrochloric acid (analytical grade) as per EPA Method 3050B [107], it was found that heavy metals are present in the natural clay. Respectively, the clay pH, moisture content, soil organic matter (SOM) and electrical conductivity were determined according to the protocol outlined in ASTM D 4972, D 2216, D 2974 and D 1125 [108]. Surface area and pore volume were measured using the Brunauer-Emmet-Teller (BET) multipoint technique using nitrogen gas adsorption at -195.976 °C. Accelerated surface area and porosity analyzer (ASAP 2020) was used for surface area determination. The clay sample was also characterized using scanning electron microscopy (SEM) and X-ray diffraction (XRD) using an FEI Nova Nano SEM 230 FE-SEM model and Rigaku Ultima IV MPD X-ray diffractometer fitted with a monochromator respectively. Other standard geotechnical parameters of the clay such as specific gravity, liquid and plastic limits, sieve analysis and hydraulic conductivity were determined according to standard procedures set out by the American Society of Testing and Materials [108].

The local GAC production procedures as well as the characterization and optimization methods used are as described by Essa et al. [42], Essa and Al-Zahrani [40], Al-

Zahrani et al. [39] and Vohra et al. [43] and briefly described herein. Date pits were obtained from Al-Maghadi Dates Factory in Al-Madinah Al-Munawwarah, Saudi Arabia. Kingdom of Saudi Arabia is the second largest producer of dates in the world. The date pits were thoroughly washed with distilled water and oven dried (Isotemp oven, Fisher) at 120 ^{o}C for 24 h. Universal cutting mill (Pulverisette 19) was used to grind the dried pits. The ground pits were then sieved to particle size range of 0.4 - 2 mm (Plate 1). From the sieved sample, 100 g was measured and thoroughly mixed with a solution of phophoric acid (54 %) prepared using 85 % (w/w) phophoric acid and impregnation ratio 1.6. The resulting slurry was evaporated in oven at 120 ^{o}C for 3 - 5 hr to remove any remaining traces of water (Plate 2). The impregnated pits (Plate 3) were then transferred into stainless tubes whose internal diameter and length are 25 mm and 300 mm respectively. The tubes were then placed inside a muffle furnace (Nabertherm, Germany) for heating (Plate 4). To allow free evolution of volatiles, the tubes were initially heated at slower rate at 5 ^{o} C/min up to carbonization temperature (hold temperature) 547 ^{o} C. Having attained the desired hold temperature value, the samples were kept inside the furnace for an activation time (hold time) of 2 hr. At the end of the activation time, the sample containing tubes were transferred to a desiccator. Upon cooling, the GAC samples were subjected to thorough washing using boiling distilled water until the washings showed almost neutral pH (Plate 5). The washed samples were drained followed by drying in an oven at 120 ^{o}C for 24 hr and finally stored in tightly closed containers to avoid any cross contamination (Plate 6). The process flow diagram is shown in Figure 3. The values used for the activation temperature, acid ratio, activation time and impregnation ratio were obtained from a previous optimization study on the production of GAC from date pits by Essa et al. [42].

Plate 1: Ground date pits

Plate 2: Semi-dried impregnated date pits

Plate 3: Mixed slurry before activation

Plate 4: Tubes ready for heating in furnace

Plate 5: Boiling to clean produced GAC

Plate 6: GAC ready to be used

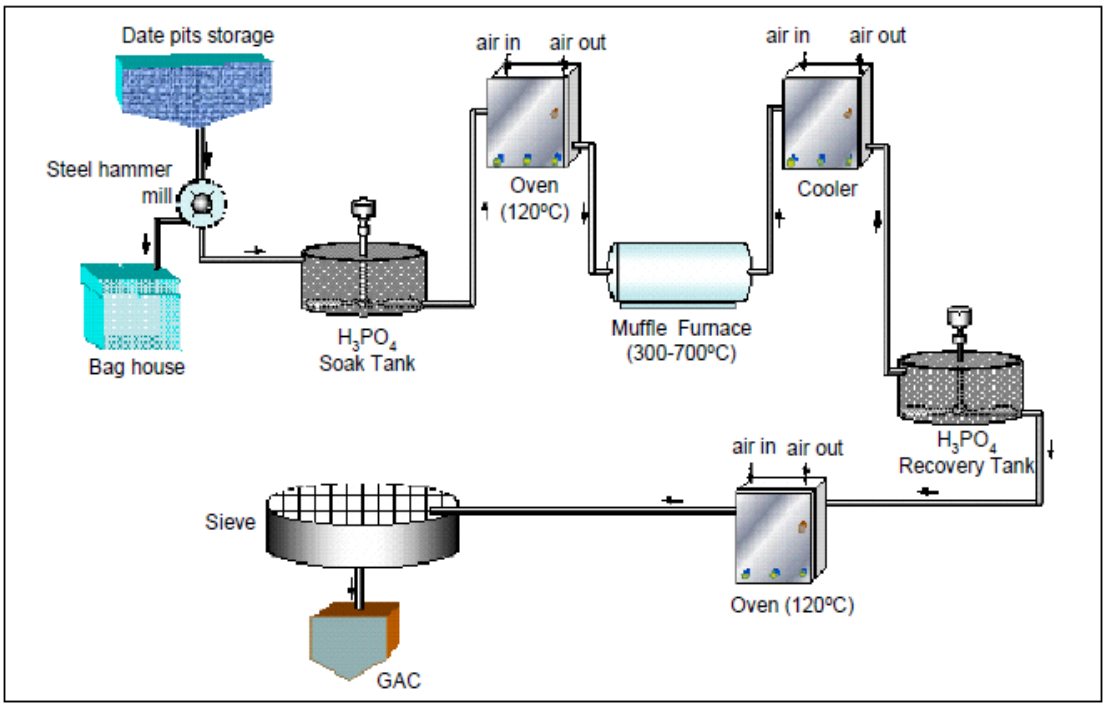

Figure 3 Process flow diagram for the production of granular activated carbon from date pits [42]

3.2 Batch Adsorption Studies - Reagents

Throughout the study, analytical grade reagents were used. Stock solutions (1000 mg/L) of the heavy metal ions prepared from their respective nitrate salts were used for the preparation of working solutions. Solutions of single and multi-component metal ions were prepared at the same concentration (20 mg/L each). pH adjustments to the desired values (2, 4, 6, 8, 10 and 12) were achieved using 0.1 N HCl or 0.01 M NaOH solution. All glassware were cleaned with dilute HNO_3 (10 % v/v) and oven dried (Isotemp oven, Fisher Scientific) at 120 °C before use.

3.3 Adsorption and Desorption Experiments

The clay mineral was powdered using a wooden pestle and sieved through mesh to obtain finer grains prior to its use in the adsorption and desorption studies. The resulting clay powder was acid washed and oven dried at 105 ^{o}C to remove

impurities. Exactly 5 g of the dried clay was mixed with 100 mL of metal ion solutions, and the resulting suspension pH was adjusted to the desired value (2, 4, 6, 8, 10 or 12) using few drops of HCl or NaOH. Batch adsorption experiments were conducted at constant room temperature of 20 ^{o}C for single metal adsorption (each component separately) and for multi-component (simultaneous presence of all the heavy metals). Different heavy metals in solutions with the clay in suspension were shaken on a horizontal rotary shaker (New Brunswick Scientific Co., Inc. USA) for 20 hours. The suspension was filtered twice; first using a 0.45 μm, 150 mm Φ Whatman membrane and secondly, using suction filtration with a finer size membrane having pore size of 0.2 μm and 47 mm Φ. For the desorption study, 1 g of the residue from the adsorption study was dried and 20 mL of 0.01 M $NaNO_3$ solution was added to the sample and stirred for 30 min. The suspension was then filtered and the filtrate was collected in vials for metal ions analysis. Method 200.2 guidelines prepared by the U.S. EPA for sample preparation procedure for spectro-chemical determination of heavy metals [109] was strictly adhered to.

Analytical Method: All filtrates from the adsorption and desorption studies were analyzed for the investigated heavy metals (i.e. Cd, Cr, Cu, Pb and Zn) using Inductively Coupled Plasma – Optical Emission Spectrometry (ICP – OES, Spectro Ciros Vision model) owing to the expected high residual concentration of heavy metals in the analyte [72]. The standards (2 % HNO_3 + tr HF) used for initial calibration verification (ICV) and continuous calibration verification (CCV) were from multi-element standards produced by CPI International. Other quality control measures stipulated in the US EPA Method 200.7 [110] and Method 200.8 [111] were adhered to. Solution containing 5 % HNO_3 was used as the blank sample for

calibration purpose. All tests were run in triplicates and the average of each of them was found.

Adsorptive Capacities: The amount of heavy metals removed (adsorbed) at equilibrium in single and multi-component adsorption studies were analyzed and interpreted using adsorptive capacity, q, percentage adsorbed onto the clay soil, R_a, and distribution coefficient, K_d, which were computed using equations (3.1), (3.2) and (3.3). Desorption results were analyzed by computing the percentage desorbed, R_d, according to equation (3.4), after 30 minutes of stirring.

$$q = \frac{(C_0 - C_e)}{M} V \qquad (3.1)$$

$$R_a = \frac{C_0 - C_e}{C_0} 100 \qquad (3.2)$$

$$K_d = \frac{C_a}{C_e} \qquad (3.3)$$

$$R_b = \frac{C_t}{C_a} 100 \qquad (3.4)$$

where C_0 initial liquid-phase concentration of sorbate (mg/L); C_a equilibrium solid-phase adsorbed concentration of sorbate onto the adsorbent; C_e equilibrium liquid-phase concentration of sorbate; C_t experimental concentration in the solution at time t (mg/L); M adsorbent mass (g); V volume of solution (mL); R_a per cent pollutant adsorbed (%); R_d per cent pollutant desorbed (%); K_d = distribution coefficient of the sorbate (L/kg). Using the calculated distribution coefficients for the heavy metals, selectivity sequence for each pH value was arrived at.

3.4 Bench-Scale Integrated Electrokinetic-Adsorption Study

3.4.1 Reactor Design and Experimental Procedures

The Lasagna reactor whose total volume is about 2000 cm^3 was fabricated. It is made up of seven (7) compartments (A, B, C, D, E, F and G) as depicted in Plate 7. The dimensions of each compartment and what it is designed to hold, is presented in Table 4 and the overall dimensions are: 24 cm (long) x 10 cm (width) x 12 cm (depth). Compartments A & B house the electrodes, C, D & E for soil while F & G for GAC. The reactor was used to treat artificially spiked natural clay with kerosene, phenol and heavy metals at given concentrations. The data collected will be used to optimize operating conditions and power consumption.

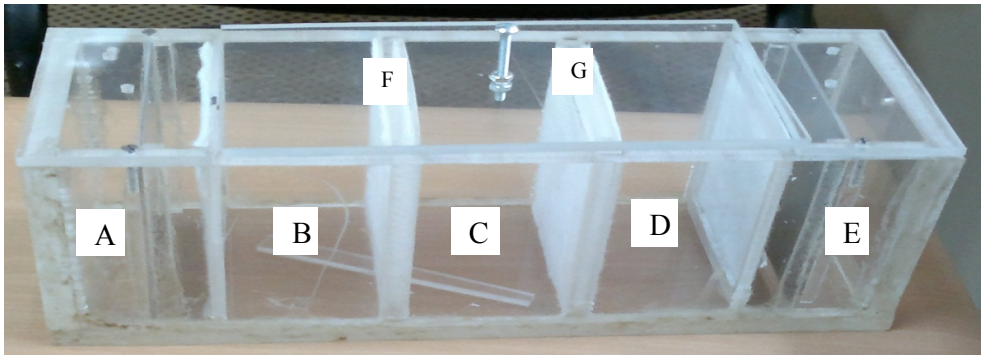

Plate 7: Reactor for electrokinetics-adsorption studies

Approximately 1 kg of local KSA soil was artificially spiked with kerosene, heavy metals (Cu, Cr, Cd, Pb, Zn and Hg) and phenol at predetermined concentrations. Thorough mixing was done using mechanical mixer (Gilson Company Inc., Plate 8) so as to achieve a homogeneous distribution of the contaminants around the soil matrix (Plate 9). The mixed spiked soil was placed in a fume-hood for drying over a period of time necessary to evaporate the solvents (hexane and distilled water). Distilled water was added to adjust the final moisture content of the soil to 33 - 70 %.

Table 4 Compartment dimensions

Compartment	Length, cm	Width, cm	Depth, cm	Volume, cm^3
A: Anode	5	10	12	600
B: Unspiked soil	6	10	12	660
C: Spiked soil	6	10	12	720
D: Unspiked soil	6	10	12	696
E: Cathode	5	10	12	600
'F' GAC	1	10	12	96
'G' GAC	1	10	12	96
			Total Soil volume	2076
			GAC volume	192

The initial conditions of the soil pH, moisture content, organic carbon and electrical conductivity were measured as well as the actual initial concentrations of the contaminants. Then, the uniformly mixed contaminated soil was placed into the cell layer by layer. Each layer was compacted with stainless steel spatula so that the amount of void space is minimized. The Lasagna cell used for the experiments consists of the cell, two graphite electrodes serving as anode and cathode, DC power supply (LG, GP - 505), process fluid reservoirs, heavy duty recirculation pump (BVP Instratec®), portable data logger (TDS - 303, Tokyo Sokki Kenkyujo Co., ltd) for real-time monitoring of temperature, electric current and voltage across the system (Plate 10). The cell was made of Plexiglas. The two electrode compartments with 240 mL working volume, placed at each end of the cell, is isolated from the soil zone by a porous Perspex plate and filter paper. The conditioning of the electrolyte was controlled by circulation of the anolyte (2N NaOH) and catholyte (1N HNO_3) using pump that is directly attached to the electrode compartments. Two planar-shaped

electrodes, 10 cm × 10 cm × 0.5 cm, was used to generate the uniform electric field. Within the described cell, two treatment zones that cut across the cell vertically bracketing the spiked soil compartment were filled with the GAC. The data monitoring system monitors electric current variation, applied voltage and temperature of the soil compartments on-line following a 30 min preset time step and automatically stores them for subsequent retrieval using floppy disc which can be read using personal computer for easy data and energy consumption analysis. The power supply provides a constant DC electric voltage for the electrokinetic test. Every week, fractions of the soil specimens were taken to determine the residual concentrations of the contaminants, soil pH, water content, organic carbon and electrical conductivity. Electrical conductivity was measured according to the method described by Sparks [35] using Accumet® XL30 conductivity meter (Fisher Scientific). Visual MINTEQ 3.0 [112] was employed to model the metal ion speciation using its dissolved concentration, pH, temperature and ionic strength. Upon the completion of each test, the electrode assemblies were disconnected and the soil specimen was extruded from the cell, sectioned into parts, weighed and preserved in glass vials for organic extraction, heavy metal digestion and subsequent analyses using the procedures outlined below.

Plate 8: Mechanical mixer

Plate 9: Contaminant mixing in progress

Plate 10: Complete experimental setup

3.4.2 Analytical Procedures for Contaminant Extraction and Analysis

Heavy Metals: Extraction of heavy metals from soil samples was performed according to guidelines spelt out in EPA Method 3050B for acid digestion of soils, sediments and sludges [113]. To briefly describe the method, 10 mL of concentrated HCl was added to 1 g of dry soil sample or 2 g of wet soil sample and covered. The sample was heated at 95 ^{0} C and refluxed for 15 min. After cooling the digestate, it was then filtered through Whatman No. 1 filter paper. The collected filterate was made up to 100 mL using distilled water and analyzed using flame atomic absorption spectrometry (AAnalyst 700, Perkin Elmer). All soil samples were extracted in duplicates except in a situation where there was insufficient quantity for duplicate extraction. EPA Method 7000B [73] was employed for heavy metal analysis using flame atomic absorption spectrometry except for mercury. A calibration curve for each heavy metal was prepared using 5-point calibration. The curve was linear with minimum correlation coefficient of at least 0.995 in each case. Other quality control

protocols such as analyzing initial calibration blank (ICB), initial calibration verification (ICV), and continuous calibration verification (CCV) samples were observed.

Mercury was analyzed using mercury analyzer (Solid Mercury Analyzer SMS 100, Perkin Elmer). Thermal decomposition, gold amalgamation and cold vapor atomic absorption spectrometry were employed by SMS 100 for sensitive measurement of mercury in solid samples according to Method 7473 [74]. Elaborate sample preparation is therefore eliminated. Following calibration using mercury standard solutions, about 1 g of soil was powdered and placed in a nickel sample boat. The boat was then heated using oxygen rich furnace in order to release all decomposition products as well as mercury. Stream of oxygen carried these products to a catalytic section of the furnace which trapped any halogens or oxides of nitrogen and sulfur in the sample. The remaining vapor that eluted from the catalytic section was selectively trapped in an amalgamation cell and rapidly heated to release mercury vapor which flowed through an absorbance cell positioned in the light path of a single wavelength atomic absorption spectrometry. Absorbance measured at a specific wavelength gave a measure of the mercury concentration in the soil sample [114].

For data analysis and calculations, the following equation was used to compute the concentrations of heavy metals in soil from the results obtained from their respective calibration curves [73].

$$\frac{mg}{kg} = \frac{A\,V}{W} \qquad (3.5)$$

where

A = mg/L of metal in digested sample from calibration curve

V = Final volume of digested soil sample, L

W = Soil sample weight used for digestion, kg

Kerosene and Phenol: EPA Method 3540C describes the procedure for extracting semi-volatile and non-volatile organics from soil matrixes [115]. Called Soxhlet Extraction, it isolates and concentrates water-insoluble (kerosene) and water soluble (phenol) organics in preparation for a variety of chromatographic procedures. The first few test samples were extracted using Method 3540C. A mixture of methylene chloride and hexane (1:1) (v/v) was used as the extraction solvent. Methylene chloride has been the preferred extraction solvent for many semi-volatile organics due to its high extraction efficiency, low cost and specification by numerous state regulatory methods [76]. It has been recommended that the sample be extracted in 7 days and analyzed in 40 days [76] after following proper sample collection, preservation and handling procedures spelt out in EPA Method 3540C [115]. A summary of the extraction procedure is described below. A representative soil sample weighing 10 g was completely mixed with 10 g of sodium sulfate and the mixture was place in a Whatman cellulose extraction thimble. The extraction solvent mixture was heated and refluxed through the soil continuously for about 16 - 24 hr or overnight as shown in Plate 11.

Plate 11: Soxhlet extraction setup

Subsequent samples were extracted using pressurized fluid extraction according to Method 3545 procedures [116]. In this regard, accelerated solvent extractor (ASE 200, Dionex) was used due to its less solvent usage and extraction time, and increased extraction efficiency [117]. Sample preparation and solvents are similar as in the Soxhlet extraction [116].

No separate extraction procedure is required for phenol, because, it will also be extracted along with kerosene from the soil sample. Volume of extract generated was then injected into the GC-MS (Clarus 580, Perkin Elmer) equipped with autosampler for analysis. The injector and detector temperatures were kept at 250 ^{0}C and 300 ^{0}C. The initial temperature was set at 50 ^{0}C, ramped at 10 ^{0}C/min to 300 ^{0}C and held at this temperature for 9 min. Carrier gas (helium) flow of 0.8 mL/min was maintained throughout. Aliquot volume of 1 µL was injected and the flow split ratio was 10. The MS was scanned using full scan mode from 50 - 550 amu at 0.9 scan/s. TPH

quantification was done by using the total chromatographic area counts using retention time range for the elution of hydrocarbon within the range C_8 - C_{16}. The pure kerosene used in this study was analyzed and was found to lie within the range of C_8 - C_{16}. External standards were prepared from the kerosene solution in hexane and 5-point calibration curve was created. Alternatively, equation 3.6 may be used for TPH quantification using only one standard TPH solution.

$$TPH\ \left(\frac{mg}{L}\right) = \frac{Total\ chromatographic\ area\ of\ sample\ x\ Concentration\ of\ standard}{Total\ chromatographic\ area\ of\ standard} \qquad (3.6)$$

Guidelines spelt out in EPA Method 8270D [104] for the quantification of semi-volatile organics by GC-MS were adhered to. The following determinative method was employed for computing contaminant concentration in the extracted soil as per EPA Method 8000C [118].

$$Concentration\ \left(\frac{\mu g}{kg}\right) = \frac{X_s\ V_t\ D}{W_s} \qquad (3.7)$$

where

X_s =calculated concentration of the analyte in the sample, µg/L

W_s = Weight of soil sample extracted, g

V_t = Total volume of the concentrated extract, µL

D = Dilution factor, if no dilution was used prior to analysis, then D = 1

3.4.3 Preliminary Electrokinetics Study

A total of three bench-scale experiments were performed to investigate the treatability of the contaminant mixture using the coupled electrokinetics-adsorption technique and to understand the operating peculiarities of the saline-sodic soil. Two of the experiments had GAC chambers bracketing the contaminated soil chamber and were operated at voltage gradients of 0.6 V/cm and 1 V/cm. The third one utilized only electrokinetics at voltage gradient of 0.6 V/cm.

3.4.3.1 Testing Program

Overall, three experiments were conducted using an initial intended concentration of 100 mg/kg for each contaminant. Three designations used are EK-GAC-1, EK-GAC-2 and EK for coupled EK and adsorption 1 and 2 and EK respectively. EK-GAC-1 utilized 1 V/cm and served to produce some preliminary information such as the feasibility of attaining reasonable percentage removal and processing fluid conditioning requirements. EK-GAC-2 and EK were then run simultaneously at 0.6 V/cm to ascertain the preference of using the integrated approach over EK alone.

3.5 Process Optimization Using Response Surface Methodology (RSM)

Important process variables such as polarity reversal rate, voltage gradient and initial contaminant concentrations were varied according to statistical experimental design using Box Benkin design. The respective response effects in terms of removal efficiencies and energy consumption were measured. Mathematical response surface predictive models were then developed (using Design Expert® software) for optimal removal rates that minimized input requirements and conditioning such as voltage gradient and pH. Design Expert® package is powerful mathematical software which

is good in experimental design and response surface modeling for comprehending the effects of independent variables and their interactions on targeted responses. Summarily, application of RSM involves three steps; design and experiments, response surface modeling using regression and finally, optimization [68].

3.5.1 Mathematical Model Development

BBD was chosen for the experimental design because of its advantages over other design methods as highlighted above. In BBD, the experimental points are hyperspherically arranged and equidistant from the central point [69]. Response Surface Methodology (RSM) was used in modeling, optimization and interpretation of the results with the help of Design-Expert® 8.0 (Stat-Ease, Inc.) platform [70, 119]. The investigated variables (called factors in RSM) were the polarity reversal rate, voltage gradient and initial contaminant concentration designated as A, B and C respectively. These variables were selected based on their known influence on contaminant remedial efficiency and were coded and varied according to Table 5. Based on the factor levels and the chosen number of central points (3), a total of fifteen (15) experiments were randomly designed for, using the BBD (Table 6) and subsequently conducted.

This experimental design was preliminarily evaluated using variance inflation factor (VIF) to check for orthogonality (independence of factors) and leverage (quantitatively measures the potential of a design point to have significant influence on the model fit) [119]. These were determined using equations 3.8 and 3.9 respectively and the results are presented in Tables 7 and 8. VIF value of 1 indicates that the factor is orthogonal to all other factors in the design. In a case whereby factors are highly correlated, then, R^2 value becomes a poor indicator of model's

predictive ability and it becomes more and more difficult to unravel how each of the investigated factors affect the response. Experimental points having high leverage values close to 1 should influence the model fit by carrying any error (experimental or measurement) into the model, as such, they should be conducted more carefully [70].

Table 5 Codification and ranges of factors

Variable	Designation	Units	Coded variable levels		
			-1	0	+1
Polarity Reversal	A	hr	0	24	48
Voltage Gradient	B	V/cm	0.2	0.6	1
Concentration	C	mg/kg	20	60	100

Table 6 Design of experimental runs using the Box-Behnken Design

Run order	Polarity reversal, A	Voltage gradient, B	Concentration, C
1	24	0.6	60
2	0	0.2	60
3	0	0.6	20
4	48	0.6	20
5	24	0.6	60
6	48	0.2	60
7	24	0.6	60
8	48	1	60
9	24	1	20
10	24	0.2	20
11	24	0.2	100
12	0	1	60
13	0	0.6	100
14	48	0.6	100
15	24	1	100

Leverage may be reduced by replicating the experimental point as shown in Table 8 for the central points (standard order 13 - 15)

$$VIF = 1/(1-R_i^2) \quad (3.8)$$

$$Leverage = p/n \quad (3.9)$$

Where R_i^2 = coefficient of determination; p = number of model terms; n = number of experiments.

Table 7 Variance inflation factor (VIF = 1, ideal; VIF > 10, high correlation among factors)

Model Terms	Standard Error	VIF	R_i^2
A	0.35	1	0
B	0.35	1	0
C	0.35	1	0
AB	0.50	1	0
AC	0.50	1	0
BC	0.50	1	0
A^2	0.52	1.01	0.01
B^2	0.52	1.01	0.01
C^2	0.52	1.01	0.01

Table 8 Leverages for experimental points

Standard order	Leverage
1	0.75
2	0.75
3	0.75
4	0.75
5	0.75
6	0.75
7	0.75
8	0.75
9	0.75
10	0.75
11	0.75
12	0.75
13	0.33
14	0.33
15	0.33
Average	0.67

Following design evaluation, the responses were fitted to a quadratic model which was fine-tuned by removing any insignificant term. This will maximize R^2 and

minimize lack of fit. The general quadratic equation for fitting models in RSM is given in equation 3.10.

$$y = \beta_0 + \sum_{i=1}^{k} \beta_i x_i + \sum_{i=1}^{k} \beta_{ii} x_i^2 + \sum_{i=1}^{k-1} \sum_{j=2}^{k} \beta_{ij} x_i x_j + \varepsilon \quad (3.10)$$

Where y = response or dependent variable; k = number of factors; β_o, β_i, β_{ii}, β_{ij} = coefficients to be fitted using regression for constant term, linear, quadratic and interaction parameters respectively; x = variables.

The developed model was evaluated using the rich diagnostic tools provided in Design-Expert® which include normal plot of residuals (to test the assumption of normality of residuals), predicted versus actual plot (to test the assumption of constant variance), Box-Cox plot (to check the need for data transformation), externally studentized residuals (to check the presence of any outlier in the data). The effects of factors were compared at a particular point in the design space using the perturbation plot. Response surface and contour plots were then generated. After thorough evaluation of the developed model, it was then validated against 'unseen' experimental results obtained separately outside the designed experimental runs presented in Table 6.

3.5.2 Use of Desirability Function in Numerical Optimization

Desirability function, being one of the mathematical methods for computation of critical values (maximum or minimum) and measuring overall success of optimizing multiple responses using geometric mean was employed for the optimization of Cd remedial efficiency. Different scenarios were also simulated and optimized to examine the synergistic or antagonistic influence of the other responses on Cd remedial efficiency [120]. A search for a combination of factor levels which

simultaneously satisfies the goals imposed on factors and responses is first carried out, followed by combining these goals into an overall Desirability function that ranges from 0 (outside of the optimization limits) to 1 (at the goal). Combining all responses into an overall Desirability eliminates favoring one response over another. The aim is not to clinch a Desirability value of 1, but to find a good set of conditions that will meet all the set goals for each factor and response. This is achieved using numerical optimization algorithms [119]. Optimal solutions (critical values of factors) may be found by differentiating equation 3.10 and equating the result to 0. To buttress the relative importance of one goal versus another, *importance* values from 1 + to 5 +'s, representing lowest to critical goals are specified. Another parameter called *weight* fine tunes how the optimization process searches for the optimal solutions. It ranges from 0.1 (low weight allows solutions that do not necessarily meet the optimal goal) to 10 (high weight will cause a search of solutions close to or beyond the stated goal). The default values for *importance* and *weight* are 3 +'s and 1 respectively. The detailed design of 8 simulation scenarios that were used in optimizing Cd remedial efficiency in the presence of other contaminants and responses is shown in Table 22 (Chapter 7).

3.6 Energy Computation in Lasagna Process

Evaluation of the total energy consumed in the Lasagna process plays an important role in the overall economics of the technology. To compute the coefficient of electroosmotic conductivity, equation (3.11) was employed.

$$Q_e = k_e i_e A \qquad (3.11)$$

where

Q_e = Electroosmotic flow, $cm^2V^{-1}s^{-1}$; i_e = DC voltage gradient applied across the soil, V/cm; A = cross-sectional area perpendicular to the flow path, cm^2

Coefficient of electroosmotic transport efficiency is given by equation (3.12).

$$k_i = \frac{Q_e}{I} \qquad (3.12)$$

where

I = electric current, A; k_i = transport efficiency, $cm^3A^{-1}s^{-1}$

Equation (3.12) may also be expressed as [2]

$$k_i = \frac{k_e}{\lambda} \qquad (3.13)$$

where

λ = conductivity of soil column, mho/cm

The transport efficiency measures the efficiency of current utilization for pumping pore fluid across the soil.

For a conventional electrokinetic system without treatment zones, with two parallel plate electrodes separated by a distance, L, the following equations applies [2].

$$P = E\ I = \frac{E^2}{R} = \frac{(i_e\ L)^2}{R} \qquad (3.14)$$

$$R = \frac{\rho\ L}{A} \qquad (3.15)$$

$$t = \frac{L}{k_e\ i_e} \qquad (3.16)$$

$$V = L\ A \qquad (3.17)$$

$$W = \frac{P\ t}{V} \qquad (3.18)$$

Substituting equations. (11), (13) and (14) in (15),

$$W = \frac{L\ i_e}{\rho\ k_e} \qquad (3.19)$$

where

P = Power consumption, kW

E = Applied voltage, V

I = current, A

R = Resistance of soil between the two electrodes, ohm

i_e = voltage gradient, V/cm

ρ = soil resistivity, ohm m

L = Electrode spacing, m

A = Cross-sectional area of soil in contact with electrodes, m^2

t = Time taken for water transported from anode to cathode, s

V = Soil volume between the two electrodes, m^3

W = Specific energy consumed, kWh/m^3 per pore volume

In the Lasagna process, contaminant transport distance is from one treatment zone to the next as against from one electrode to another in conventional electrokinetics. If a number of equally spaced treatment zones are considered to be separated at a distance, d, between the electrodes, then treatment time per pore volume of liquid transported between any two adjacent treatment zones is given by modifying equation (3.16).

$$t_{TZ} = \frac{d}{k_e\ i_e} \qquad (3.20)$$

Similarly, equation (3.21) was obtained after modifying equation (3.19) to determine the specific energy consumed in kWh per m^3 of soil treated per pore volume between adjacent treatment zones.

$$W = \frac{P\ t_{TZ}}{V} = \frac{d\ i_e}{\rho\ k_e} \qquad (3.21)$$

Equation (3.21) indicates that low energy consumption will result from smaller treatment zone spacing. However, from an overall cost standpoint, this energy saving may be balanced by higher material and installation costs which will result due to the increased number of treatment zones required.

CHAPTER 4

SINGLE AND MULTI-COMPONENT ADSORPTION OF HEAVY METALS ONTO SALINE-SODIC SOIL

4.1 Introduction

Heavy metal ions in waters are toxic to human and aquatic animals even at low concentrations. They are usually stable and non-biodegradable within the ecosystem. As a result, they tend to bioaccumulate in living tissues thereby causing some serious health concerns. According to the World Health Organization [121], some of the heavy metals of most immediate concern are lead (Pb), cadmium (Cd), copper (Cu), chromium (Cr) and zinc (Zn). Copper and zinc are essential dietary nutrients that our body need in trace amounts. However, intake of these trace elements beyond or below certain thresholds may cause health problem including gastrointestinal disturbance, liver and kidney failure, prostate cancer and bone anomalies [122, 123]. Saudi Arabian Standards Organization (SASO) limits the maximum level of Cu and Zn in drinking water to 1 mg/L and 5 mg/L respectively [124]. Chromium is essential for several human metabolic processes, but affects human physiology, accumulates in the food chain and causes many ailments when present in larger concentrations [125]. Cr^{6+} is more hazardous to health than Cr^{3+} due to the former's high toxicity. Conversely, Pb and Cd have no essential function to plants and animals apart from causing different carcinogenic, mutagenic and chronic diseases in humans [126-130]. SASO limits these trace elements in drinking water to a maximum of 50 µg/L, 5 µg/L and 50 µg/L for Pb, Cd and Cr respectively [124].

Various treatment techniques including adsorption, precipitation, ion exchange and reverse osmosis have been employed to eliminate or reduce these toxic heavy metal concentrations in water and wastewater. Adsorption on solid surfaces is the most common one and efforts are being made continuously to develop new, low cost and efficient adsorbents for removal of heavy metals. For the removal of toxic heavy metals, recently, many efforts have been focused on adsorbents such as activated carbon, clay and sediments in riverbeds and in suspension. Over the years, the role played by adsorbents in water and wastewater treatment had been critically and elaborately investigated [127].

Several low cost adsorbents such as agricultural/industrial wastes and natural/synthetic clay minerals have been used as effective adsorbents for removal of heavy metals, organics, and radionuclides [131-142]. Hence, in the past decades, clay minerals have been used as effective adsorbents for heavy metal removal in water treatment because of their strong ion-exchange and complex formation abilities with the heavy metals [143, 144]. However, few investigations have been reported on natural clay application for simultaneous removal of multi-component heavy metal removal from water or wastewater. It is expected that, when several heavy metals exist in the water or wastewater stream, some will be more difficult to be removed than others and also competitive environment is created. For example, Cd ions are generally more difficult to be removed using adsorption compared to others such as Pb and Cu [143]. In addition, to our best knowledge, local clay from Al-Hassa Oasis, Saudi Arabia has not been tested for feasibility of removal of heavy metals from water and wastewater streams. Knowing the sorption and desorption characteristics of the heavy metals on the clay minerals, will in no small measure, aid in modeling the behavior of the soil when contaminated by these heavy metals. It will also be useful in

designing amendments and increasing fixation of the heavy metals on the soil in case of contamination by these species [131]. Prediction of the behavior of soils of arbitrary composition may also be achieved through studying sorption and desorption behavior of these clay minerals [131]. The clay buffer capacity and by extension, the initial pH play an importance role in the mobility of the heavy metals in the clay. Alkaline pH condition enhances the precipitation of the heavy metals thereby reducing their mobility. In this report, the adsorptive capacity of local Saudi Arabian clay from Al-Hassa Oasis was tested for single and multi-component heavy metals removal in simulated wastewater streams at different initial pH. The investigation focused on the competitive sorption and desorption behavior of five (5) heavy metals (Cd, Cr, Cu, Pb, Zn) onto local clay.

4.2 Results and Discussion

Findings of this study will be presented and discussed under the following headings: characteristics of the clay soil, single and competitive adsorption studies, selectivity sequence and statistical comparison and desorption study.

4.2.1 Characteristics of the Clay Soil

Table 9 summarizes the physico-chemical properties of the clay sample obtained from the numerous analyses carried out as outlined above. The pH value of the investigated clay is naturally alkaline (9.53), which promotes heavy metals precipitation and adsorption onto the clay surface. Soil organic matter (4.3 %) plays an importance role in the adsorption of heavy metal ions even in soils where its value is very low [35]. This is because, SOM possesses very high specific surface area that may reach up to 800 – 900 m^2/g and a cation exchange capacity (CEC) which may range between 150 and 300 cmol/kg [145].

Table 9 Physical and chemical properties of the clay

Property	Value
pH (ASTM D 4972)	9.53
Moisture content, % (ASTM D 2216)	3.91
Soil organic matter, % (ASTM D 2974)	4.30
Hydraulic conductivity, cm/s (ASTM D 5084)	6.91081×10^{-09}
Electrical conductivity, mS/cm (ASTM D 1125)	56.17
Average pore width (by BET*), Å	75.64
BET Specific surface area, m^2/g (UOP964)	42.13
Pore volume, cm^3/g (UOP964)	0.08
Specific gravity (ASTM D 854)	2.77
Liquid limit (ASTM D 4318)	44.71
Plastic limit (ASTM D 4318)	25.95
Plasticity index	18.76
USCS classification (ASTM D 2487)	CL (Clay)
Particle size distribution (ASTM D 422)	
Clay, %	78
Silt, %	6
Very fine sand, %	10
Fine sand, %	5
Medium sand, %	1

*BET - Branaur-Emmett-Teller

Stevenson [145] posited that the majority of a surface soil's CEC is in fact attributable to its SOM. Soil electrical conductivity (EC) varies with the amount of moisture held by soil particles. Hence, sands have a low EC, followed by silts while clays have the highest EC. It has strong correlation to soil particle size and texture [146]. Soil EC as defined by Grisso et al. [146] 'is the ability of a material to transmit (conduct) an electrical current'. Electrical conductivity of clay typically lies between 10 and 1000 milli Siemens per meter. The EC of the clay sample is 5617 milli Siemens per meter which implies that it has an excess of dissolved salts [35, 146]. The clay surface area (42 m^2/g) will give it ability to adsorb heavy metals on its surface.

Reddi and Inyang [147] posited that the water contents at which clay soil transit from one state to the other represent its entire physico-chemical behavior. Plastic limit gives a measure of the water content at which transition from semi-solid to plastic state occurs while liquid limit represents the water content needed for the clay soil to

begin exhibiting flow characteristics similar to liquids. For the clay soil used in this study, its plastic and liquid limits are 25.95 and 44.71 respectively (Table 9). Scanning Electron Microscope (SEM) is generally used to investigate surfaces, structures, morphologies, and forms of materials. Figure 4 depicts micrograph of the clay soil which clearly revealed the surface texture and porosity of the clay soil. The clay surface area will enhance the contact area and facilitate adsorption of positively charged ions. It will also make it possible for the clay soil to accommodate heavy metals on its active sites through ion exchange and complexation. Furthermore, result of the elemental analysis carried out is depicted in Figure 5. The dominant elements are O and Si whose percentage compositions are 53 % and 18 % respectively. Other elements present in lesser quantities are Ca, Al, Fe, Na, Cl, K and Mg. The mineralogical composition using XRD revealed that the clay is mainly composed of montmorillonite; quartz and calcite are also present in lesser quantities. Montmorillonite has been described by Reddi and Inyang [147] to possess a 2:1 layer structure, with extensive isomorphous substitution of iron and magnesium for aluminum in the octahedral sheets, the layer of which are separated by several sheets of water molecules. Belonging to the secondary minerals, montmorillonite has the highest specific surface area, plastic and liquid limits, hence serves as good adsorbent [147]. In acidic environment, calcite may be leached away or decomposed to yield carbon dioxide, thereby creating more pores in the solid matrix. It may also help raise the buffer capacity of the clay soil due to the presence of carbonate.

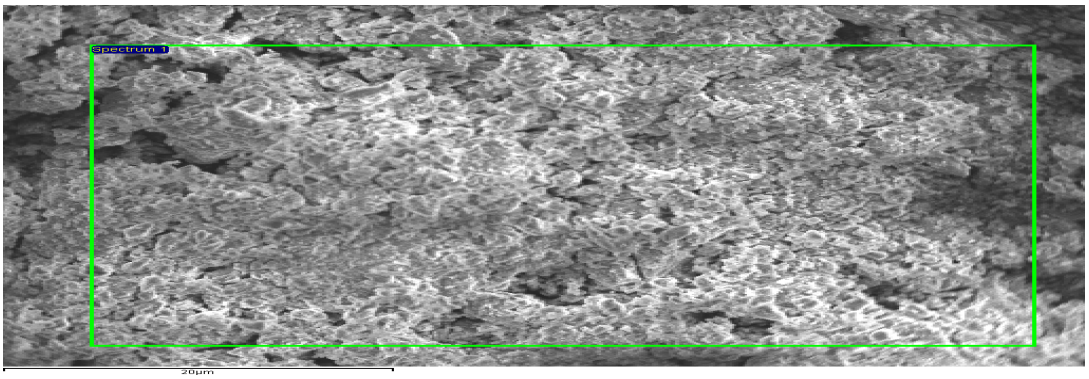

Figure 4 Scanning electron micrograph of clay at 40,000 magnification

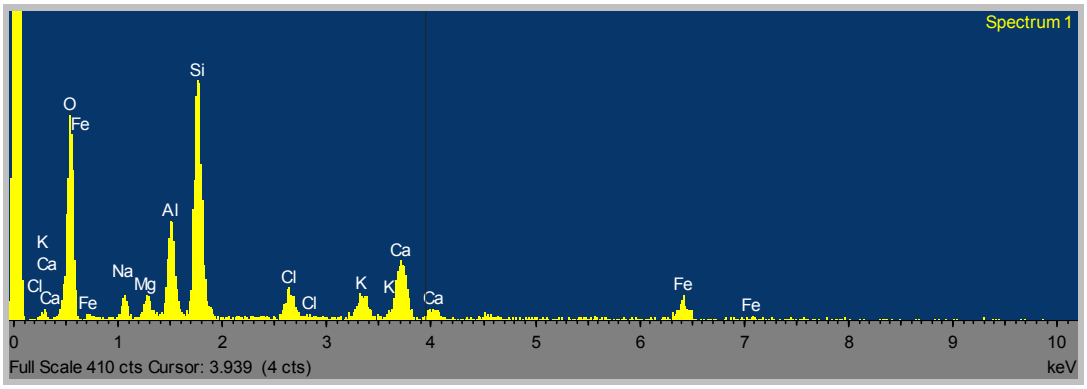

Figure 5 Elemental composition of the clay mineral

4.2.2 Single and Competitive Adsorption Studies

4.2.3 Cadmium ions

Due to different ionic forms of the heavy metals and ionization state of the surface functional groups, pH plays the most significant role in adsorption studies [143]. The first systematic studies of Cd ions adsorption from aqueous solutions using activated carbons (ACs) were reported by Huang and Ostovic [148]. From Figure 6, single component adsorption of Cd ions increases with an increase in pH of the solution. The amount of Cd ions adsorbed was smallest at pH values less than 4, but increases at higher pH values. In the same vein, the lowest percentage removal from solution was observed to be 90.2 % (at pH = 2) as shown in Figure 7, but remained more or less

constant at pH values greater than 10. Similar trend was observed by Ferro-Garcia et al. [149] and Huang and Ostovic [148] using different ACs as adsorbents. At lower pH, hydrogen ions are adsorbed onto the clay surface, thus, suppressing Cd ions adsorption. Further increase in the hydrogen ions concentration (decreasing pH) will only lower the adsorptive capacity of Cd ions [129]. As the pH increases, hydrogen ions concentration decreases, providing more space for Cd ions to be adsorbed onto the clay surface. Although Ferro-Garcia et al. [149] have reported extremely low percentage adsorption (< 5 %) of Cd ions onto different ACs (olive stone, peach stone and Almond shell), the present study found high percentage adsorption (90.2 %) of Cd ions onto clay even at low pH values. This observed difference may arise due to the fact that clay soil is negatively charged even at low pH, thus having higher capacity for the adsorption of positive ions, whereas carbon surface is positively charged at low pH, which enables the electrostatic repulsive interactions between the cations and the positively charge carbon surface to prevail [149]. From the aqueous speciation of Cd ions, it remains mainly as Cd^{2+} up to about pH = 8 [144].

In the presence of competitive ions (Cr, Cu, Pb and Zn), Cd ions adsorption was found to be suppressed as depicted in Figure 6, but exhibited similar trend as in single component adsorption, that is, percentage removal increases with an increase in pH as shown in Figure 8. The effect of competitive adsorption has reduced the percentage removal from 90.2 % (in single component adsorption) to 72.24 % (in multi-component adsorption) which gives a percentage decrease of about 20 %. At pH values greater than 10, complete removal was achieved (Figures 7 - 8). This is because more ions are competing for a limited number of adsorption sites on the clay surface. Cd ions were found to be the least adsorbed during competitive adsorption. This finding is in agreement with earlier studies on competitive adsorption of Cd ions

onto clay soil as corroborated by Srivastava et al. [144], Benjamin and Leckie [150] and Biddappa et al. [151]. Low adsorption of Cd ions in the presence of other competing heavy metal ions may not be unconnected with its relatively low electronegativity value. Futalan et al. [130] suggested that adsorptive capacities of metal ions are influenced by their electronegativity values. Beyond pH = 8, Cd ions removal was not affected by the presence of other metals (Figure 6). Regardless of the presence of other metals in solution, Cd ions removal increased with increasing solution pH (Figure 8).

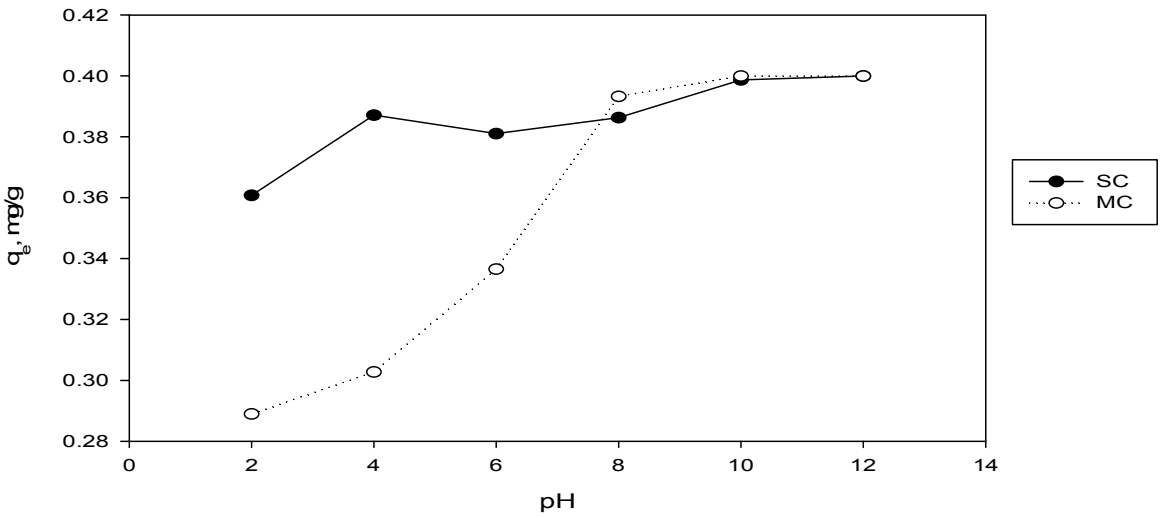

Figure 6 Effect of pH on the adsorptive capacity of clay for cadmium for both single component and multi-component adsorption scenarios

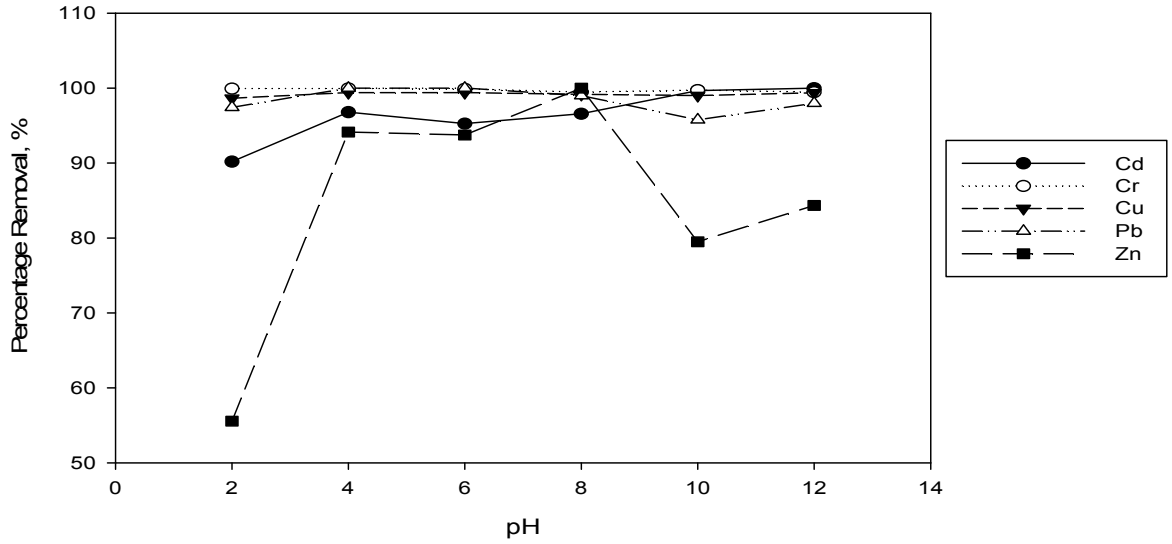

Figure 7 Percentage of heavy metals removed against pH for single component adsorption scenario

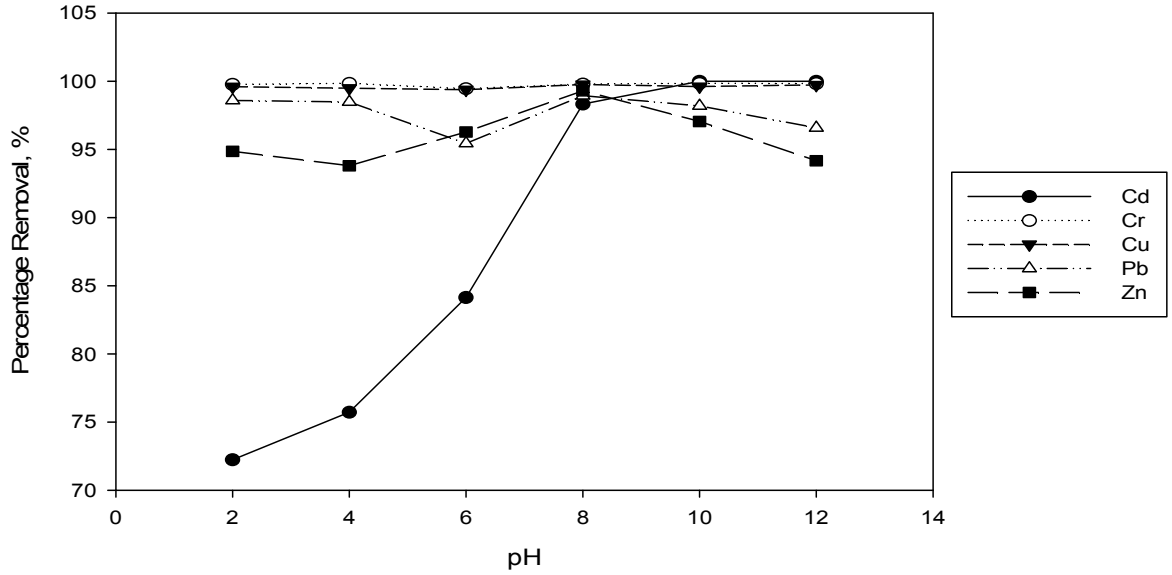

Figure 8 Percentage of heavy metals removed against pH for multi- component adsorption scenario

4.2.4 Chromium ions

For the single component adsorption study of Cr ions, Figure 9 shows that Cr ions adsorption was highest at pH = 4. This is similar to the results obtained when lignite coal and bituminous coal were used as adsorbents as reported by Kannan and Vanangamudi [152]. The percentage removal remained fairly constant and maximum up to pH =6, then, declined at higher pH values (Figure 7). Also Huang and Wu [153,

154] observed similar trend for Cr ions adsorption on calcined charcoal and Fitrasorb – 400 activated carbons. This observation was attributed to reduction which occurs in acidic solutions of Cr^{6+} to Cr^{3+}, and adsorption of Cr^{6+} was much larger than that of Cr^{3+} as investigated by Huang and Wu [153, 154]. Overall, Cr ions adsorption onto clay minerals was found to be extremely good irrespective of the pH value, in all cases, exceeding 99 % as shown in Figure 7.

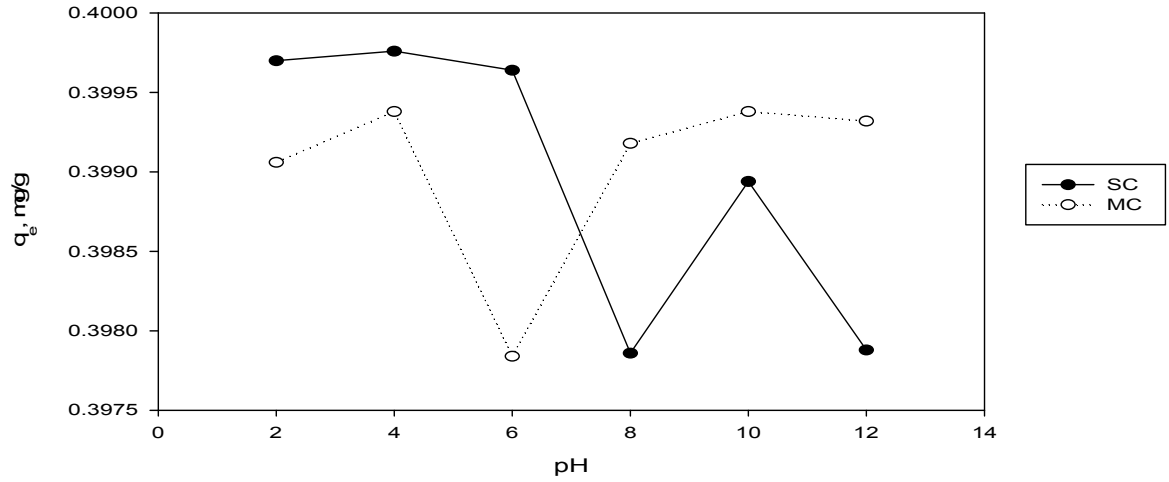

Figure 9 Effect of pH on the adsorptive capacity of clay for chromium for both single component and multi-component adsorption scenarios

The competitive effect of adsorption on Cr ions lead to reduction in their adsorptive capacities up to pH = 6 in the multi-component adsorption scenario. But, beyond pH = 7, the adsorptive capacities of Cr ions are higher than their single component adsorptive capacities (Figure 9). This was as a result of the reduction in the adsorptive capacities of Cu, Pb and Zn ions. The highest difference in SC and MC adsorptive capacities of Cr ions was observed to be at pH = 6. Also, in the MC adsorption of Cr ions, their percentage removals at all pH values were greater than 99 % as shown in Figure 8. It is worth noting that Cr ions have the highest adsorptive capacities, hence, highest percentage adsorption onto the clay minerals for both SC and MC adsorption scenarios. Similar conclusions were drawn by Covelo et al. [131] where they found

the sorption selectivity of Cd, Cr, Cu, Ni, Pb and Zn on kaolinite clay to follow the following order at pH = 4.5: Cr > Pb > Zn > Cd > Ni > Cu.

4.2.5 Copper ions

Adsorption of Cu ions in SC scenario (Figure 10) was observed to be highest between pH values 4 and 6. Bekkouche et al. [143] also found out that the optimum pH for Cu ions removal from a single component solution using titanium dioxide to be 6. In another related studies, Bansal and Goyal [125] reported Cu ions removal using powdered activated carbon at different pH values was considerable at pH values less than 7. In addition, Khan and Khattak [155, 156] found the optimum pH range for Cu ions removal to be 4.2 – 5.1. Similar findings were corroborated by Goyal et al. [157]. The low adsorption within the pH range 2 – 4 may be attributed to high solubility and ionization of copper salt in the acidic medium. The maximum adsorption in the pH range 4 – 6 might be due to partial hydrolysis of Cu^{2+} which results in the formation of $Cu(OH)^{+}$ and $Cu(OH)_2$ whose adsorption capacities are higher than that of Cu^{2+} [155]. Beyond pH = 6, lower adsorption of Cu may be attributed to the precipitation of Cu ions as $Cu(OH)_2$, which in turn, lowers the availability of the clay surface due to occupation or blockage or a large portion of the clay surface. The percentage removals have been extremely high for each pH value investigated, with pH = 2 having the least percentage removal of 98.65 % (Figure 7) thereby rendering Cu ions to have the second largest adsorptive capacity in the single component scenario after Cr ions.

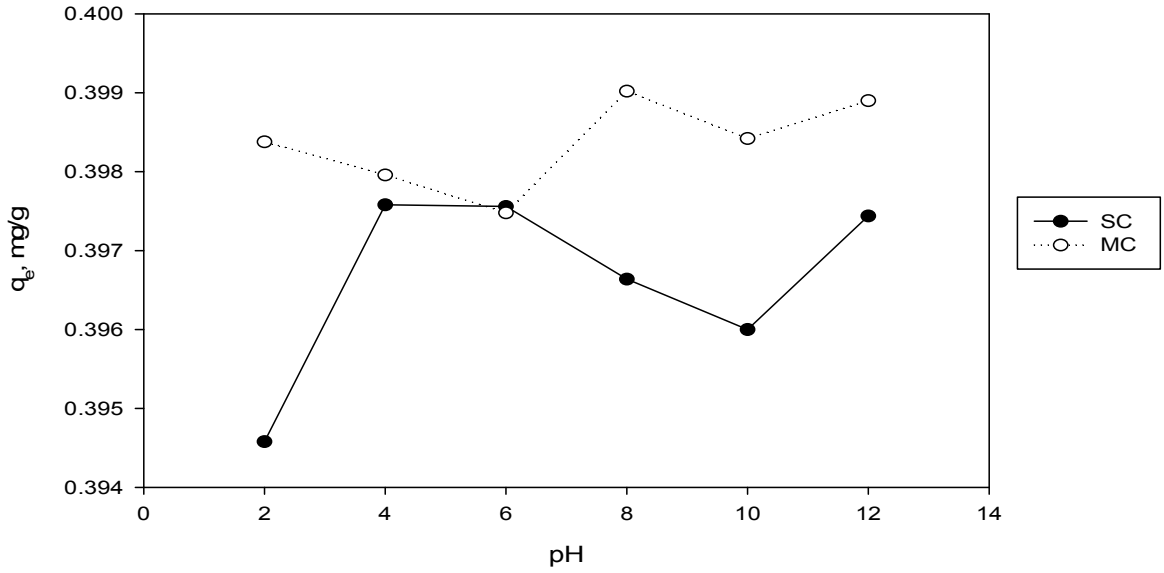

Figure 10 Effect of pH on the adsorptive capacity of clay for copper for both single component and multi-component adsorption scenarios

Figure 10 depicts higher adsorptive capacity for Cu ions in the multi-component scenario, with the percentage removals ranging from 99.37 to 99.76 % (Figure 8). Srivastava et al. [144] have shown that greater proportions of the hydroxyl species $CuOH^{+}$, $Cu(OH)_3^{-}$ and $Cu(OH)_{2\ (aq)}$ (with higher adsorptive capacities than Cu^{2+}) were formed in the multi-component scenario, as compare to the single component scenario. As such, adsorption was higher in the MC scenario.

4.2.6 Lead ions

Removal of Pb ions was attributed to adsorption and precipitation onto the clay surface and within the pores. In SC scenario, adsorptive capacity of Pb ions increased with increasing pH of the solution up to pH = 6, beyond which it started declining (Figure 11). Increase in Pb ions adsorption with pH was also noticed and reported by Reed et al. [158] and Corapcioglu and Huang [159]. Formation of $Pb(OH)_2$ at higher pH values greater than 10, lead to the removal of Pb ions via adsorption and precipitation. Complete removals (100 %) were noted at pH values of 4 and 6 (Figure 7)

Apparently, the competitive adsorption of other heavy metals ions onto the clay minerals has lowered Pb ions adsorptive capacity up to pH = 8, as compared with the single component scenario (Figure 11). Thereafter, Pb ions became more adsorbed onto the clay minerals (pH = 10). For all the pH values investigated, more than 95 % of Pb ions were adsorbed onto the adsorbent in MC scenario (Figure 8).

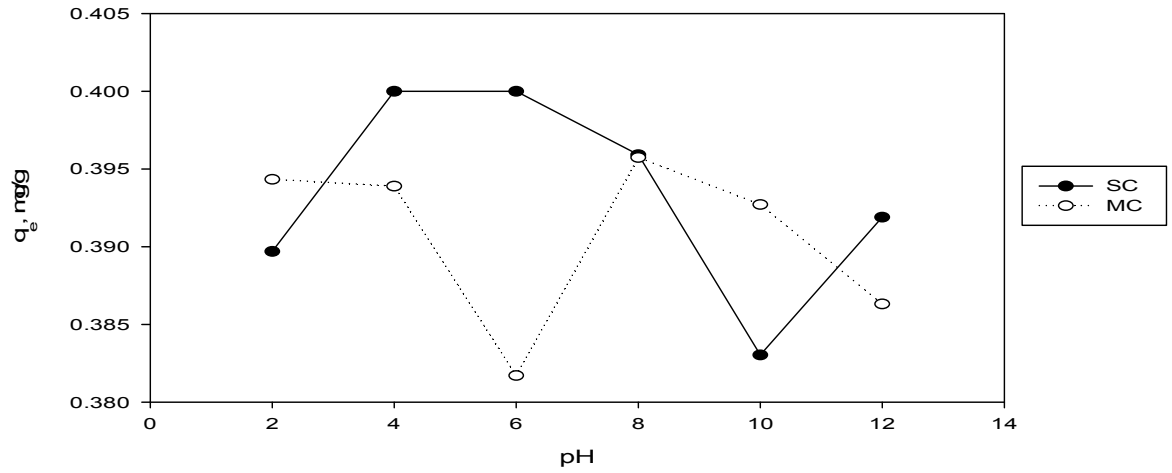

Figure 11 Effect of pH on the adsorptive capacity of clay for lead for both single component and multi-component adsorption scenarios

4.2.7 Zinc ions

Adsorption of Zn ions was observed to be increased with increasing pH up to pH = 8, where all Zn ions were removed in SC scenario (Figures 7 and 12). Lower adsorptive capacity was noticed below pH = 4 as corroborated by Ferro-Garcia et al. [149]. Zn ions were the least adsorbed in the SC scenario, having the lowest percentage removal of 55.56 % (Figure 7). Adsorptive capacity increased in the MC scenario, moving a step forward, from the least adsorbed in the SC scenario to the second least adsorbed after Cd ions (Figure 8). Similar selectivity of Zn ions over Cd ions during adsorption was reported by Srivastava et al. [144] and Covelo et al. [131]. From Table 10, the selectivity sequence for the adsorption of the investigated heavy metals onto the tested

clay minerals in SC and MC scenarios are Cr > Pb > Cu > Cd > Zn and Cr > Cu > Pb > Cd > Zn respectively . Forbes et al. [160] and Srivastava et al. [144] have reported similar selectivity sequence (MC scenario). It is to be noted that selectivity of Cd ions was the most affected in the presence of other metals ions, followed by Pb.

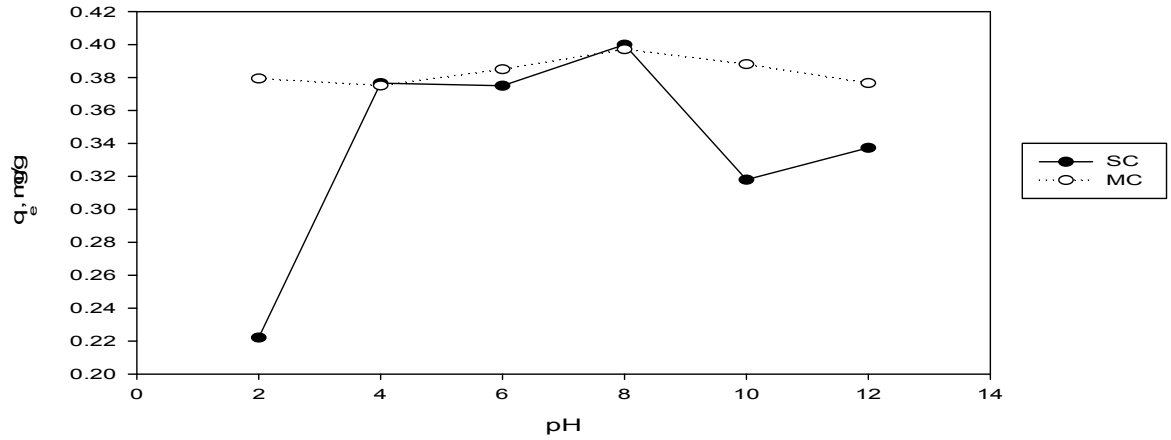

Figure 12 Effect of pH on the adsorptive capacity of clay for zinc for both single component and multi-component adsorption scenarios

4.3 Selectivity Sequence

Selectivity sequences for pH 2, 4, 6, 8, 10 and 12 for SC and MC scenarios are presented in Table 10 together with the associated overall selectivity sequence for each scenario. These sequences were arrived at, based on the distribution coefficient of the heavy metals as presented in the table. For both scenarios, two ions that lie on opposite extreme ends are Cr and Zn. This is because, the former have the overall highest distribution coefficient while the latter have the lowest. It can be seen how Pb ions became highest selective at pH 4 and 6 (SC scenario) but became substituted by Cd ions in alkaline condition. It is to be noted that, the selectivity of Cd ions increases with increase in pH for both scenarios. As presented in Table 10, the values of the distribution coefficients generally increases with increasing selectivity of clay for the

heavy metals and vice versa. For instance, Cd ions were completely adsorbed onto the clay minerals at pH 12 in SC scenario, giving their aqueous concentration to be zero and distribution coefficient to be infinite. Pb and Zn ions also experienced complete removal at pH values 4 - 6 and 8 respectively.

4.4 Desorption Study

Multi-component desorption study undertaken revealed that Cr ions were the least desorbed (Figure 13), having percentage desorption of 0.18 %, followed by Cd and Cu ions. Zn and Pb ions were desorbed most, as indicated by their percentage desorption values of 6.55 and 3.49 respectively. Selectivity sequence during desorption may be written as Cr < Cd < Cu < Pb < Zn. Different selectivity sequences for different soil components were reported by Covelo et al. [131, 161] from which they found the selectivity sequences to be highly dependent on clay material used.

Table 10 Distribution coefficients and selectivity sequences for various pH values

	Single component distribution coefficients, K_d, L/kg					Selectivity sequence
pH	Cd	Cr	Cu	Pb	Zn	
2	184.08	26646.67	1456.01	756.70	24.99	Cr > Cu > Pb > Cd > Zn
4	603.05	33313.33	3285.79	*	321.88	Pb > Cr > Cu > Cd > Zn
6	402.83	22202.22	3258.69	*	300.00	Pb > Cr > Cu > Cd > Zn
8	564.80	3718.32	2360.95	1940.78	*	Zn > Cr > Cu > Pb > Cd
10	6133.85	7527.17	1980.00	451.70	77.56	Cr > Cd > Cu > Pb > Zn
12	*	3753.58	3105.00	967.65	107.80	Cd > Cr > Cu > Pb > Zn
Average	-	16193.55	2574.41	-	-	Cr > Pb > Cu > Cd > Zn
	Multi-component distribution coefficients, K_d, L/Kg					
pH	Cd	Cr	Cu	Pb	Zn	Selectivity sequence
2	52.07	8490.64	4918.27	1393.43	368.73	Cr > Cu > Pb > Zn > Cd
4	62.30	12883.23	3901.57	1291.48	302.58	Cr > Cu > Pb > Zn > Cd
6	106.18	3683.70	3154.60	417.64	516.91	Cr > Cu > Pb > Zn > Cd
8	1174.03	9736.10	8143.27	1857.93	2837.14	Cr > Cu > Zn > Pb > Cd
10	*	12883.23	5043.29	1078.90	656.82	Cr > Cd > Cu > Pb > Zn
12	*	11744.71	7252.73	564.80	322.76	Cd > Cr > Cu > Pb > Zn
Average	-	9903.60	5402.29	1100.70	834.16	Cr > Cu > Pb > Cd > Zn

*Indicates 100 % removal from solution

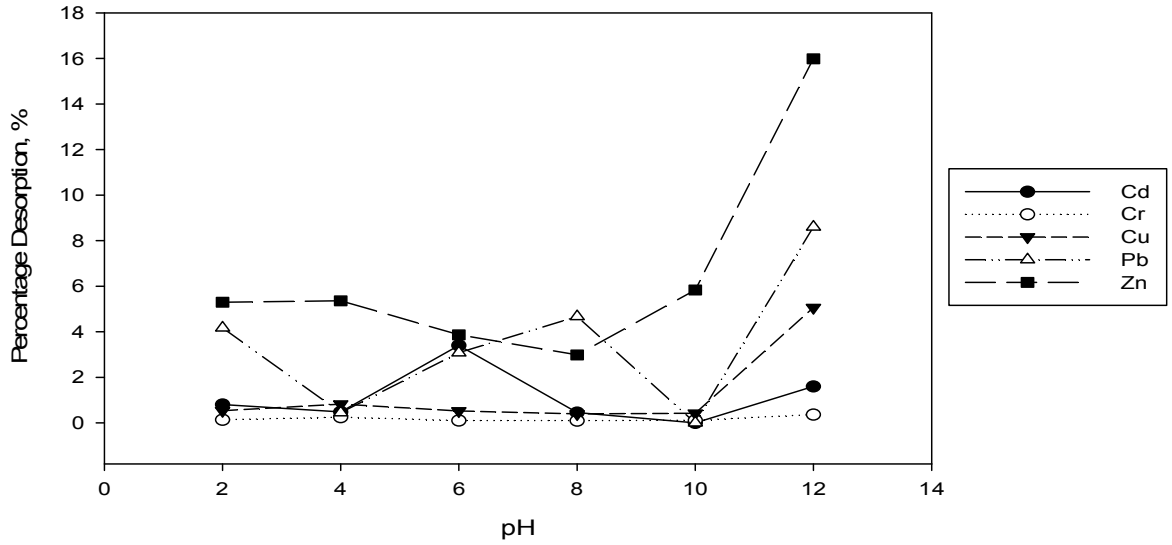

Figure 13 Percentage desorption of heavy metals against pH for multi- component adsorption scenario

4.5 Conclusion

The adsorption and desorption behaviors of Cd, Cr, Cu, Pb and Zn ions onto natural clay minerals were investigated in single and multi-component scenarios. Cr ions were found to be the highest adsorbed and the least desorbed during multi-component adsorption and desorption respectively. Conversely, Zn ions were the least adsorbed and the highest desorbed in single component adsorption and multi-component desorption respectively. Adsorptive capacities of Cu and Zn ions were observed to be higher in the MC adsorption scenario than in the SC scenario. The adsorption selectivity sequences for the SC and MC scenarios were Cr > Pb > Cu > Cd > Zn and Cr > Cu > Pb > Cd > Zn respectively. Remarkable removals were observed at almost all the pH values, with some of the removals reaching 100 % while others were mostly 99 % for the different pH values. pH has slightly affected the adsorptive capacities of all investigated heavy metals in the SC and MC scenarios. Adsorptive capacities of Cr, Cu, Pb and Zn were seen to have increased with increasing pH, up to around the neutral pH (6 and 8), whereas the adsorptive capacity of Cd ions increased with increase in the pH values in both scenarios. In the case of Cr ions, higher

percentage removal was noticed between pH values 2 and 6 (in SC scenario) and 4 and 8 – 12 (in MC scenario). Desorption study has revealed a selectivity sequence Cr < Cd < Cu < Pb < Zn with the highest percentage desorption occurring at pH = 12 (15.98 % desorption) for Zn ions. From the results, Pb ions became highest selective at pH 4 and 6 (SC scenario) but exchanged position with Cd ions in alkaline condition (pH 12). Conclusively, initial pH plays a significant role in competitive adsorption and desorption of the investigated heavy metals onto clay minerals and the local clay used in this study has proved to be a candidate adsorbent for heavy metal removal in wastewater streams. This study allows for a better understanding of SC and MC adsorption behavior of the heavy metals onto the clay minerals. The knowledge derived herein, may be brought to the fore when remediating a clay soil contaminated by these metals.

CHAPTER 5

PRELIMINARY INTEGRATED ELECTROKINETICS-ADSORPTION REMEDIATION EXPERIMENTS

5.1 Introduction

Rapid proliferating industrialization has been recorded in recent decades. One of the major environmental consequences of these progressive achievements is the improper release of elevated amounts of variety of organic and inorganic pollutants into the environment. These pollutants could enter the environment directly as a result of accidents, spills during transportation, and leakage from waste disposal sites, storage sites and industrial facilities etc, thereby contaminating the environment. Co-occurrence of complex chemical mixtures such as total petroleum hydrocarbons (TPH), phenols, heavy metals (such as Cr, Cd, Cu, Zn, Pb and Hg) , radionuclides and pesticides at remediation sites pose potential dangers to human health and the environment, and further complicate the remediation process. Some of the pollutants encountered in contaminated soils may be treated using processes like biodegradation, vapor extraction, chemical oxidation, thermal desorption, and incineration. Satisfactory results may not be obtained when these treatment processes are applied to low-permeability soils or those sites contaminated by mixed contaminants (inorganic and organic wastes) because of the difficulty in accessing the contaminants to uniformly deliver treatment reagents. Therefore, innovative remediation technologies must be developed to study the in situ removal of contaminant mixture from soil to

ensure a sustainable environment. This has given birth to an important area of current research in in situ soil remediation technology [1, 13, 162, 163].

It has been observed that contaminated soils do not contain single contaminants. Several pollutants appear in the soil as mixed components. In reality, soil polluted with organic contaminants often contains other contaminants such as heavy metals. The implication of the presence of the different nature of the two contaminant groups is that there may be synergistic or antagonistic effects on their respective removal using electrokinetic remediation technique [18, 21]. Reddy [22] posited that the presence of mixed contaminants will retard individual contaminant migration and removal. Also, as organic pollutants are removed by electroosmotic flow and heavy metals by electromigration, the solubility as well as hydrophobicity disparities between the organic pollutants and heavy metals indicates the complexity of electrokinetic remediation of soils polluted with mixed contaminants. To date, several studies have been conducted using electrokinetics (EK) for mixed contamination [19, 30, 31, 33]. Of the several electrokinetic remediation techniques, Lasagna process has been found to yield the best removal efficiency of organic contaminants from soils [17]. The general concept of the Lasagna process is the transportation of contaminants from contaminated soil section into treatment zones using major electrokinetic transport mechanisms (i.e. electroosmosis or electromigration). Once at the treatment zones, the contaminants may be removed from the pore water by sorption, degradation or immobilization depending on treatment zone design [2, 13-15]. Detailed studies of all previous works on the Lasagna process which span from bench scale investigations to full field-scale remediation of contaminated soils have been reported elsewhere [2, 12-15, 34, 37, 38, 53, 56]. Lasagna process usually uses

activated carbon as the sorbent material to improve the removal of contaminants from contaminated soil [13, 37, 38].

The main aim of this study is to investigate the possible application of the coupled electrokinetics-adsorption innovative technique that combines electrokinetics and adsorption using locally produced granular activated carbon (GAC) from date palm pits for remediation of local saline-sodic soil contaminated with mixture of toxic pollutants comprising of petroleum byproduct (kerosene), organic compound (phenol) and heavy metals (Cr, Cu, Cd, Zn, Pb and Hg).

5.2 Results and Discussion

5.2.1 Clay and GAC characteristics

Some of the physico-chemical properties of the saline-soil are presented in Table 11. The mineralogical composition obtained from the XRD result, shows that the soil consists mainly of montmorillonite, quartz and calcite minerals. Scanning electron microscopy revealed the dominant elements to be O and Si whose percentage compositions are 53.11 % and 18.46 % respectively. Other elements present in lesser quantities are Ca (7.09 %), Al (6.76 %), Fe (5.20 %), Na (2.69 %), Cl (2.69 %), K (2.29 %) and Mg (1.73 %). The GAC used in the present study was produced locally from date palm pits as described elsewhere [40, 43].

Table 11 Physico-chemical properties of saline-sodic soil [164]

Property	Value
pH (ASTM D 4972)	9.00
Moisture content, % (ASTM D 2216)	3.91
Soil organic matter, % (ASTM D 2974)	3.26
Electrical conductivity, dS/m (ASTM D 1125)	8.62

From Table 11, the soil pH (9.00) indicates that it contains appreciable soluble salts capable of undergoing alkaline hydrolysis as is seen sodium carbonate [36]. The hydrolysis of calcite ($CaCO_3$) produces a pH of about 8 – 8.2 in soils. This may be limited by its low solubility. In addition, Na^+ ions do not strongly compete with H^+ ions for exchange sites as does Ca^{2+} ions which are strongly and more tightly held on the soil surface. The inability of the displaced Na^+ ions to inactivate OH^- ions results in an increased soil pH, which is usually greater than 8.2. Similarly, for soil whose pH is greater than 8.2, its exchangeable sodium percentage is greater than 15 [36]. The presence of calcite coupled with alkaline hydrolysis of sodium carbonate give a high electrical conductivity to the soil (8.62 dS/m). The role of soil organic matter (SOM) in heavy metal adsorption is not to be underrated by its low value (3.26 %). This is because of the high specific surface area and cation exchange capacity possessed by SOM, which may reach up to 800 – 900 m^2/g and 150 - 300 cmol/kg respectively [145]. The physico-chemical properties and morphological characteristics of the clay and GAC are detailed elsewhere [40, 164].

5.2.2 Single and Competitive Adsorption of Heavy Metals on Clay

Lukman *et al.* [164] found out that the adsorptive capacities of Cu and Zn ions were higher in the multi-component adsorption scenario than in the single component scenario as presented in Figures 14 and 15. The adsorption selectivity sequences obtained using the coefficient of distribution for the single and multi-component scenarios were Cr > Pb > Cu > Cd > Zn and Cr > Cu > Pb > Cd > Zn respectively [164]. Srivastava et al. [144] reported a similar selectivity sequence for the multi-component scenario. Yong et al. [165] identified the general factors that influence selectivity sequence to be ionic size or activity, first hydrolysis constant, soil type and pH of the system. From the multi-component desorption study presented in Figure 16,

it can be inferred that trivalent Cr ions were tightly held by the soil surface, thus having the least percentage desorption, followed by Cd and Cu ions. Reddy and his co-workers [166-168] reported that trivalent Cr ions adsorb highly to soil solids and form cationic species that are insoluble over a wide range of pH. This is in line with the present findings (Figures 15 and 16) which revealed a high selectivity for the trivalent Cr during multi-component adsorption and desorption tests. It may be argued that the solubility of heavy metal ions at alkaline pH is very low due to their precipitation as insoluble hydroxides. However, in this study, the main focus is not on the adsorbed or precipitated species, but rather, on the mobile or dissolved species that can be removed via electromigration or electroosmotic flow during electrokinetic remediation. Hence, percentage removal (Figures 14 and 15) refers to the amount adsorbed by the soil minerals plus any precipitated metal species.

5.2.3 Soil pH Distribution during Coupled Electrokinetics-Adsorption Remediation

The pH value of the investigated clay is naturally alkaline (pH = 9), which promotes heavy metals precipitation and adsorption onto the clay surface depending on the metal speciation. At the end of the 21-day period, the pH distribution within the soil was found to be approximately 12 (Figure 17) for all the three runs despite dissimilar application of voltage gradients which might be expected to increase the rate of production of H^+ and OH^- radicals and their subsequent migration to the opposite electrodes for a higher

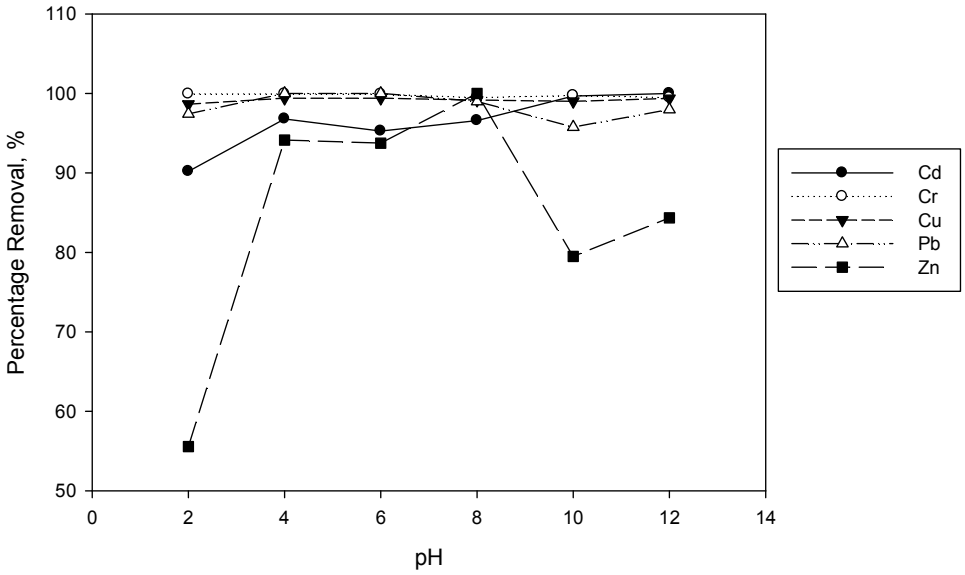

Figure 14 Percentage of heavy metals adsorbed plus any precipitated species at different pH for single component adsorption scenario [164]

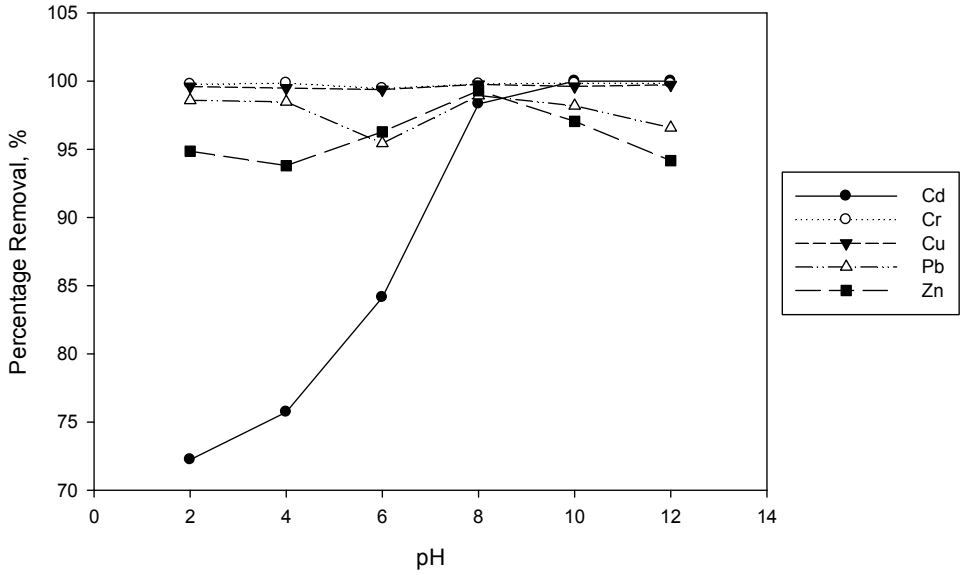

Figure 15 Percentage of heavy metals adsorbed plus any precipitated species at different pH for multi-component adsorption scenario [164]

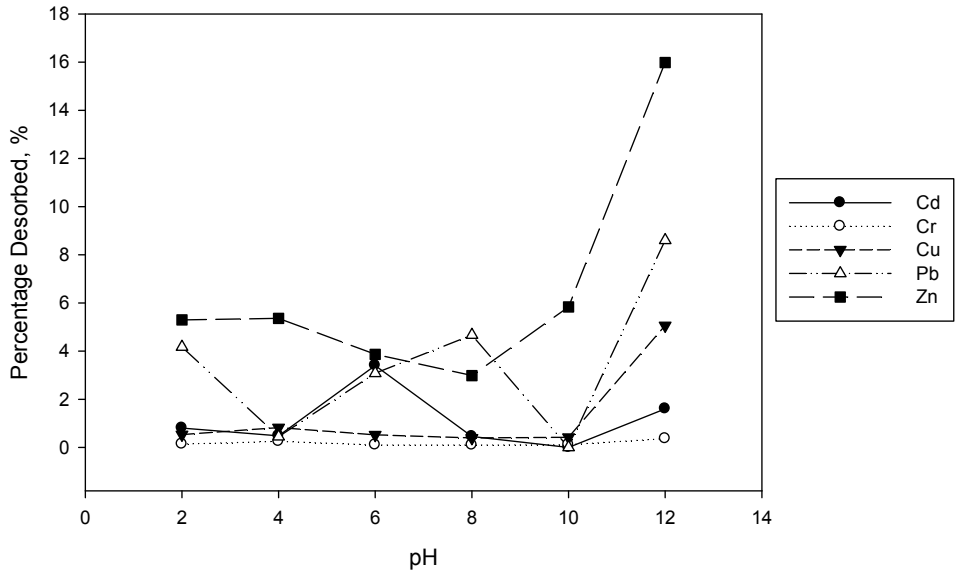

Figure 16 Percentage of heavy metals desorbed plus any precipitated species at different pH for multi-component desorption scenario [164]

voltage gradient. This high pH environment might be explained by the presence of calcite in the soil minerals which increases the acid buffering capacity of the soil. It is expected that the carbonates will neutralize the H^+ ions generated at the anode which suppresses the development and migration of acidic pH front near the anode. Results obtained for electrokinetic remediation of glacial till by Reddy and his co-workers [166] have corroborated this finding. Bipolar effect was also investigated for EK-GAC-2, but pH gradient is not observed, hence bipolar effect is not present.

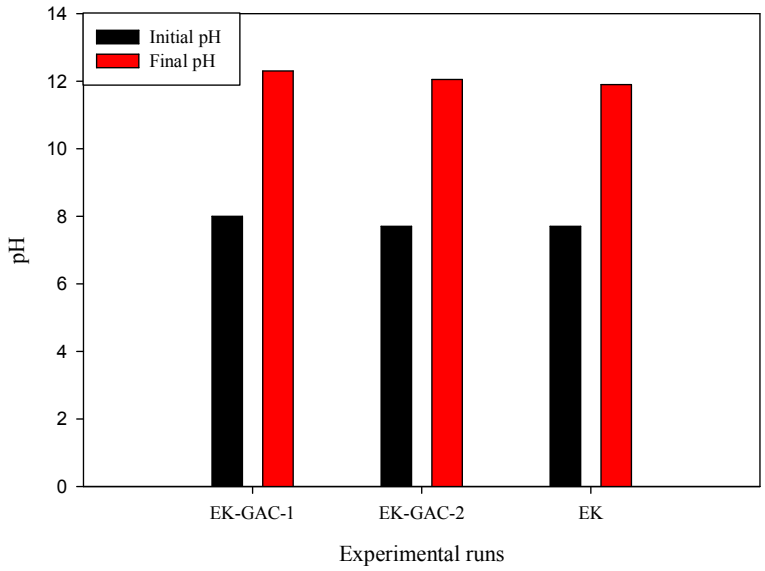

Figure 17 pH variation

5.2.4 Soil Moisture Content, Organic Matter and Electrical Conductivity

Soil moisture content enhances dissolved contaminant transport by ionic migration and electroosmosis and hence affects removal efficiency. In the present study, the GAC chamber was initially saturated with water while the spiked soil specimen was kept at an initial moisture content of 33 % in each case. This value increased to 52.6, 38.46 and 35.11 % for EK-GAC-1, EK-GAC-2 and EK respectively at the end of the 21-day period. Absence of GAC chambers in the EK run may be responsible for its lowest moisture content at the end of the run. Soil organic matter plays an important role in the adsorption of heavy metal ions even in soils where its value is very low [35]. This is because, SOM possesses very high specific surface area and cation exchange capacity (CEC) which may range between 150 and 300 cmol/kg [145]. The majority of a surface soil's CEC is in fact attributable to its soil organic matter. The initial SOM for the spiked chambers of EK-GAC-1, EK-GAC-2 and EK were 8.22,

6.38 and 6.38 % respectively. At the end of the experiments, these initial values decreased for EK-GAC-1 and EK-GAC-2 and increased slightly for EK.

Soil electrical conductivity (EC) varies with the amount of moisture held by soil particles. Electrical conductivity of clay typically lies between 0.01 and 1 dS/m. Abrol *et al.* [36] and Sparks [35] have classified soils whose EC and pH are greater than 4 dS/m and 8.2 (at 25 °C) to be saline-sodic. The EC of the pristine clay sample is 8.62 dS/m which indicates that it has an excess of dissolved salts which makes it to be classified as saline-sodic soil with exchangeable sodium percentage (ESP) of more than 15. Upon spiking the soil, the EC jumped to 47.3 dS/m due to increase in the dissolved ions and decreased at the end of the runs to 31.7 and 43.2 dS/m for EK-GAC-2 and EK respectively (Figure 18). Higher reduction in EC of EK-GAC-2 may be explained by the higher contaminant removal efficiency. In the case of EK-GAC-1, the spiked EC was 24.56 dS/m which increased to 38.3 dS/m at the end of the test. This increase may be attributed to the higher voltage gradient (1V/cm) used in this test which sped the rate of the electrochemical decomposition of water (at the electrodes) and degradation of the processing fluids.

5.2.5 Variations of Current, Temperature and Cumulative Electroosmotic Flow

The average electric current recorded for EK-GAC-1, EK-GAC-2 and EK are 0.88, 0.61 and 0.71 A respectively. Maximum current of 2.8 A was recorded by EK-GAC-1 test and may be attributed to its higher voltage gradient which facilitates faster ionic movement in pore fluid. Dynamic changes in the solution chemistry may be responsible for the observed fluctuating current trend observed in all the tests. Maturi and Reddy (2008) observed somewhat similar current fluctuation. The current values

recorded in the tests are 2 – 3 orders of magnitude higher than those obtained in similar studies employing the Lasagna process and electrokinetics only. This unique and important observation may be explained by the salinity and sodicity levels of the investigated soil which provided large amount of dissolved ions in the pore fluid for effective current conduction. High current flow through the soil may have significant impact on the soil temperature, electroosmotic flow rate, electrode and processing fluid deterioration, removal efficiency and energy consumption. The average temperature recorded for EK-GAC-2 and EK are 28.5 and 30 ^{o}C respectively. For the same tests, the maximum temperature is 34.6 and 40.5 ^{o}C respectively. High temperature will reduce the soil moisture content due to pore fluid evaporation and subsequent reduction in current and electroosmotic flow.

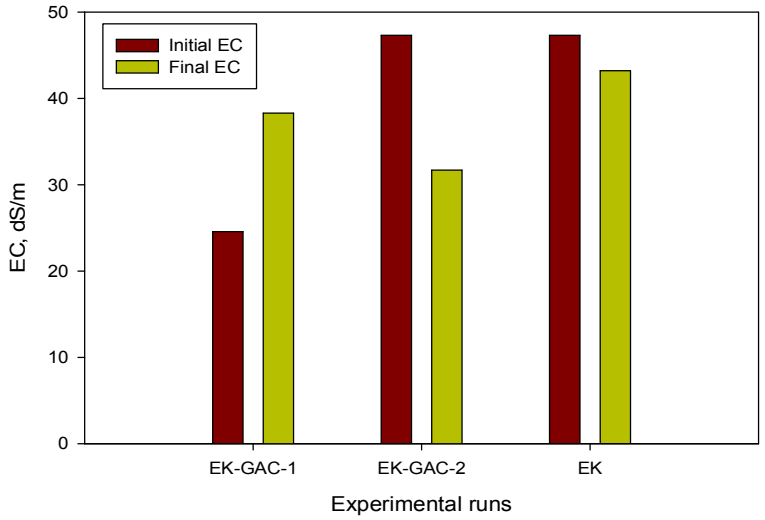

Figure 18 Variation of electrical conductivity

Though thermal effects due to temperature rise have not been reported to be significant in bench-scale studies [2], our finding from this study reveals that increasing the voltage gradient more than 1 V/cm leads to considerable rise in the soil

temperature which may not be neglected for practical purposes and modeling studies. As such, the general notion of using 1 V/cm for most bench-scale studies needs to be investigated if the soil possesses some properties that were not studied before. Electroosmotic flow is maintained throughout the duration of the tests, EK-GAC-2 and EK tests maintain an average pore volume of 0.75 and 0.66 respectively. Total electroosmotic volumes are 1388 and 1214 mL which translated into total pore volumes flushed to be 17.35 and 15.17 for EK-GAC-2 and EK tests respectively. Expectedly, the maximum temperature and electroosmotic flow recorded coincided with the period in which maximum current was recorded. Electroosmotic flow is not influenced by hydraulic gradient in this study as it occurs even under negative hydraulic gradient. Higher electroosmotic flow is expected to occur in the test with higher voltage gradient. It is obvious that the soil zeta potential is not reversed in this study which could reverse the electroosmotic flow. This is because it remains unidirectional throughout the test period.

5.2.6 Contaminant Removal Efficiency

After the operational period of 21 days, significant removal is observed for most of the contaminants in all the tests as presented in Figure 19. Highest and lowest percent removal is observed in phenol and Zn ions respectively. Only phenol achieved 100 % removal possible because it is miscible with water and behaves in the same way as other cationic species [169]. Acar and his co-workers [6] achieved similar percent removal after two pore volumes were flushed. Lukman *et al.* [164] observed that Zn is the least selective by this soil in competitive aqueous medium, most especially in the alkaline region. From Zn speciation using its Pourbaix diagram [170], it may be said that Zn precipitates as zinc hydroxide at the initial soil pH despite its existence in the

form of hydroxo-complexes at pH > 11. Calcareous soils, similar to the one studied here, have been found to perform relatively poorly for Zinc removal [171].

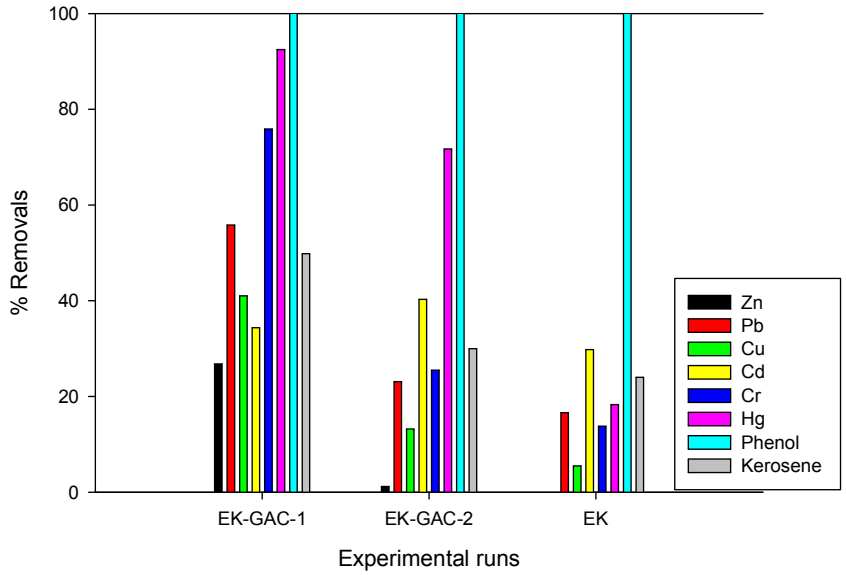

Figure 19 Comparison of the contaminant removal efficiencies for all the tests

Among the trace elements studied in EK-GAC-1 and EK-GAC-2 tests, Hg removal was highest (92.49 %). This may be attributed to the presence of excess Cl^- under aerobic conditions and subsequent formation and migration of the mercury complex $HgCl_4^{2-}$ according to the following reaction in equation 5.1 [172].

$$O_2 + 2Hg + 8Cl^- + 2H_2O \rightarrow 2HgCl_4^{2-} + 4OH^- \qquad (5.1)$$

Visual MINTEQ 3.0 was employed to model the Hg speciation before and after the first experimental run (EK-GAC-1) using its dissolved concentration, pH, temperature and ionic strength. It was assumed that all dissolved Hg species are removed at the end of the experimental run (i.e. 3 weeks). Table 12 provides the hydroxocomplexes present. The species having the highest initial % of total Hg concentration and

removal efficiency is $Hg(OH)_2$ (aq) which suggests that precipitated mercury hydroxides can redissolve at high alkaline pH values encountered in this study. The formation of complexes with OH^- anions that have increased pore fluid solubility may be attributed to the redissolution of $Hg(OH)_2$ (aq) and its subsequent high removal efficiency. Each of the species have been removed by the process, with the dominant removal of $Hg(OH)_2$ (aq) corresponding to the actual removal efficiency of Hg during this experimental run (Figure 19).

Table 12 Modeling of Hg speciation using Visual MINTEQ 3.0 for EK-GAC-1

Initial Hg species	Concentration, mol/L	Final Hg species	Concentration, mol/L	% Removed
$Hg(OH)_2$ (aq)	4.30e-04	$Hg(OH)_2$ (aq)	3.98e-04	92.49
Hg^{+2}	9.04e-14	Hg^{+2}	1.73e-22	1.91e-07
Hg_2OH^{+3}	4.23e-22	Hg_2OH^{+3}	4.03e-35	9.53e-12
$Hg_3(OH)_3^{+3}$	1.79e-22	$Hg_3(OH)_3^{+3}$	3.77e-35	2.11e-11
$HgOH^+$	2.82e-09	$HgOH^+$	1.11e-13	3.93e-03

Figure 20 depicts how precipitated metal hydroxides can redissolve at high pH values. This occurs due to the formation of complexes with OH^- anions. These complexes are negatively charged and have increased pore fluid solubility. Consequently the removal efficiency of these heavy metals is enhanced even under high alkaline condition prevailing in the present study.

Higher electroosmotic flow observed in EK-GAC-1 and EK-GAC-2 tests may be responsible for higher removal of kerosene in these tests than EK test (Figure 19). Generally, introducing GAC chambers in EK-GAC-2 test lead to higher percent removal of all contaminants than the case without the GAC chambers (EK test). In addition, higher voltage gradient produced higher percent removal (EK-GAC-1 and EK-GAC-2 tests).

5.2.7 Conditioning and Energy Consumption

Due to the rapid electrochemical decomposition of water at the electrodes and subsequent generation of H^+ and OH^- ions at the anode and cathode respectively, there was need to condition the anode and cathode chambers with H^+ and OH^- neutralizing chemicals. 2 N $NaOH$ and 1 N HNO_3 were used as the anolyte and catholyte respectively. Automatic processing fluid recycling was intended, but due to the soil salinity and sodicity which led to the passage of high current in the soil, periodic monitoring of the processing fluids pH was necessary. For the EK-GAC-1 test, the catholyte becomes completely basic ($pH \approx 13$) after 6 hr, while the anolyte lasted up to 12 – 18 hr before becoming completely acidic ($pH \approx 0.5$).For the EK-GAC-2 and EK tests, the catholyte may last up to 12 hr before it needed replacement.

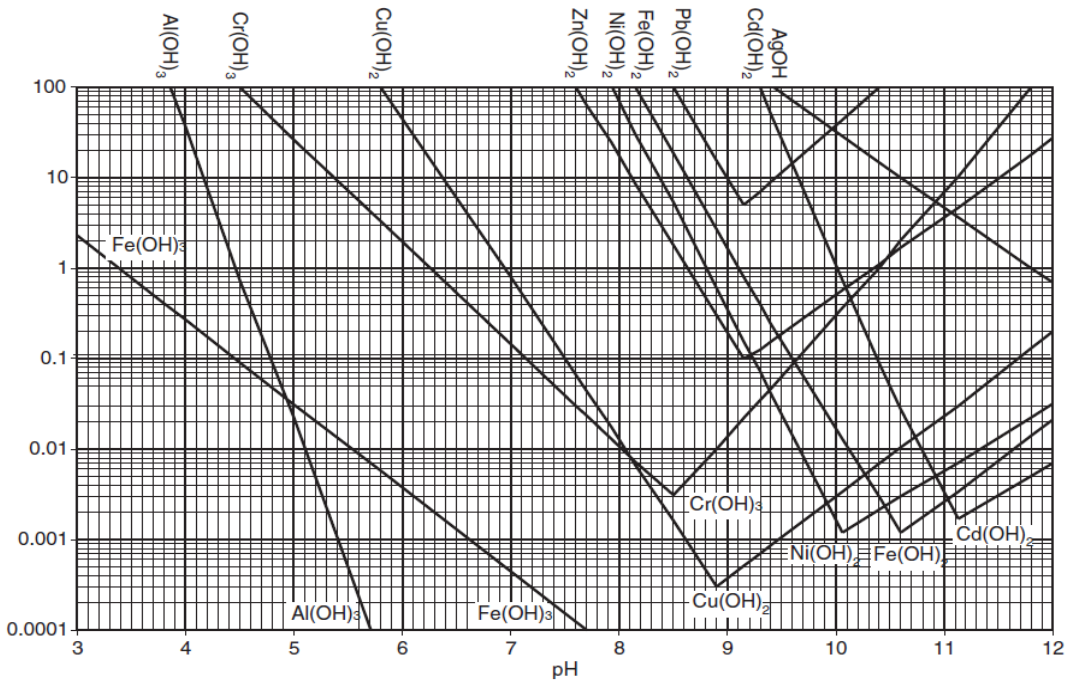

Figure 20 Variation of theoretical solubilities of some heavy metal hydroxides with pH [173]

Higher current flow in EK test led to higher rate of processing fluids deterioration and higher energy consumption. The total energy consumed per m^3 of soil treated during the 21- day period is estimated at 4273, 1777 and 2068 kWhr / m^3 for EK-GAC-1, EK-GAC-2 and EK tests respectively.

5.3 Conclusion

The potential of coupling electrokinetics and adsorption using locally produced granular activated carbon from date palm pits for the remediation of natural saline-sodic soil was investigated. The soil was spiked with kerosene, phenol, Cr, Cd, Cu, Zn, Pb and Hg at given concentrations and three tests (EK-GAC-1, EK-GAC-2 and EK) were run for a period of 21 days. Application of voltage gradient of 1 V/cm to the spiked soil led to high current generation, high electroosmotic flow, high rate of deterioration of processing fluids and anode electrodes, high percent removal and high energy consumption. Phenol and Zn were found to have the highest and lowest removal efficiency. For the 21-day period of continuous electrokinetics-adsorption experimental run, efficiency for the removal of Zn, Pb, Cu, Cd, Cr, Hg, phenol and kerosene were found to reach 26.8, 55.8, 41.0, 34.4, 75.9, 92.49, 100.0 and 49.8 % respectively. Despite the high selectivity of trivalent Cr exhibited by the clay soil, the alkaline pH maintained for most of the experimental duration has led to the formation of hydroxocomplexes which were removed due to electromigration. Hence, high percentage removal of the trivalent Cr was recorded. The results obtained suggest that integrating adsorption into electrokinetic technology is a promising solution for removal of contaminant mixture from saline-sodic soils. It is suggested that different types of electrodes should be investigated (for this type of soil) together with the operating parameters (such as polarity reversal rate, pulse and continuous current

application) affecting percent removal for simultaneous optimization of the Lasagna process.

CHAPTER 6

GEOCHEMICAL MIGRATION OF TRIVALENT CHROMIUM SPECIES IN SALINE-SODIC SOIL DURING LASAGNA PROCESS

6.1 Introduction

In 1909, Freundlich and Neumann [174] provided the general name "electrokinetic phenomena" to refer to the electrically driven mass flow of dissolved contaminants and pore fluid transport in soils induced by an applied DC voltage. It is made up of transport of pore fluid via electroosmosis (EO) and transport of ions or charged species via electromigration [175]. The direction and quantity of contaminant movement is influenced by the contaminant concentration, solubility, speciation, degree of hydrophobicity, soil type and structure, and the mobility of contaminant ions, as well as the interfacial chemistry and the conductivity of the soil pore fluid [57]. The remedial efficiency generally depends on the nature of the contaminants, and soil properties, such as pH, permeability, adsorption capacity, buffering capacity

and geochemical processes (such as acid/base reactions and migration, dissolution/precipitation, redox reactions, complexation, speciation) [60, 175].

The geochemical properties of the most stable forms of Cr, i.e., trivalent and hexavalent Cr has been extensively studied in different types of soils (kaolin, glacial till, etc.) by Reddy and his co-workers and other investigators [166-168, 176-181]. The trivalent Cr, though considered relatively non-toxic compared to the hexavalent Cr, exists in the subsurface environments as cation, Cr^{3+} and in the following hydroxocomplex forms; $Cr(OH)_4^-$, $CrOH^{2+}$ and $Cr(OH)_3^0$. Cr^{3+} and $CrOH^{2+}$ ions. They are mostly prevalent at soil pH values less than 6, while $Cr(OH)_4^-$ and $Cr(OH)_3^0$ ions prevails when pH is greater than 11.8. The redox state also affects the Cr form with a reduced state favoring the presence of the trivalent Cr while an oxidized state favors the existence of the hexavalent Cr. Most of the trivalent Cr species are less mobile because of their low solubility over a wide pH range (< 12) and may be readily adsorbed by the negatively charged clay surfaces. There exists a redox state in the subsurface environment because of the generation of oxygen and hydrogen gases at the electrodes in addition to the possible presence of iron (reducing agent), manganese (oxidizing agent) or microorganisms. The redox potential (Eh) and soil pH determines the possible oxidation of Cr from the trivalent to hexavalent form as shown in Figure 21. Chinthamreddy and Reddy [167] have found no significant oxidation of trivalent Cr in high buffering capacity soil such as glacial till.

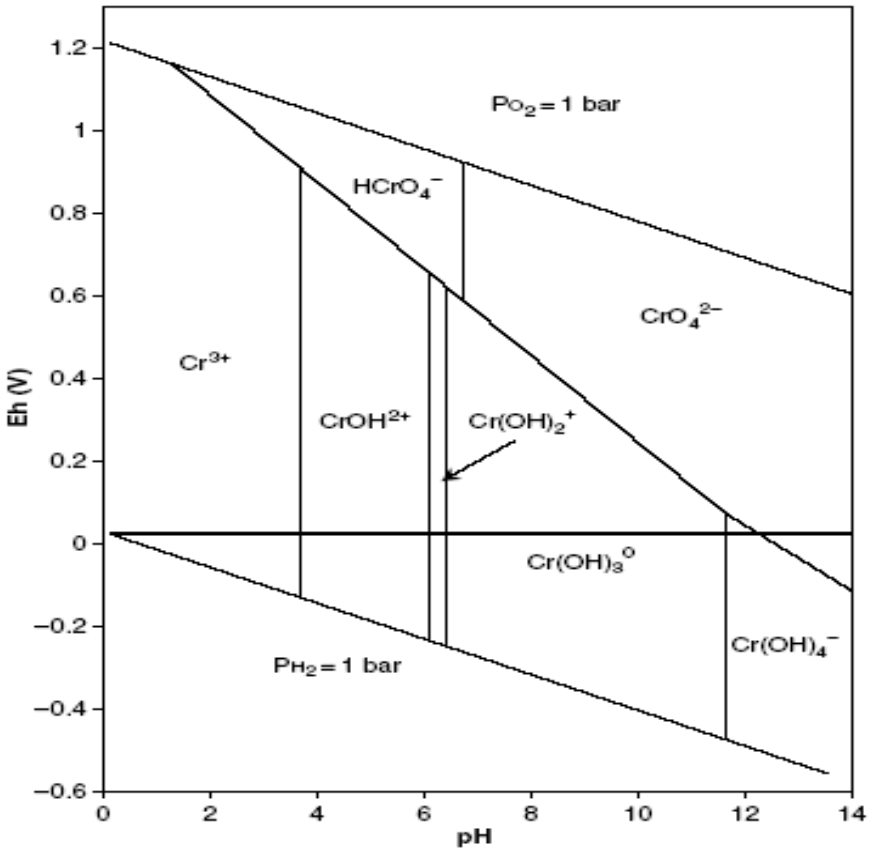

Figure 21 Redox potential (Eh) – pH diagram for Cr – O – H system [182]

Some microbially-driven biotransformation processes may affect the soil physico-chemical properties after electrokinetic remediation because of the passage of electric current and development of pH gradients [165]. These lead to original soil mineral degradation and alteration via biotransformation. While biotransformation deals with the bioweathering and alteration or degradation of clay minerals, biomineralization refers to the formation of amorphous and crystalline materials from aqueous ions by biologically mediated processes such as diagenesis [183]. In addition to current and pH gradients, heavy metals can also affect the following biological assays: soil microbial biomass carbon, enzyme activity, basal soil respiration and earthworm assays and seed assays [5, 184-186]. Given the aforementioned intricacies of the

geochemical behavior and migration of trivalent Cr in soil during electrokinetic remediation. This study was aimed at investigating trivalent Cr migration and remedial efficiency in high buffering capacity and alkaline soil during electrokinetic study in addition to the impacts of the soil remediation on the physico-chemical properties of the soil. A carefully designed experiment using BBD was used to study the interaction effects of voltage gradient, initial contaminant concentration and polarity reversal rate on the trivalent Cr remedial efficiency in saline-sodic soil that was artificially spiked with Cr, Cu, Cd, Pb, Hg, phenol and kerosene using RSM modeling and optimization tools.

6.2 Results and Discussion

6.2.1 Characterization

Natural saline-sodic clay, obtained from Al-Hassa Oasis, Saudi Arabia was used in this study. The soil has the following characteristics: pH (8.3), moisture content (3.91 %), soil organic matter (2.59 %), electrical conductivity (15.24 dS/m), specific surface area (9.07 m^2/g), pore volume (0.014 cm^3/g), pore size (62.55 Å) – mineralogy from x-ray diffraction (XRD); quartz (SiO_2) (87.4 %), calcite ($CaCO_3$) (5.2 %) and dolomite ($CaMg(CO_3)_2$) (7.4 %). X-ray fluorescence spectroscopy (XRF) revealed the soil consists of the following elements: Ca (37.64 %), Si (34.73 %), Fe (10.41 %), Al (7.6 %), K (3.42 %), Mg (2.48 %), Pd (2.85 %) and Ti (0.86 %). These properties were determined using methods of the American Society of Testing and Materials (ASTM) standards and were reported elsewhere [164].

6.2.2 Coupled Electrokinetics-Adsorption Study

Fifteen (15) bench-scale experiments (Figure 22), each having a 21-day run time, were designed and performed to investigate the migration and distribution of trivalent

Cr in a contaminant mixture using the coupled electrokinetics-adsorption technique and to understand the operating variables' effects on saline-sodic soil.

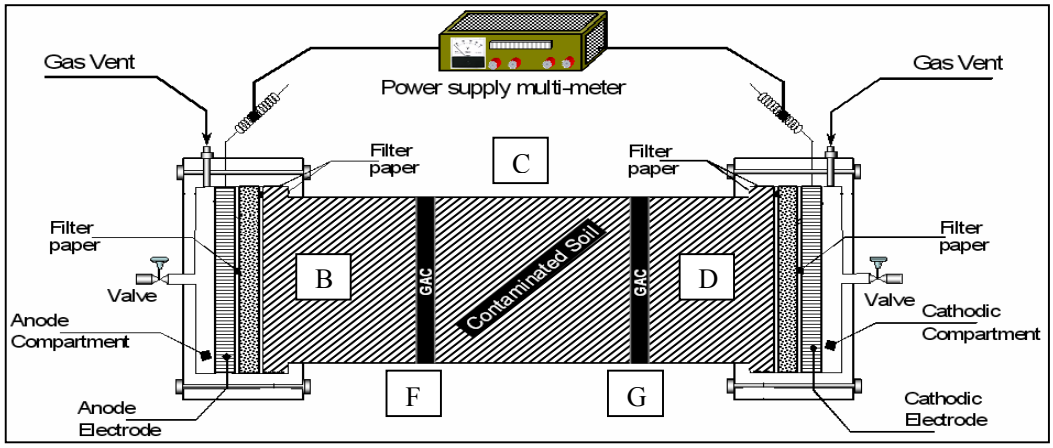

Figure 22 Coupled electrokinetics-adsorption experimental setup

Discussion of the monitored results obtained after performing thirteen (13) tests (Table 13) with 3 center points was focused on geochemical processes affecting sorption/desorption and migration/removal mechanisms such as the development of acid/base fronts, migration and reactions, dissolution/precipitation, oxidation/reduction reactions, complexation and metallic ion speciation. In addition, presentation of the developed mathematical models and discussion on how the factors affect the respective responses was done.

Table 13 Design of experimental runs using the Box-Behnken Design

Run order	Polarity reversal, A (hr)	Voltage gradient, B (V/cm)	Concentration, C (mg/kg)	Remedial efficiency, %
1	0	0.6	20	0.00
2	48	0.6	20	0.00
3	24	1	20	0.00
4	24	1	100	0.00
5	24	0.6	60	79.97
6	0	1	60	72.73
7	24	0.2	20	0.00
8	0	0.2	60	36.93
9	48	1	60	65.66
10	48	0.6	100	0.00
11	0	0.6	100	25.50
12	24	0.2	100	0.00
13	48	0.2	60	34.88

6.2.3 Soil pH distribution, Electrical Conductivity, Bipolar Effects, Electroosmotic flow and Current

Soil pH and Electrical Conductivity: The soil pH (8.3) indicates that it contains appreciable soluble salts capable of undergoing alkaline hydrolysis as is seen with sodium carbonate [36]. The hydrolysis of calcite and dolomite may be limited by their low solubility, thus producing a pH of about 8 – 8.2 in soils. In addition, Na^+ ions do not strongly compete with H^+ ions for exchange sites as does Ca^{2+} ions that are strongly and more tightly held on the soil surface. The inability of the displaced Na^+ ions to inactivate OH^- ions results in increased soil pH, which is usually greater than 8.2. Moreover, for a soil whose pH is greater than 8.2, its exchangeable sodium percentage has to be greater than 15 [36]. Presence of calcite and dolomite coupled with alkaline hydrolysis of sodium carbonate give high electrical conductivity to the soil (15.24 dS/m).

The saline-sodic nature of the soil necessitated the use of processing fluids (2 N NaOH and 1 N HNO_3) to continuously neutralize the rapidly generated H^+ and OH^- ions at the anode and cathode respectively. These fluids were monitored every 8 hours and replaced as they degraded. HNO_3 and NaOH are strong acid and base respectively, and dissociate completely according to the following reactions.

$$HNO_3(l) \rightarrow H^+(aq) + NO_3^-(aq) \quad (6.1)$$

$$NaOH(aq) \rightarrow Na^+(aq) + OH^-(aq) \quad (6.2)$$

Because of the electrochemical decomposition of water, OH^- and H^+ ions were produced at the cathode and anode respectively as shown in equations 6.3 and 6.4.

$$4H_2O(l) + 4e^- \rightarrow H_2(g) + 4OH^-(aq) \quad (6.3)$$

$$2H_2O(l) \rightarrow O_2(g) + 4H^+(aq) + 4e^- \quad (6.4)$$

The electrochemically generated H^+ and OH^- ions due to water electrolysis at the anode and cathode respectively were neutralized to form water molecules (equation 6.5) because of the OH^- and H^+ ions produced from the dissociation of the catholyte and anolyte respectively as shown in equations 6.2 and 6.1.

$$H^+(aq) + OH^-(aq) \rightarrow H_2O(l) \quad (6.5)$$

The oxygen and hydrogen gases generated may be vented out, while some amount may go into the soil and alter the redox chemistry [187]. Na^+ and NO_3^- ions migrated into the soil to the opposite electrodes thereby increasing the electrical conductivity as the treatment process progressed. A sustained and variable electroosmotic flow was observed due to the migration of the Na^+ ions, which could have enhanced the

migration of the double layer complexes toward the cathode, while nitrate ions could have been involved in complex formation with the cations [167]. This electroosmotic flow led to a decreasing volume of the anolyte and an increasing volume of the catholyte over time. Hence, refilling the anolyte was necessary even before it degraded completely. In addition, since the processing fluids are finite in volume and the electrochemical decomposition of water at the electrodes is continuous for the test duration, then, a time was reached when all the ions in the processing fluids were exhausted. Consequently, rise and fall in catholyte pH and anolyte pH respectively were expected before the complete replacement of the processing fluids. Now, OH^- ions generated at the cathode according to equation 6.3 migrated into soil toward the anode. In this migration process, soil pH rose (Figure 23) and metal hydroxides were formed which could have precipitated and reduced the electrical conductivity (Figure 24) and increased current consumption near the cathode [5]. At the same time, soluble hydroxocomplexes were formed with the cations due to the complexing property of the hydroxyl ions [65, 188]. On the other hand, hydrogen ions generated at the anode (equation 6.3) migrated toward the cathode. This process may lead to soil protonation or desorption of indigenous and spiked heavy metals, hence increasing the electrical conductivity (Figure 24) [166]. Given the presence of calcite and dolomite in the soil minerals, the developing acid front may have been buffered by the carbonate mineral, thereby hindering any fall in the soil pH (Figure 23). From the forgoing discussion, it is clear that, there was an overall increase in the soil pH and electrical conductivity (Figure 24) as the integrated electrokinetics-adsorption remediation progressed. Results obtained for electrokinetic remediation of high buffering capacity glacial till by Reddy and his co-workers [166, 168, 177, 189] have corroborated these findings. The transient nature of the acid/base front migration and

reactions may have been responsible for the lower final values of some pH and EC than the preceding 1st or 2nd week values. In addition, the electroosmotic flow (Figure 25) undoubtedly varied spatially and temporally as it also depends on the soil zeta potential, processing fluids pH, pore fluid viscosity and permittivity [175, 190-192].

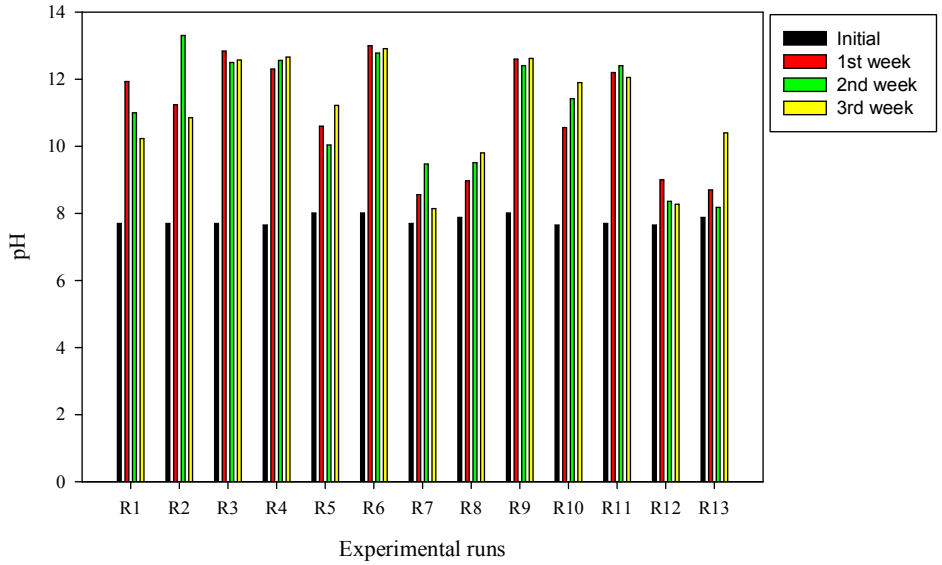

Figure 23 Weekly pH variation

It was observed from Figure 23 that the average initial soil pH after spiking was within the range 7.7 - 8, lower than the original soil pH (8.3), while the final pH ranged from 8 - 12.9. The lower initial pH was due to the acidity of the contaminant solutions, while the higher final pH values resulted from the high buffering capacity of the soil, which neutralized the generated acidic front from equation 6.4 but allowed the migration of the basic front generated from equation 6.3. Consequently, all weekly pH values were higher than the initially spiked soil pH for all the tests. Additionally, low pH rise (8 - 10.4) was observed for all the tests conducted using 0.2 V/cm (R7-8, R12-13) whereas highest pH (12.6 - 12. 9) were recorded for all tests conducted using

1 V/cm (R3-4, R6, R9) consistently. High voltage gradient led to the passage of high amount of current, which increased the rate of the electrochemical decomposition of the electrolyte and enhanced subsequent migration of the basic front into the soil. This basic front migration was responsible for raising the soil pH. This observed effect of the voltage gradient on the soil pH were successfully modeled mathematically and the coded linear model equation at 5 % significant level (0.05 p-value) is presented in equation 6.6 while the graphical presentation of the significant influential factors together with 3D response surface and contour plots are given in Figure 26 (a) and (b).

$$\text{Soil pH} = 11.07+0.097*A+1.77*B+0.39*C \quad (6.6)$$

Where A = polarity reversal, hr; B = voltage gradient, V/cm; C = concentration, mg/kg.

Anderson and Whitcomb [70] have reported that R^2 is biased, hence, a more accurate, less biased and better goodness-of-fit statistic called adjusted R^2 was computed for evaluating the model accuracy. The model's R^2 and adjusted R^2 (unbiased estimate of the coefficient of determination) were 0.7725 and 0.7105 respectively. High values of R^2 are essential for modeling the experimental design space, while in identification of significant factors R^2 value does not matter, for significant factors will remain significant [70]. It is very clear that model equation, perturbation and 3D response surface plots have shown the significant influence of voltage gradient on the soil pH over the other factors (polarity reversal rate and initial contaminant concentration). The relative contribution or effect of any given model term is directly proportional to its coefficient. Perturbation plot (Figure 26 (a)) revealed a sequence of relative

influence of the operating parameters on the target response as follows: voltage gradient > concentration > polarity reversal.

Bipolar Effects: The two treatment zones F and G contain 100 % granular activated carbon which has the potential to be used as electrode material due to its electrical conducting properties [13]. The sides of the GAC chambers facing anode and cathode electrodes tend to behave as bipolar electrodes by acting as cathode and anode while the inner sides behave as anode and cathode respectively. These bipolar electrodes would be expected to generate H^+ and OH^- ions depending on whether the side is acting as anode or cathode [2] and may be expected to alter the pH distribution in the soil profile. These bipolar effects were investigated at the end of R11 and the pH profile is presented in Figure 27. The pH profile shows the variation of pH within the unspiked chambers B and D, spiked chamber C and GAC chambers F and G. The pH ranged from 11.9 (near the anode) to 12.6 (near the cathode) which suggest that bipolar effects did not manifest due to the presence of carbonate minerals that impact high acid buffering capacity.

Sparks [35] posited that electrical conductivity (EC) is the best index for the assessment of soil salinity. As important as this parameter is, most works on electrokinetic remediation failed to at least report the soil electrical conductivity, let alone, monitor its variation over the treatment duration. Electrical conductivity greatly influences electrokinetic remediation, because it determines the amount of current flowing through the soil.

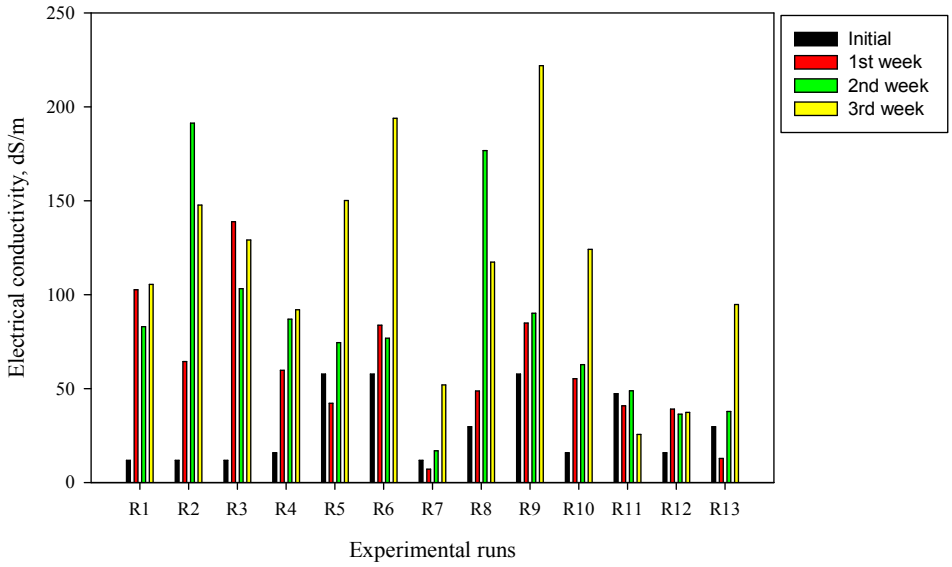

Figure 24 Weekly soil electrical conductivity variation

The usual voltage gradient of 1 V/cm for bench-scale studies [54] when applied to saline-sodic soils would lead to high electric current flow. Lukman *et al.* [188] have reported that, this would lead to excessive soil heating, reduction in the soil moisture content, high energy and process fluid consumption, high electroosmotic flow rate (Figure 25), and in some cases, higher percentage removal of contaminants. EC is simultaneously influenced by many soil properties, viz; water content, soluble salts, grain size, humus, temperature, texture and cation exchange capacity (CEC) [193]. The 1st week EC data show that tests conducted using 1 V/cm (R3, 9, 6) possessed the highest EC values with R1 (0.6 V/cm) coming second highest. No discernible trend was visible in the case of initial contaminant concentration - despite its influence on the EC as depicted in Figure 26 (c). Similar trend was observed for the 3rd week, where R9 and 6 have the highest EC values (Figure 24). A general increase of EC with time and voltage gradient (Figure 26 (c) and (d)) was observed (except for R11). The reason for this observation has been elaborately discussed above. These

variations and impacts of the influential investigated factors have been modeled and presented in the 3D response surface plot in Figure 26 (d). Perturbation plot (Figure 26 (c)) revealed a sequence of relative influence of the operating parameters on the soil electrical conductivity as follows: concentration > voltage gradient > polarity reversal.

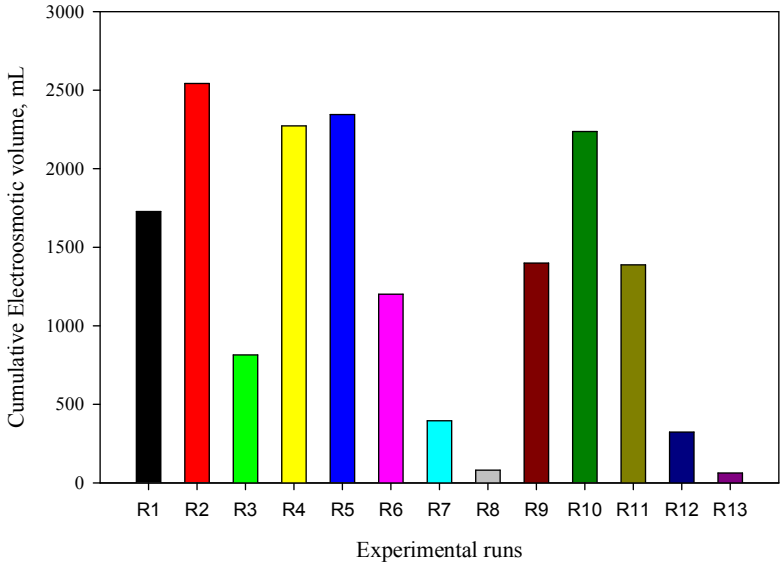

Figure 25 Cumulative electroosmotic volume for each test

Electroosmotic flow: The cumulative electroosmotic volume for all the tests presented in Figure 25 shows that R2 (20 mg/kg), R5 (60 mg/kg) and R4 (100 mg/kg) have the highest values, indicating that low contaminant concentration leads to high electroosmotic flow. Other parameters that may influence electroosmotic flow are clay zeta potential, voltage gradient, time-dependent fluid properties such as dielectric constant and viscosity [194]. Equation 6.7 shows the electroosmotic velocity as derived according to Helmholtz – Smoluchowski (H - S) theory.

$$v_e = \frac{\varepsilon_s \zeta}{\eta} E = k_e E \qquad (6.7)$$

Where

v_e = electroosmotic velocity;

ε_s = pore fluid permittivity;

η = pore fluid viscosity;

ζ = soil zeta potential;

k_e = coefficient of electroosmotic conductivity;

E = voltage gradient.

These parameters make the measured electroosmotic volume for all the tests to vary temporally. The reduction of the thickness of the diffuse double layer resulting from higher ionic concentration with subsequent higher ionic strength causes reduction in the electroosmotic flow [195], hence higher concentrations usually yield lower electroosmotic volume (Figure 25). Reddy *et al.* [195] have observed a similar trend. The electroosmotic volume usually decreased with time because of the increase in electrical conductivity with time (Figure 24) that led to higher ionic strength as the treatment proceeded. Moreover, voltage gradient has been observed to be most influential to the electroosmotic flow (Figure 28). The least electroosmotic volumes recorded belong to the lowest voltage gradient used (0.2 V/cm), that is, in the case of R7, R12, R8 and R13. This is because; high voltage gradient caused the passage of high electric current, which led to a high electromigration with subsequent substantial transfer of momentum to the surrounding pore-fluid molecules [195]. The soil zeta potential, defined as the electrical potential existing at the junction between the fixed and mobile parts of the electrical double, is influenced by the type and concentration of dissolved ions in the pore fluid in addition to the pore fluid chemistry. Clay soils,

being negatively charged, usually possess negative zeta potential. At low pH below the point of zero charge (PZC), zeta potential may become positive because of excessive protonation and increase in ionic strength resulting from increased dissolution of metal ions in the pore fluid and their subsequent adsorption onto the soil particles and compression of the electrical double layer [196]. Reversal of the zeta potential charge could reverse the direction of the electroosmotic velocity as shown in equation 6.7. At high pH values, such as those encountered in this study, deprotonation and metal hydroxide precipitation could maintain a negative zeta potential, hence, electroosmotic flow will remain unidirectional as observed in all the tests. Electroosmotic flow has not been influenced by hydraulic gradient in this study as it occurs even under negative hydraulic. Equation 6.8 presents the model equation (R^2 = 0.946 and adjusted R^2 = 0.9057) relating the electroosmotic volume to the factors. Voltage gradient appears to be the most influential, followed by polarity reversal rate and initial contaminant concentration (Figure 28 (a)). At high voltage gradient (1 V/cm), the decrease in the electroosmotic volume (Figure 28 (b)) may be attributed to the development of bubbles within the electrode chambers, due to temperature rise, which then seeps into the soil to reduce the soil saturation with subsequent reduction in the electroosmotic volume [188].

$$\text{Sqrt (Electroosmotic volume, mL)} = 49 + 2.57 * A + 11.68 * B + 1.22 * C + 5.26 * B * C - 5.34 * A^2 - 20.95 * B^2 \quad (6.8)$$

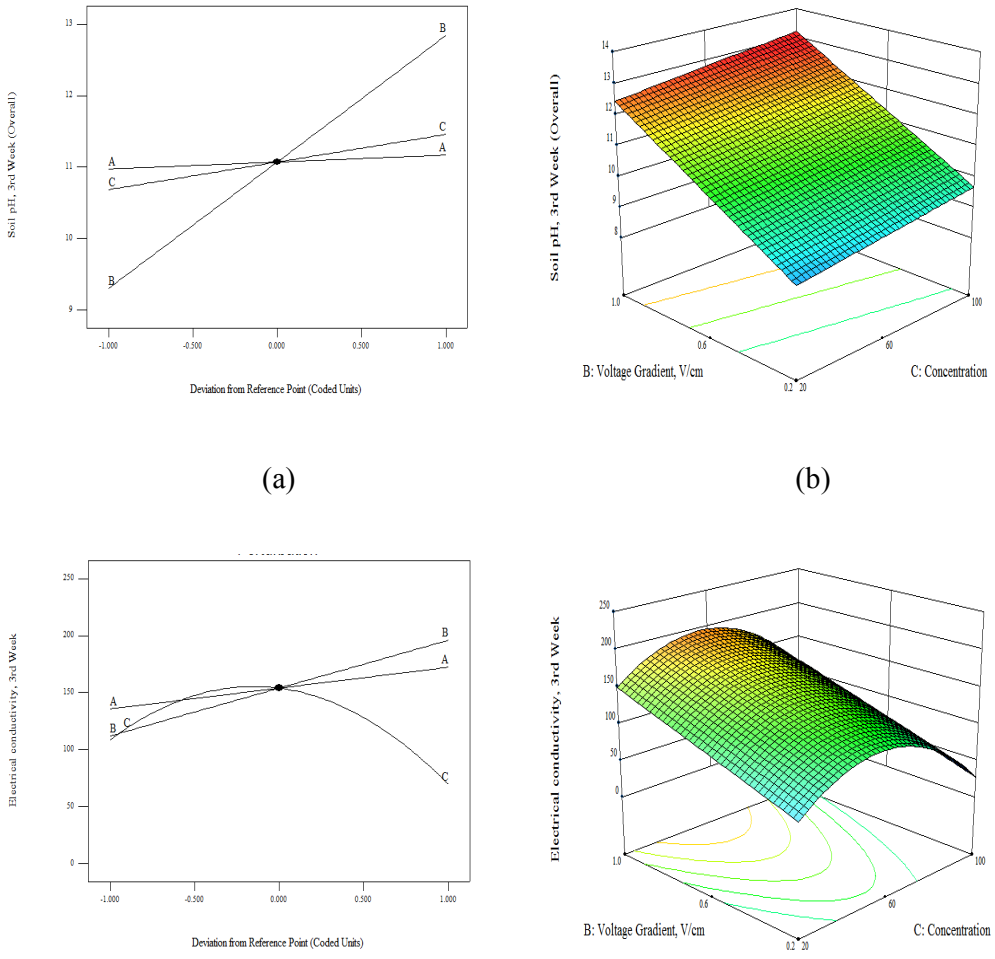

Figure 26 Perturbation plots showing the relative significance of factors on soil pH (a) and electrical conductivity (c) (left). 3D response surface and contour plots showing how the influential factors affect soil pH (b) and electrical conductivity (d) (Right)

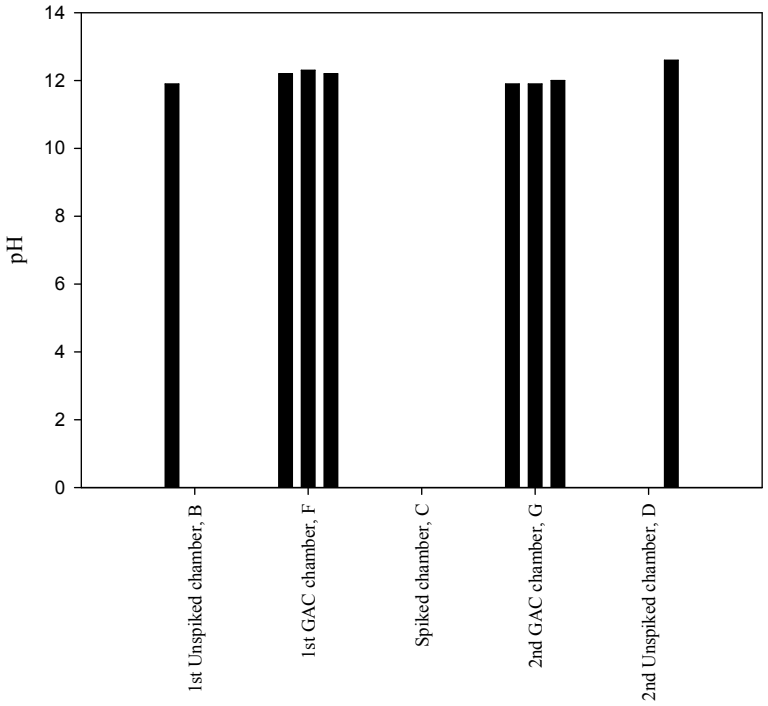

Figure 27 pH profile with two GAC treatment zones for investigating bipolar effects (R11)

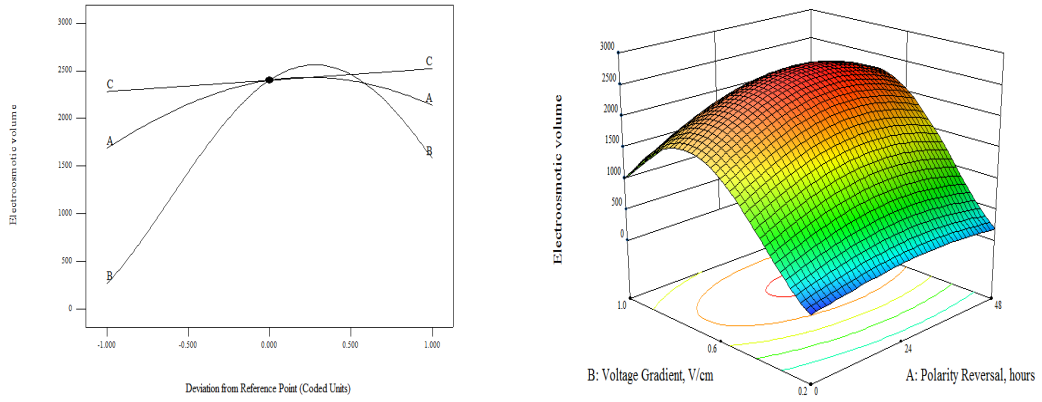

Figure 28 (a) Perturbation plot showing the relative significance of factors on electroosmotic volume. (b) 3D response surface and contour plots showing the influence of voltage gradient on cumulative electroosmotic volume

Current and Temperature: Table 14 presents the average electric current recorded for each test during the 3-week test duration in descending order of magnitude to show how it was influenced by the applied voltage gradient and how it correspondingly affected the soil pH. Clearly, the higher the voltage gradient, the more amount of current was passed through soil which resulted in rapid generation of H^+ and OH^- ions and subsequent rise in soil pH (Table 14). The current was usually low at the beginning of the tests (Figure 29 (a)), rose gradually as the tests continued and then declined, sometimes to a stable value, while in some instances, kept on fluctuating according to the time-dependent geochemical processes taking place such as ionic dissolution and precipitation, degradation of the processing fluids. Study conducted by Maturi and Reddy [31] corroborated the fluctuating current trend. Upon application of the driving force, the voltage gradient, the processing fluids and pore fluid migrated while the dissolved ions electromigrated to opposite poles. These processes led to an increase in the ionic strength of the pore fluid thereby increasing the current flow to a maximum value. The observed decline of the current to a stable value may be attributed to the electromigration of cations and anions to the respective electrode with subsequent possible precipitation of the cations due to increase in the soil pH as the test progressed [195, 197]. Temporal geochemical processes such as mineral and chemical dissolution and neutralization reactions taking place in the electrode chambers also contributed to the variation of the electric current. A maximum value of 5.13 A was recorded for R6 whose average current was 3.02 A. This current is considered extremely high, considering the fact that it is about two orders of magnitude greater than the recorded current values for other bench-scale studies that employed the Lasagna process (< 30 mA) in other soil as shown in Table 2.1. Other studies using electrokinetic remediation only using voltage gradient of 1

V/cm or higher, have reported higher values but usually less than 300 mA [189, 195, 198]. Using low voltage gradient of 0.2 V/cm has only resulted in reducing the current to about 130 – 210 mA (Table 14). This unique and important observation may be explained by the high salinity and sodicity of the investigated soil which provides large amount of dissolved salts and minerals (carbonates) in the pore fluid for sustained high electrical conduction. High current flow through the soil will significantly affect the soil temperature, electroosmotic flow rate, electrode material and processing fluids degradation, soil pH, geochemical processes, remedial efficiency and energy consumption. In a related study by Lukman *et al.* [188], they recorded a similar high current (2.8 A). To emphasize on the effect of the electric current on the soil temperature, current and temperature readings recorded using a time step of 30 min is presented in Figure 29 for R11 (voltage gradient = 0.6 V/cm). This test had 0.61 A and 28.45 ^{o}C as the average current and temperature respectively. The maximum values were 0.91 A and 34.6 ^{o}C respectively which were recorded under room temperature of 24^{o}C. It is clear from Figure 29 that low current leads to low soil temperature and vice-versa. In a preliminary study conducted by Lukman *et al.* [188] using 1 V/cm, 36.34 ^{o}C and 47 ^{o}C were the average and maximum soil temperatures, indicating that the soil becomes very hot when using 1 V/cm. While soil heating may be advantageous in increasing the volatility of organics, solubility of minerals (carbonates) and reduction in pore fluid viscosity which will increase electroosmotic flow, it may also be undesirable since it will reduce the soil moisture content due to pore fluid evaporation with subsequent reduction in current and electroosmotic flow. In addition, it will increase soil electrical conductivity and energy expenditure [2]. Previous studies have not reported significant rise of soil temperature during bench-scale tests [2]. A linear model was obtained (equation 6.9)

which relates the factors to the average electric current whose respective R^2 and adjusted R^2 are 0.9556 and 0.9435. The perturbation and response surface plots (Figure 30) also revealed the significant influence of the applied voltage gradient over initial contaminant concentration and polarity reversal rate.

$$\text{Sqrt (Average current)} = 1 + 0.020 * A + 0.59 * B - 0.059 * C \quad (6.9)$$

Table 14 Comparing electrical current with voltage gradient and soil pH for all tests

Run	Current, A	Voltage gradient, V/cm	pH
R6	3.02	1	12.9
R9	2.65	1	12.6
R3	2.25	1	12.6
R4	2.04	1	12.7
R2	1.32	0.6	10.9
R1	1.17	0.6	10.2
R10	1.12	0.6	11.9
R5	1.03	0.6	11.2
R11	0.61	0.6	12.0
R8	0.21	0.2	9.8
R12	0.15	0.2	8.3
R7	0.14	0.2	8.1
R13	0.13	0.2	10.4

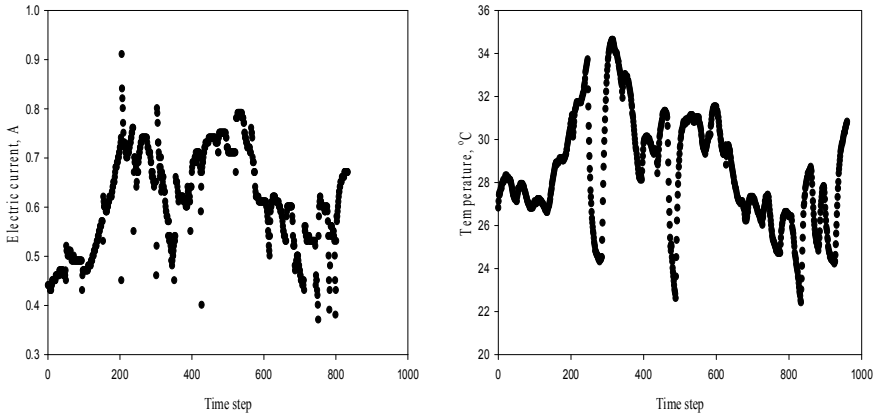

(a) (b)

Figure 29 Comparing variations of electric current with soil temperature: (a) current (b) temperature

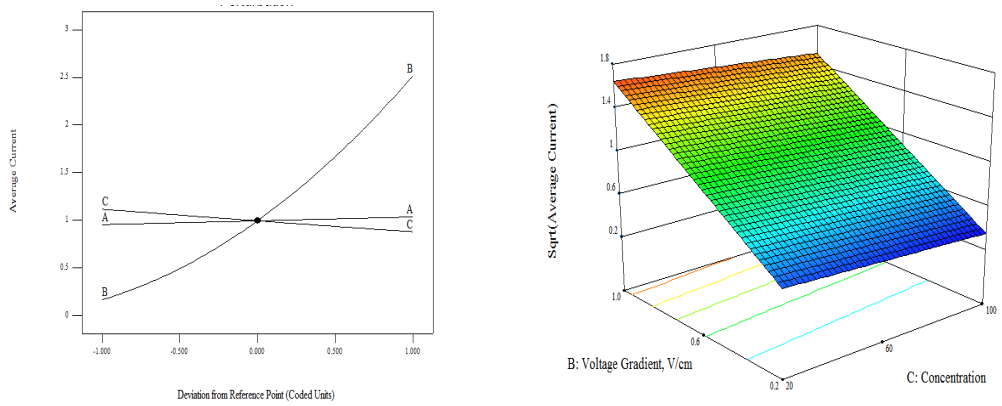

(a) (b)

Figure 30 (a) Perturbation plot showing the relative significance of factors on average electric current. (b) 3D response surface and contour plots showing the influence of voltage gradient on average electric current

6.3 Trivalent Chromium Migration, Model Validation and Optimization

Figure 31 presented the distribution and migration of trivalent Cr from the contaminated chamber, C, to the GAC chambers F and G for all the thirteen (13) tests. This migration becomes more pronounced for tests R5, R6 and R9. In the case of R6 (no polarity reversal), significant trivalent Cr migration took place from the contaminated chamber, C, to the GAC chamber, F, near the anode. This observation may be attributed to the formation of high amount of negatively charged metal hydroxocomplexes at pH 12.9, which are then attracted to the anode via electromigration but become adsorbed onto the GAC in chamber F during the transport process. Visual MINTEQ 3.0 [112] was employed to model the trivalent Cr ion speciation for R5 from the weekly monitoring data using the dissolved concentration, pH, temperature and ionic strength. The speciation diagram presented in Figure 32 reveals the increasing dominance of the negatively charged complex $Cr(OH)_4^-$ and the decreasing concentration of aqueous $Cr(OH)_3$ at pH 11.2. This

explains the greater movement of the trivalent Cr species toward the anode in R6 at pH 12.9. Pourbaix [199] and Chinthamreddy and Reddy [176] have already asserted that $Cr(OH)_4^-$ ions will become the dominant species at pH values greater than 11.8, thus, trivalent Cr solubility increases. However, under normal soil pH, trivalent Cr has limited solubility and highly adsorbs to soil [166, 176]. In a related study by Reddy and Chinthamreddy [168] which involved an alkaline and high acid buffering soil called glacial till, they did not observe significant trivalent Cr migration and no removal. Although, the soil redox state may be dynamic because of the generation of oxygen and hydrogen gases at the electrodes in addition to the possible presence of iron (reducing agent), manganese (oxidizing agent) or microorganisms that can oxidize the trivalent Cr to the hexavalent form; oxidation of trivalent Cr does not take place appreciably in high buffering capacity soil such as saline-sodic soil [167]. For this reason, hexavalent Cr was not studied. Migration of the trivalent Cr from the contaminated chamber to the GAC chambers indicated remarkable remedial efficiency for some of the tests (R5, R6 and R9) while others indicated low or no removal at all (R1-R4, R7, R10 and R12). There is zero remedial efficiency when there was accumulation of the contaminant at the sampling location thereby having the residual concentration (C_o) to be greater than the initial (C), in which case, $C_o/C > 1$. Hence Figure 31 utilized C_0/C to indicate the migration of trivalent Cr when $C_o/C < 1$ or its accumulation at any given location or chamber when $C_o/C > 1$.

The tests were sorted in decreasing order of remedial efficiency (Table 15) to reveal some salient points that will help in providing adequate connection between factors and responses. Highest remedial efficiencies (34.88 - 79.97 %) were recorded for tests involving 60 mg/kg initial trivalent Cr concentration, whereas no removal was recorded for all tests involving 20 mg/kg. Only one test involving 100 mg/kg recorded

some remedial efficiency (Table 15). Low remedial efficiency at 20 mg/kg may be attributed to the availability of adsorption sites for trivalent Cr ions coupled with the high selectivity for Cr for this particular soil type [164] at the given concentration. At higher concentrations (100 mg/kg) and pH, trivalent Cr may precipitate as $Cr(OH)_3$, thus, rendering it immobile [195]. Even with low electric current, electroosmotic flow and voltage gradient (0.2 V/cm), 34.88 % and 36.93 % of the trivalent Cr was removed from the contaminated chamber in tests R13 and R8 respectively. Polarity reversal rate did not show any discernible pattern. Hence, there is need for simultaneous optimization of these three factors for optimal removal of the trivalent Cr.

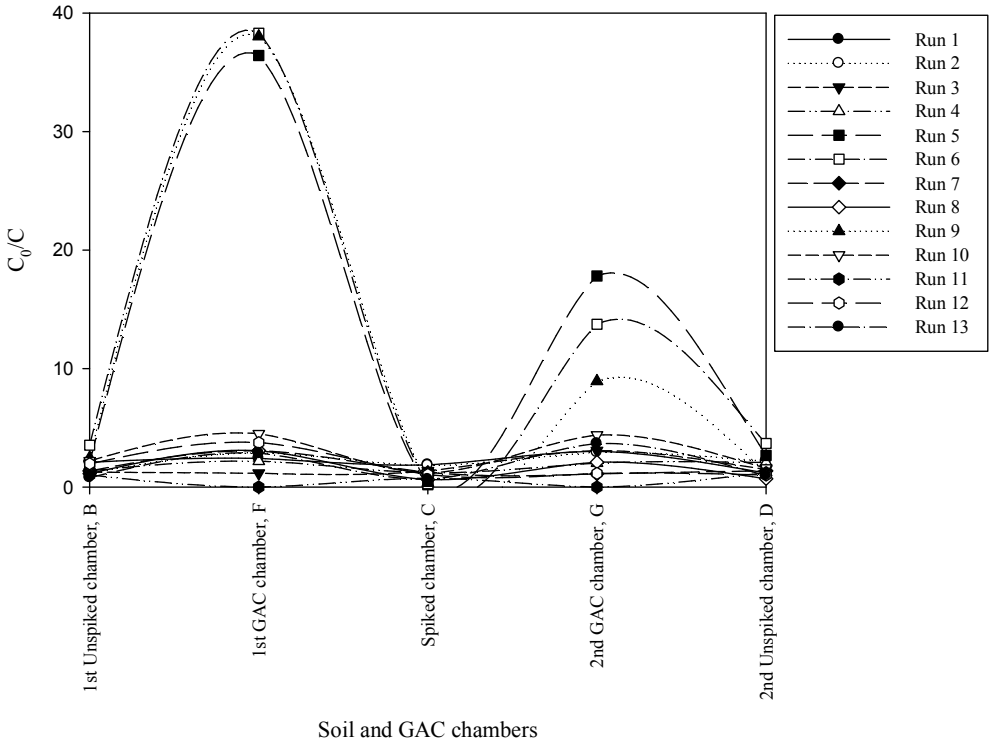

Figure 31 Trivalent Cr distribution and migration from the contaminated chamber to the GAC chambers after 13 tests

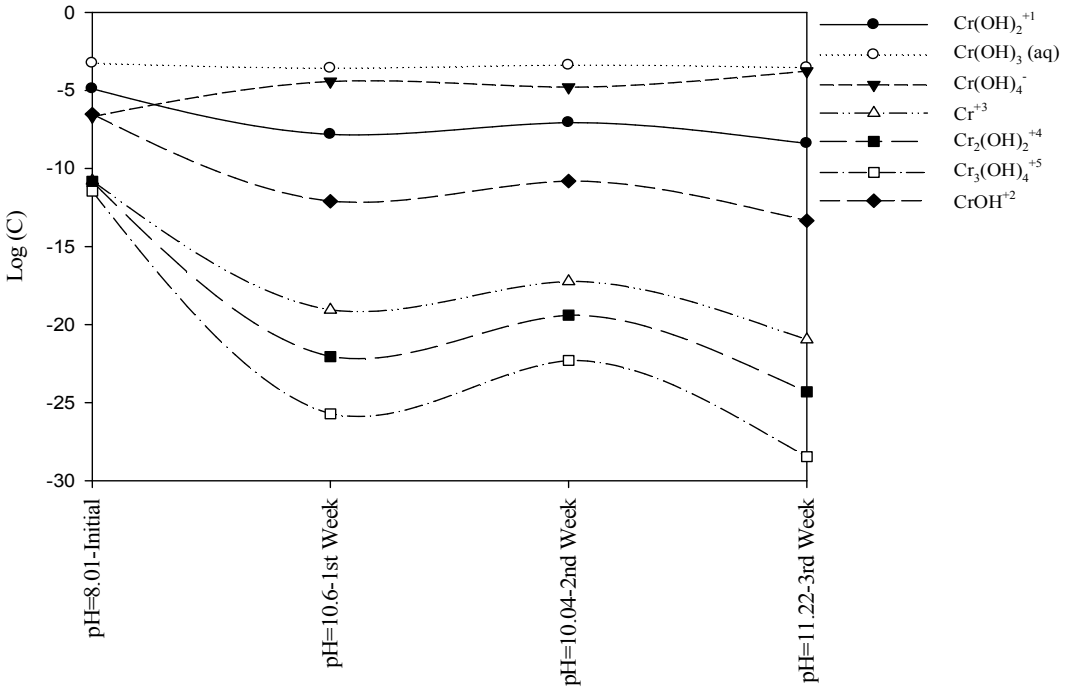

Figure 32 Speciation diagram for trivalent Cr species at different weekly pH values

It is important to note that high voltage gradient (1 V/cm) or passage of high electric current does not necessarily translate into high remedial efficiency but will definitely increase the energy expenditure. At high voltage gradient, current is high, leading to high electroosmotic flow toward cathode. This opposite flow may interfere with the electromigration of the anionic trivalent Cr species that are migrating toward the anode, thus, reducing the overall remedial efficiency. Electromigration constitute the major transport mechanism for charged species whose rate is 10 – 300 times higher than the advective electroosmotic transport [9]. At low voltage gradient (0.2 V/cm), extremely low electroosmotic flow takes place and sustained electromigration prevails. The weekly percentage removal of trivalent Cr from the contaminated

chamber is presented in Figure 33. The dynamic and temporal changes in the geochemical processes controlling the contaminant removal are attributable to the observed trends in the weekly percentage removal.

Table 15 Comparing trivalent Cr remedial efficiency with factors and some responses

Runs	Remedial efficiency, %	Current, A	Residual pH	Electroosmotic volume, mL	Polarity reversal rate, hr	Voltage gradient, V/cm	Initial Cr concentration, mg/L
R5	79.97	1.03	11.2	2344.50	24	0.6	60
R6	72.73	3.02	12.9	1201.50	0	1	60
R9	65.66	2.65	12.6	1399.50	48	1	60
R8	36.93	0.21	9.8	81.00	0	0.2	60
R13	34.88	0.13	10.4	63.00	48	0.2	60
R11	25.50	0.61	12.0	1387.84	0	0.6	100
R1	0.00	1.17	10.2	1728.00	0	0.6	20
R2	0.00	1.32	10.9	2542.50	48	0.6	20
R3	0.00	2.25	12.6	814.50	24	1	20
R4	0.00	2.04	12.7	2272.50	24	1	100
R7	0.00	0.14	8.1	396.00	24	0.2	20
R10	0.00	1.12	11.9	2236.50	48	0.6	100
R12	0.00	0.15	8.3	324.00	24	0.2	100

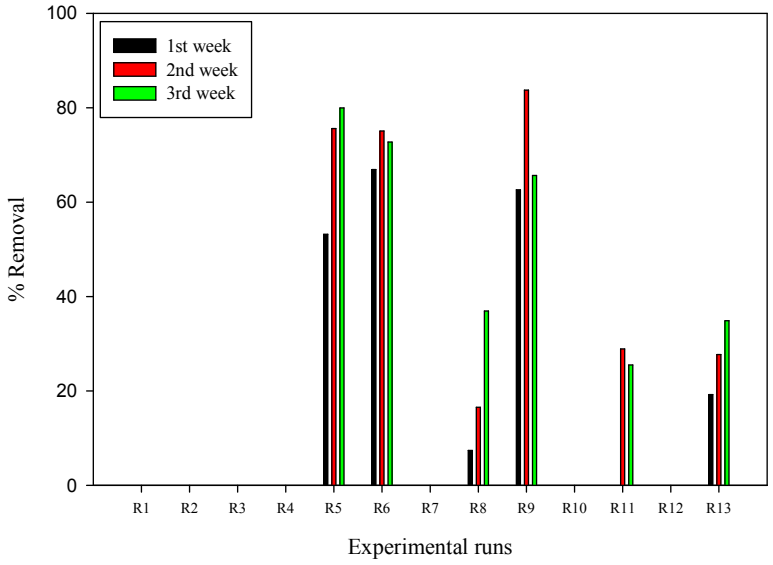

Figure 33 Weekly percentage removal of trivalent Cr for 13 tests

Equation 6.10 relates the investigated factors to the remedial efficiency with 0.9335 and 0.8966 as the R^2 and adjusted R^2 values respectively.

$$\text{Sqrt (Cr, remedial efficiency)} = 8.78 - 0.71 * A + 0.58 * B + 0.63 * C - 1.50 * B^2 - 7.39 * C^2 \quad (6.10)$$

Perturbation plot (Figure 34 (a)) also supports the observed influence of the initial Cr concentration on the remedial efficiency, followed by voltage gradient, then, polarity reversal rate. The investigated factor levels can be used to determine the optimal conditions required to achieve maximum remedial efficiency as depicted in the 3D response surface plot (Figure 34 (b)).

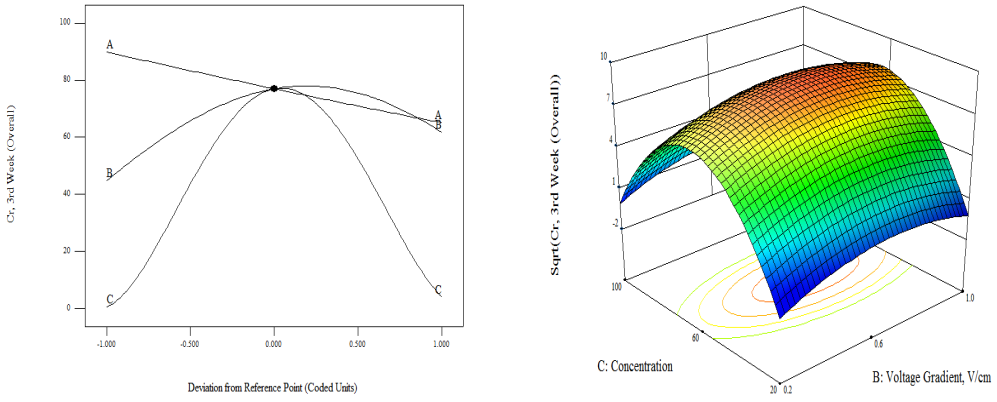

(a) (b)

Figure 34 (a) Perturbation plot showing the relative significance of factors on trivalent Cr remedial efficiency. (b) 3D response surface and contour plots showing the influence of initial contaminant concentration on trivalent Cr remedial efficiency

Model Validation: To validate the practical applicability of the developed models affecting the remedial efficiency (equation 6.10) and soil pH (equation 6.6), an additional experimental test was run at a voltage gradient of 1 V/cm, initial contaminant concentration of 44.15 mg/kg and without polarity reversal (Table 16).

Results of the model validation showed that the experimental results lie within 90 % confidence interval (CI) and prediction interval (PI) with associated prediction error of 2.35 % and 32.64 % for soil pH and remedial efficiency respectively. Since the validation results fall within the prediction interval, then, the outcome of the confirmation test was a success [70]. Hence, the models can provide good approximations necessary to move in the proper direction.

Table 16 Experimental validation of trivalent Cr remedial efficiency and soil pH using voltage gradient = 1V/cm; average concentration = 44.15 mg/kg; polarity reversal rate = 0 hr

Response	Experimental result	Model prediction	Prediction error, %	90% CI* low	90% CI high	90% PI** low	90% PI high
Cr, Remedial efficiency	75.88	51.11	32.64	31.17	75.95	18.36	100.00
Residual soil pH	12.3	12.6	2.35	11.7	13.5	10.8	14.0

*Confidence interval; **Prediction interval

Optimization of Trivalent Chromium Removal: Numerical optimization was employed here to find the optimal factor levels that will specifically target maximum remedial efficiency of trivalent Cr while optimizing all the other contaminant remedial efficiencies and responses (Figure 35). An overall Desirability value of 0.715 was obtained and its variation based on the influential factors (initial concentration and voltage gradient) is depicted in Figure 36. Optimal conditions required to achieve effective trivalent Cr removal at 60 mg/kg are presented in Table 17. Overall Desirability of 0.715 was attained at the following optimal conditions: voltage gradient = 0.36 V/cm; polarity reversal rate = 17.63 hr; soil pH = 10.0. Under these conditions, the expected trivalent Cr remedial efficiency was 64.75 %.

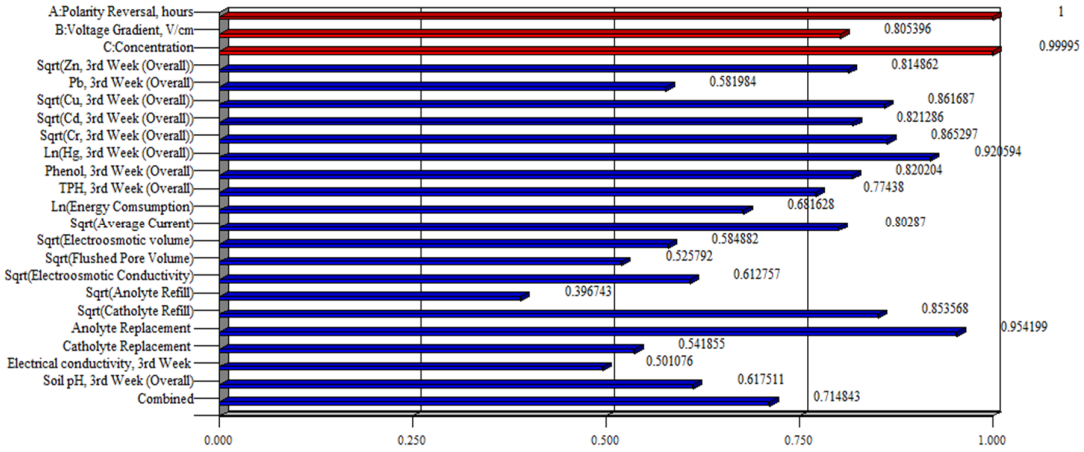

Figure 35 Combined and individual response Desirability values for all responses and factors

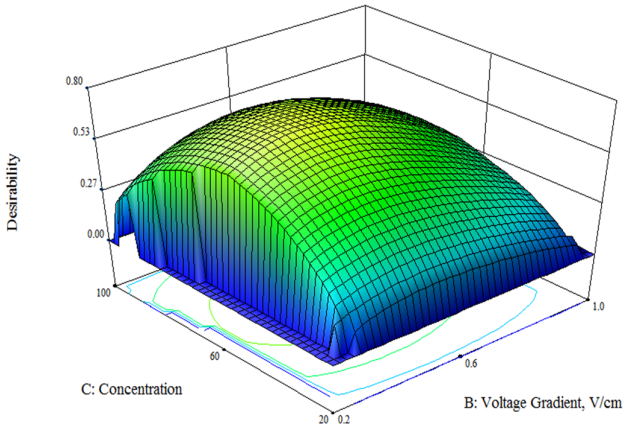

Figure 36 3D surface plot of the overall Desirability variation relative to influential factors

Table 4.8

Table 17 Optimal factor levels required to maximize remedial efficiency of trivalent Cr

Item	Value
Polarity reversal, hours	17.63
Voltage gradient, V/cm	0.36
Concentration, mg/kg	60.00
Expected remedial efficiency of trivalent Cr	64.75
Expected residual soil pH	10.00
Desirability	0.715

6.4 Impacts of the Integrated Electrokinetic Remediation on Soil Physico-Chemical Properties

Preceding sections have elaborately discussed and modeled the impacts of the proposed remediation technique on the soil pH and electrical conductivity. Additionally, the passage of electric current and soil pH gradients [5, 184-186] will result in the following physico-chemical interactions: (1) Possible dissolution of the clay minerals beyond a pH range of 7 - 9; (2) dissolution of available soil salts such as carbonates; (3) production of cementitious products resulting from the precipitation of metal ions at pH values corresponding to their hydroxide solubility values; and (4) soil structural changes which affects its engineering characteristics [5]. Surface area, pore volume and size (Table 18), mineralogical compositions (Table 19) and elemental constituents (Table 20) were analyzed, before and after the test for R5. At the end of the test (pH = 11.2), the soil specific surface area increased (9.07 to 11.21 m^2/g) with corresponding increase in the pore volume and size. These results have confirmed that some dissolution of the soil minerals took place during the electrokinetic remediation process due to variations in the pore fluid chemistry. Soil pores are due to the presence of interlayer spaces that become prominent in 2:1 clay mineral types such as montmorillonite and smectite [35, 165, 200]. Table 19 presents the mineral transformation where dolomite completely disappeared; calcite and quartz

were altered and degraded respectively, after the test. The constituent soil elements were not spared as the amount of each one either increased or decreased after the test as shown in Table 20. These observations may be explained by microbially-driven biotransformation processes involving dissolution and precipitation, which take place under both aerobic and anaerobic conditions. This leads to mineral dissolution and formation of new minerals from aqueous ions (biomineralization) as noticed in Table 19 [165]. Yong *et al*. [165] have asserted that the scientific basis for biomineralization is still not well understood.

Table 18 Values of soil surface area, pore volume and size, before and after treatment

Description	BET* Surface area, m^2/g	Pore volume, cm^3/g	Pore size, Å
Before	9.07	0.014	62.55
After	11.21	0.045	163.24

*BET - Brunauer-Emmett-Teller

Table 19 Soil mineralogical transformations before and after treatment

Phase name	Before, %	After, %
Quartz, SiO_2	87.4	55.3
Calcite, $CaCO_3$	5.2	44.7
Dolomite, $CaMg(CO_3)_2$	7.4	-

Table 20 Values of constituent soil elements, before and after treatment

Element	Before, %	After, %
Ca	37.64	42.06
Si	34.73	23.42
Fe	10.41	15.06
Al	7.6	9.55
K	3.42	4.61
Mg	2.48	2.49
Pd	2.85	1.46
Ti	0.86	1.35

6.5 Conclusion

The study reported herein, investigated the migration of trivalent Cr ions from a multiple contaminated natural saline-sodic soil. The soil salinity and sodicity, which provided large amount of dissolved salts and minerals (carbonates) in the pore fluid for sustained high electrical conduction, were responsible for the extremely high electric current flow. This led to excessive soil heating, high energy and process fluid consumption, high electroosmotic volume, and in some cases, higher percentage removal of trivalent Cr. Significant migration of Cr from the contaminated chamber to the granular activated carbon chamber was recorded which led to highest remedial efficiencies (79.97 – 34.88 %) for tests involving 60 mg/kg initial trivalent Cr concentration, whereas no removal was recorded for all tests involving 20 mg/kg. Even under low electric current, electroosmotic flow and voltage gradient (0.2 V/cm), up to 36.93 % of the trivalent Cr was removed from the contaminated chamber. It has been shown that high voltage gradient (1 V/cm) or passage of high electric current does not necessarily translate into high remedial efficiency. Bipolar effects did not manifest due to the presence of carbonate minerals that impact high acid buffering capacity. For test without polarity reversal, trivalent Cr moved toward the anode due to the formation of high amount of anionic $Cr(OH)_4^-$ hydroxocomplex at high pH, which was further attracted to the anode via electromigration. Non-adsorption of this ion onto the negatively charged clay soil due to the possession of a similar charge increased its availability and mobility. Speciation modeling using Visual MINTEQ 3.0 reveals the increasing dominance of the anionic $Cr(OH)_4^-$ and the decreasing concentration of aqueous $Cr(OH)_3$ at pH 11.2. Effects of voltage gradient, initial contaminant concentration and polarity reversal rate on the effective removal of Cr

ions were experimentally studied using the Box-Behnken Design of experiment and mathematically modeled and numerically optimized using Response Surface Methodology. Results of the model validation showed that the experimental results lie within 90 % confidence interval and prediction interval with associated prediction error of 2.35 % and 32.64 % for soil pH and trivalent Cr remedial efficiency respectively. Overall Desirability of 0.715 was attained at the following optimal conditions: voltage gradient = 0.36 V/cm; polarity reversal rate = 17.63 hr; soil pH = 10.0. Under these conditions, the expected trivalent Cr remedial efficiency was 64.75 %. Passage of electric current and variations in the pore fluid chemistry led to soil mineral dissolution and alteration via biotransformation.

CHAPTER 7

APPLICATION OF NUMERICAL OPTIMIZATION TO CADMIUM REMOVAL FROM SALINE-SODIC SOIL

7.1 Introduction

In situ treatment technologies for contaminated soils and groundwater has been the subject of a great deal of research in the last three decades owing to their attendant advantages; potential lower cost, less environmental disruption and reduction in worker exposure to hazardous materials [13, 195]. Particularly, synergistic coupling of electrokinetics (EK) with other remediation techniques such as adsorption, bioremediation or advanced oxidation has been found to have an edge over all other promising in situ treatments when applied to low permeability soils present at many contaminated sites [12, 17, 188]. Of particular note, is the successful integration of electrokinetics with adsorption, popularly called the Lasagna process, for remediating soils contaminated by single or multiple contaminants under field, pilot and bench scales [12, 13, 188]. These contaminants may be heavy metals, polar and nonpolar organics, radionuclides, any charged cationic or anionic species or any combination thereof.

Electrokinetic remediation depends on the application of low DC voltage to mobilize and transport contaminants from the contaminated section to the treatment zones for in situ treatment or collection points for ex situ treatment. Other factors affecting

contaminant migration include polarity reversal and initial contaminant concentration and soil type in addition to the following geochemical processes: migration of acid and base fronts and reactions, dissolution and precipitation of metallic ions, oxidation and reduction (redox) reactions, complexation and ionic speciation [175, 194]. The operating variables such as voltage gradient and polarity reversal have significant influence on the geochemical processes, energy expenditure and contaminant remedial efficiency. These characteristics make application of optimal voltage gradient and effective remediation of saline-sodic soils very challenging. There is need to study these operating variables using modeling and optimization approaches to understand their impacts on contaminant remedial efficiency, energy expenditure, electroosmotic conductivity, soil electrical conductivity and pH. To this end, empirical modeling using Response Surface Methodology (RSM) offers great and numerous advantages. - large amount of information from a small number of experiments, evaluation of simultaneous interaction effects of the independent parameters on the responses and simultaneous optimization of multiple factors and responses for obtaining optimal conditions [68, 69]. The traditional one-factor-at-a-time (OFAT) optimization approach will never uncover interactions of factors which is the key success of RSM [70]. Hence, investigating the effects of the operating factors on the removal of mixed contaminants using several responses to arrive at optimal conditions is an invaluable effort. In this study, the interaction effects of voltage gradient, initial contaminant concentration and polarity reversal rate on the effective removal of Cd ions from a multiple contaminated natural saline-sodic soil were experimentally studied using the Box-Behnken Design. Mathematical model development and numerical optimization using RSM for elaborate investigations into

optimal conditions for factors and responses that will reduce the cost of the integrated electrokinetics-adsorption remediation of the contaminated soil were carried out.

7.2 Results and Discussions

7.2.1 Heavy Metal Migration and Removal

Results presented in Table 21 have shown remarkable remedial efficiency for some of the tests while others indicated low or no removal at all. Zero remedial efficiency implies that the initial and final Cd concentrations are the same, as such, the ratio of the residual (C_0) to initial concentration (C) will be unity (1) or there was accumulation of the contaminant at the sampling location thereby making the final concentration to be greater than the initial in which case $C_0/C > 1$. Of particular note, are those tests involving 20 mg/kg all have zero remedial efficiency. It is expected that a higher initial contaminant concentration will lead to a higher remedial efficiency due to possible saturation of the adsorption sites on the soil minerals.

Table 21 Design of experimental runs using the Box-Behnken Design

Run order	Polarity reversal, A	Voltage gradient, B	Concentration, C	3rd Week remedial efficiency, %
1	24	0.6	60	91.99
2	0	0.2	60	18.16
3	0	0.6	20	0.00
4	48	0.6	20	0.00
5	24	0.6	60	82.79
6	48	0.2	60	0.00
7	24	0.6	60	96.50
8	48	1	60	0.00
9	24	1	20	0.00
10	24	0.2	20	0.00
11	24	0.2	100	1.47
12	0	1	60	28.60
13	0	0.6	100	40.33
14	48	0.6	100	0.00
15	24	1	100	28.79

Table 22 Assignment of goals, importance and weight to factors and responses for 8 scenarios

Scenarios	Optimization parameters & goals						
	Cd removal efficiency	Factors, A, B, C	Energy consumed	Other contaminants*	Other responses**	Weight	Importance
Case 1	maximize	in range	-	-	-	default - 1	default - 3
Case 2	maximize	A-in range; B-min; C-max	-	-	-	default - 1	default - 3
Case 3	maximize	A-in range; B-min; C-max	minimize	-	-	default - 1	default - 3
Case 4	maximize	A-in range; B-min; C-max	minimize	-	-	Energy-10	Energy + Cd - 5
Case 5	maximize	A-in range; B-min; C-max	minimize	in range	-	Energy-10	Energy + Cd - 5
Case 6	maximize	A-in range; B-min; C-max	minimize	maximize	-	Energy-10	Energy + Cd - 5
Case 7	maximize	A-in range; B-min; C-max	minimize	maximize	-	Energy-10	Energy + All contaminants - 5
Case 8	maximize	A-in range; B-min; C-max	minimize	maximize	optimize***	Energy-10	Energy + All contaminants - 5

*Zn, Pb, Cu, Cr, Phenol, TPH (total petroleum hydrocarbon) (3rd week)

**Zn, Pb, Cu, Cd, Cr, Hg (2nd week), average current, electroosmotic volume (EOV), flushed pore volume (PV), electroosmotic conductivity (k_e), anolyte refill, catholyte refill, anolyte replacement, catholyte replacement, electrical conductivity (EC) (2nd & 3rd weeks), soil pH (2nd & 3rd weeks).

***Maximize: Contaminant removal efficiencies, EOV, PV, k_e - minimize: replacement & refill of processing fluids, EC, soil pH

Low remedial efficiency at 20 mg/kg may be attributed to the availability of adsorption sites for Cd ions coupled with the high selectivity for Cd for this particular soil type at the given concentration [164, 195]. However, Reddy et al. [195] found that Cd migration and removal was lower at concentrations greater than 250 mg/kg. Figure 37 illustrates heavy metals mobilization and subsequent migration from the soil chambers to the GAC chambers. Unspiked chambers B and D border the anode and cathode respectively. Most of these metal ions (Cd, Hg, Cu, Zn) migrated significantly from the contaminated chamber to the GAC chamber toward the anode. This significant migration from the contaminated chamber toward the anode could be attributed to the formation of a high amount of negatively charged metal hydroxocomplexes at pH 12 which are then attracted to the anode via electromigration but become adsorbed onto the GAC during the transport process. Visual MINTEQ 3.0 [112] was employed to model the metal ion speciation after the test (Run 13) using their dissolved concentration, pH, temperature and ionic strength. The speciation result presented in Table 23 suggests the dominance of the negatively charged hydroxocomplexes which explains the movement of these ions toward the anode.

While Figure 37 utilized C_0/C to indicate the migration ($C_0/C < 1$) or accumulation ($C_0/C > 1$) of contaminants at any given location or chamber, Table 24 provides the actual initial and final concentrations of these contaminants in each chamber which enable the computation of the mass balance for each heavy metal ion. Good mass balance was obtained for some heavy metals like Cu (94.57 %) and Zn (85.90 %) and low for Hg (33.94 %). Several reasons have been put forward by previous investigators to explain the discrepancies in mass balance that is sometimes encountered during electrokinetic remediation [168, 195, 201] - some of the major reasons identified have been the contaminant adsorption onto the electrode and

Geotextile materials (which houses the GAC in the two chambers) and non-uniform distribution of contaminants within the small soil sample (about 2 g) which was taken for acid digestion and analysis. Also noted from Table 24 is the presence of some indigenous heavy metals in the natural unspiked soil and GAC which, in most cases, migrated away from their original locations to the GAC or electrode chambers.

7.2.2 Mathematical Modeling Using Response Surface Methodology (RSM)

Following the preliminary evaluation of the design using variance inflation factor and leverage which checked for orthogonality and the potential of a design point to significantly influence the model fit respectively, results obtained from the fifteen (15) tests presented in Table 21 were fitted to a quadratic model (equation 3.10). The response data were transformed using square root power transformation following the Box-Cox plot from the Design-Expert® program which suggested that power transformation be carried out. However, only significant model interaction effects based on 5 % significant level (i.e. $p < 0.05$) are included in the model equation (Table 5. 8), hence the term reduced quadratic model signifies dropping some insignificant model terms from the quadratic model equation. This will help improve the model prediction accuracy by increasing the adjusted and predicted R^2 [70].

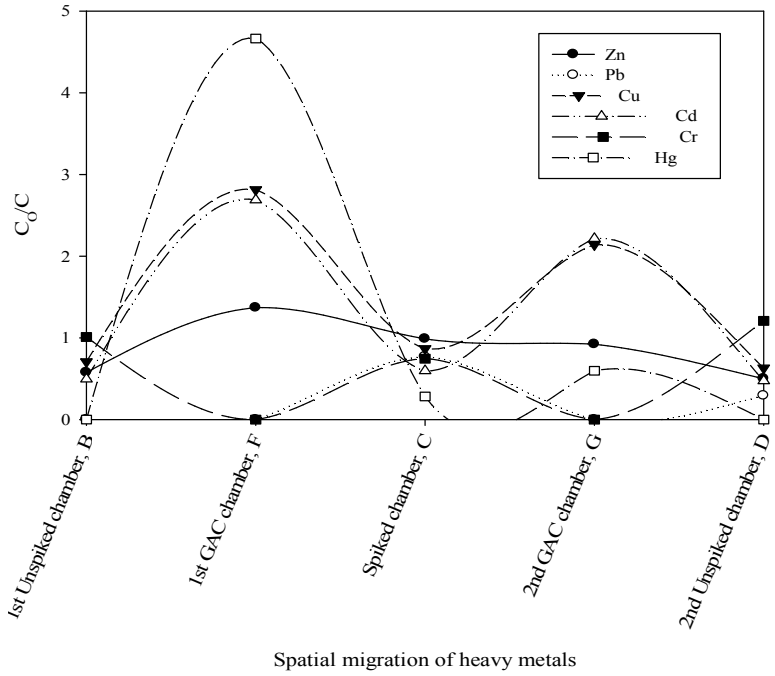

Figure 37 Heavy metal migration from the contaminated chamber to the GAC chambers

Table 23 Metal ion speciation using Visual MINTEQ 3.0 at pH 12

Component	Species formula	% of total concentration
$Hg(OH)_2$	$Hg(OH)_2$	100
Zn^{+2}	$Zn(OH)_2$ (aq)	19.229
	$Zn(OH)_3^-$	66.904
	$Zn(OH)_4^{-2}$	13.864
Pb^{+2}	$PbOH^+$	0.03
	$Pb(OH)_2$ (aq)	8.329
	$Pb(OH)_3^-$	91.64
Cu^{+2}	$Cu(OH)_4^{-2}$	14.202
	$Cu(OH)_3^-$	83.28
	$Cu(OH)_2$ (aq)	2.516
Cd^{+2}	Cd^{+2}	0.025
	$CdOH^+$	1.764
	$Cd(OH)_2$ (aq)	88.541
	$Cd(OH)_3^-$	9.542
	$Cd(OH)_4^{-2}$	0.127
$Cr(OH)_2^{+1}$	$Cr(OH)_3$ (aq)	20.883
	$Cr(OH)_4^-$	79.117

Table 24 Sample mass balance (Run 13) for the heavy metals

Spiked chamber, C - Run 13						
Contaminants,	Zn	Pb	Cu	Cd	Cr	Hg
Initial concentration, mg/kg	91.45	97.85	76.65	98.45	77.95	127.92
Residual concentration, mg/kg	90.38	75.23	66.50	58.75	58.08	36.14
1st Unspiked chamber, B						
Initial concentration, mg/kg	14.35	22.90	8.05	16.10	12.65	0.00
Residual concentration, mg/kg	8.28	0.00	5.70	7.98	12.79	0.00
2nd Unspiked chamber, D						
Initial concentration, mg/kg	14.35	22.90	8.05	16.10	12.65	0.00
Residual concentration, mg/kg	7.18	6.70	5.075	7.63	15.28	0.00
1st GAC chamber, F						
Initial concentration, mg/kg	4.88	0.00	3.83	4.13	6.90	2.23
Residual concentration, mg/kg	6.68	0.00	10.775	11.10	0.00	10.40
2nd GAC chamber, G						
Initial concentration, mg/kg	4.88	0.00	3.83	4.13	6.90	2.23
Residual concentration, mg/kg	4.50	0.00	8.20	9.15	0.00	1.33
Mass balance, %	85.90	36.92	94.57	55.00	60.36	33.94

The analysis of variance (ANOVA) given in Table 25 shows that the model and given model terms (linear, interaction and curvature) are significant with an associated insignificant lack of fit. Lack of fit (LoF) is important in determining the variation of

the data around the fitted model; hence, it is required to be insignificant for the model to fit the data well. Positive and negative coefficients in the coded response function indicate synergistic and antagonistic effects respectively. Moreover, the relative contribution of any given model term may be directly proportional to its coefficient.

Sqrt (Cd remedial efficiency) = 9.5 -1.99 * A + 0.65 * B + 1.62 * C - 1.59 * A * C + 1.04 * B * C - 3.58 * A^2 - 3.52 * B^2 - 4.34 * C^2 (7.1)

Where A = polarity reversal, hr; B = voltage gradient, V/cm; C = concentration, mg/kg.

Equation 7.1 is written out using coded factors, as such, direct substitution of the actual factor levels or values is not possible without decodification. Equation 7.2 is used to convert the actual factor levels to the coded ones prior to substitution into equation 3.10 for any response predictive purpose.

$$x_i = \frac{X_i - \frac{\left(X_{high} + X_{low}\right)}{2}}{\frac{\left(X_{high} - X_{low}\right)}{2}} \qquad (7.2)$$

Where x_i = new coded value; X_i = actual value from data whose range is X_{low} - X_{high}.

Table 26 presents statistical parameters necessary for evaluating the model quality and prediction ability. Anderson and Whitcomb [70] reported that R^2 is biased, hence, a more accurate, less biased and better goodness-of-fit statistic called adjusted R^2 was computed for evaluating the model accuracy. Adjusted R^2 value was high (0.9666) and had to differ from the predicted R^2 by at most 0.2 to ensure absence of outliers in the data set.

Table 25 Significant levels of model, lack of fit and individual model terms at 5 % ($p < 0.05$)

ANOVA for Response Surface Reduced Quadratic Model						
Source	Sum of Squares	df	Mean Square	F Value	p-value Prob > F	
Model	211.79	8	26.47	51.61	< 0.0001	**significant**
A-Polarity Reversal, hours	31.84	1	31.84	62.06	0.0002	
B-Voltage Gradient, V/cm	3.43	1	3.43	6.69	0.0415	
C-Concentration	20.90	1	20.90	40.73	0.0007	
AC	10.08	1	10.08	19.65	0.0044	
BC	4.31	1	4.31	8.40	0.0274	
A^2	47.31	1	47.31	92.23	< 0.0001	
B^2	45.81	1	45.81	89.31	< 0.0001	
C^2	69.46	1	69.46	135.40	< 0.0001	
Residual	3.08	6	0.51			
Lack of Fit	2.80	4	0.70	5.12	0.1699	**not significant**
Pure Error	0.27	2	0.14			
Cor Total	214.87	14				

Adequate precision gives a measure of signal to noise ratio (≥ 4) while predicted residual error sum of squares provides a measure of how the developed model fits each point in the design.

Table 26 Some salient characteristics of the overall Cd removal model

R^2	Adjusted R^2	Predicted R^2	Adequate Precision	Standard deviation	Mean	*C.V., %	**PRESS
0.9857	0.9666	0.8747	17.92	0.72	3.40	21.04	26.93

*C.V. – Coefficient of variation; **PRESS – Predicted residual sum of squares

7.2.3 Model Diagnostics

Figure 38 presents the normal plot of residuals which is used to check the ANOVA assumption for normality of residuals. The points are expected to follow a straight line if the residuals follow a normal distribution [70]. However, some scatter is usually expected even with normal data. For an untransformed data which shows some definite patterns, then, transformation of the response data may yield better analysis results. To test the assumption of constant variance inherent in the ANOVA, a plot of the residuals versus the ascending predicted response (Figure 39) is used. While a random scatter is desirable, similar to the one presented in Figure 39, an expanding variance with megaphone pattern indicates possible need for response transformation. A random scatter is needed in the plot of residuals versus the experimental run order presented in Figure 40 to eliminate the existence of lurking variables that may have influenced the response during the experiment which were not included in the study. Any trend could indicate the presence of a time-related lurking variable capable of ruining the analysis. Randomization and blocking will eliminate such lurking variables. Given the adjusted R^2 in Table 26, a high model prediction accuracy is expected as shown in Figure 41. Even distribution of points on either side of the straight line demonstrates good ability of the model in predicting the actual responses.

It has the advantage of detecting a value or group of values that the model will have some difficulty in predicting. Figure 42 helps to detect the presence of outliers (points lying outside the boundary straight lines) in the data which mostly occur due to typographical errors and mistakes or imperfections during experimental run or analysis that lead to collection of wrong data point. Outliers do not fit well to models. Though several conditions could indicate the need for data transformation as highlighted above, the specific test that checks the need for data transformation is the Box-Cox plot [202] presented in Figure 43. If the lambda value lies within the 95 % confidence interval, then, no transformation is needed. Already, square root transformation was carried out on the response data to bring the lambda value within the 95 % confidence interval as shown in Figure 43.

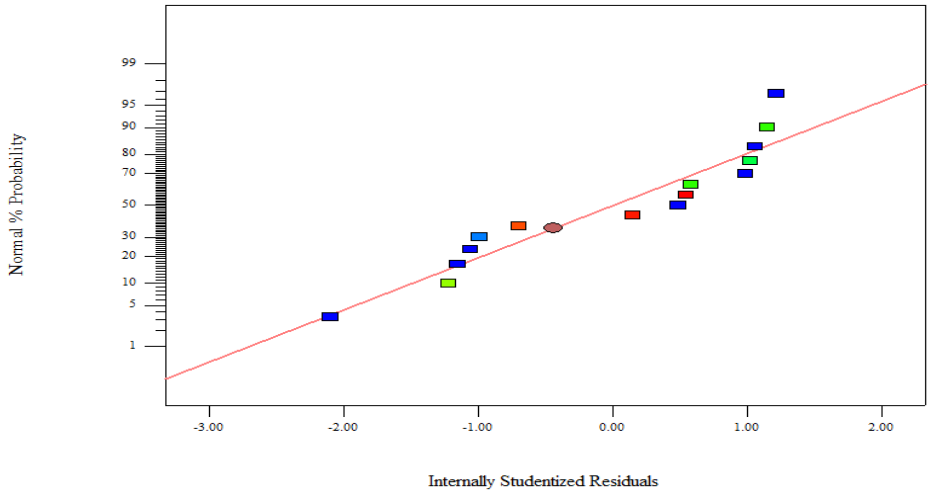

Figure 38 Normal plot of residuals for normality check

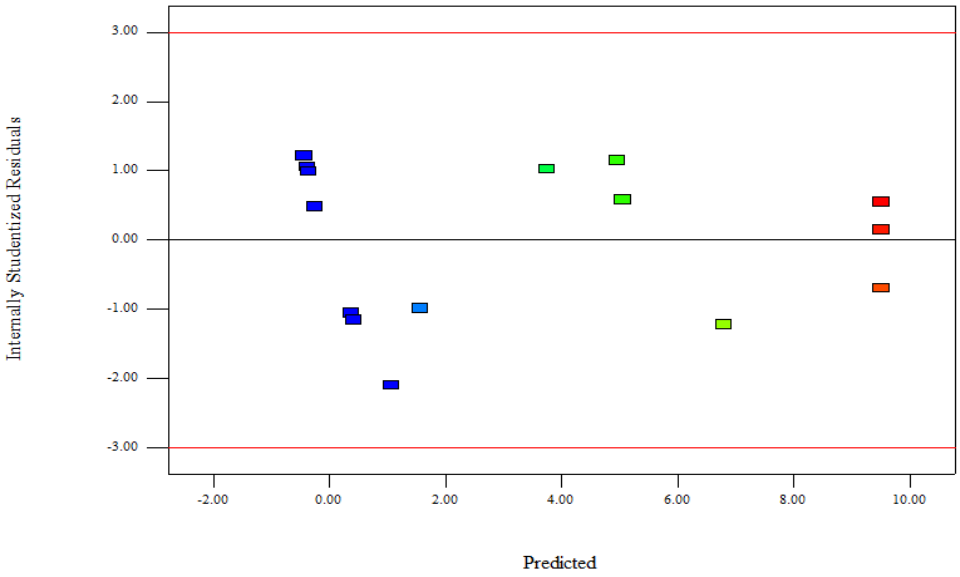

Figure 39 Plot of residuals versus predicted response for constant variance check

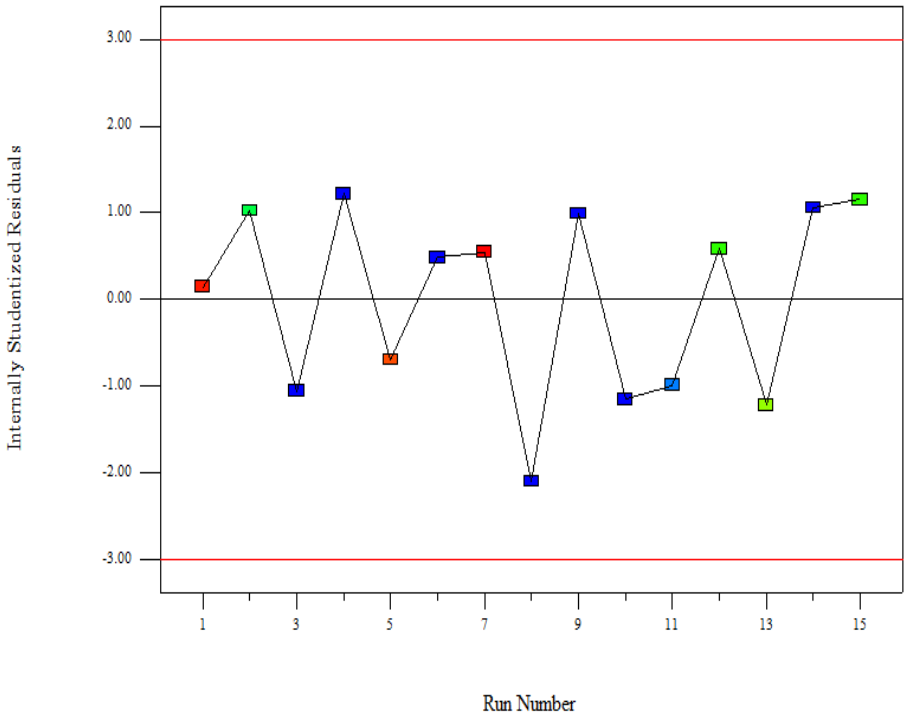

Figure 40 Plot of residuals versus experimental runs for checking lurking variables

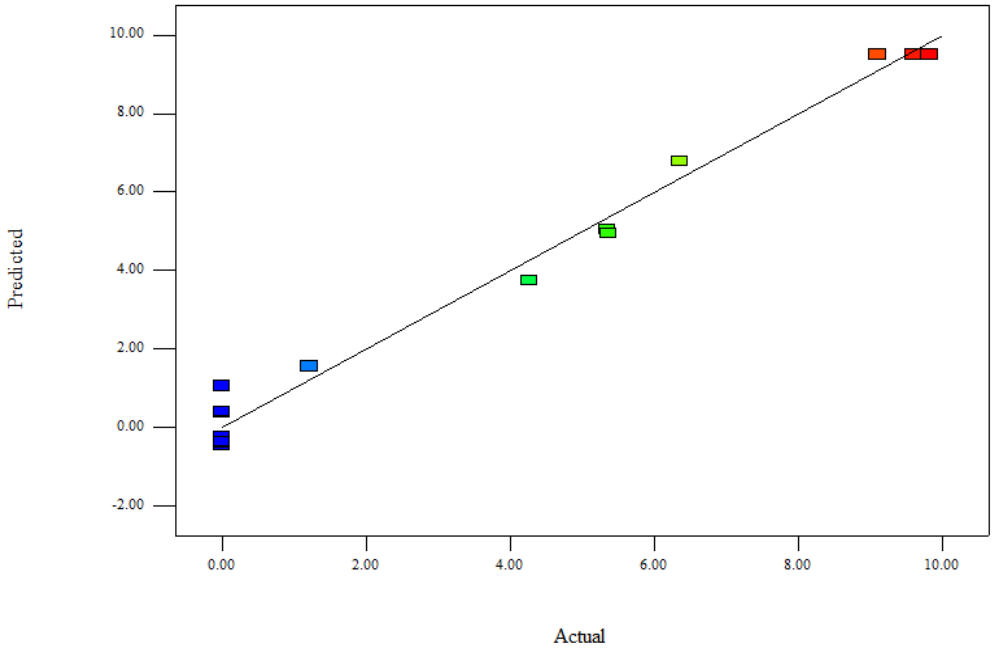

Figure 41 Plot of model predicted values versus experimental results

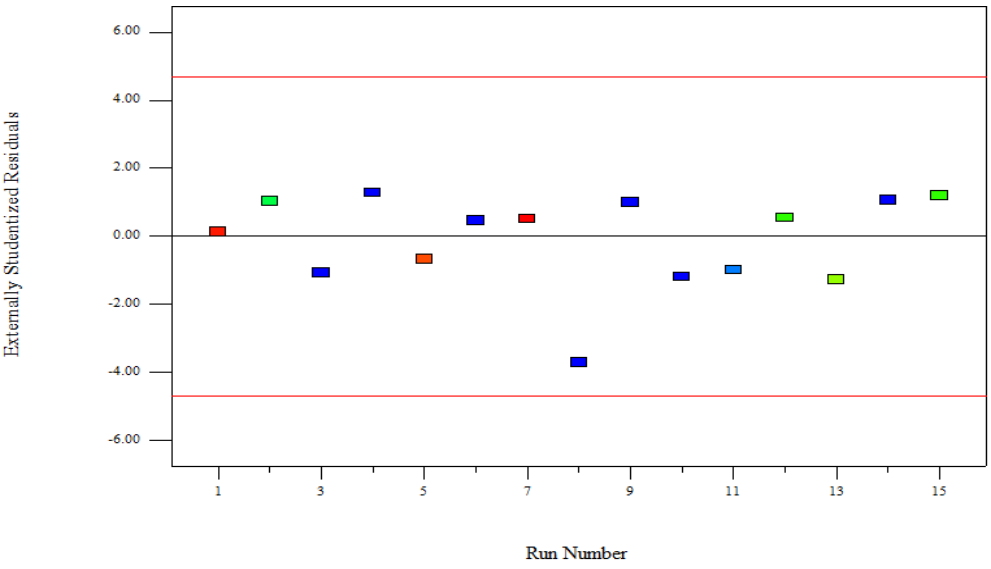

Figure 42 Plot of externally studentized residuals for checking outliers

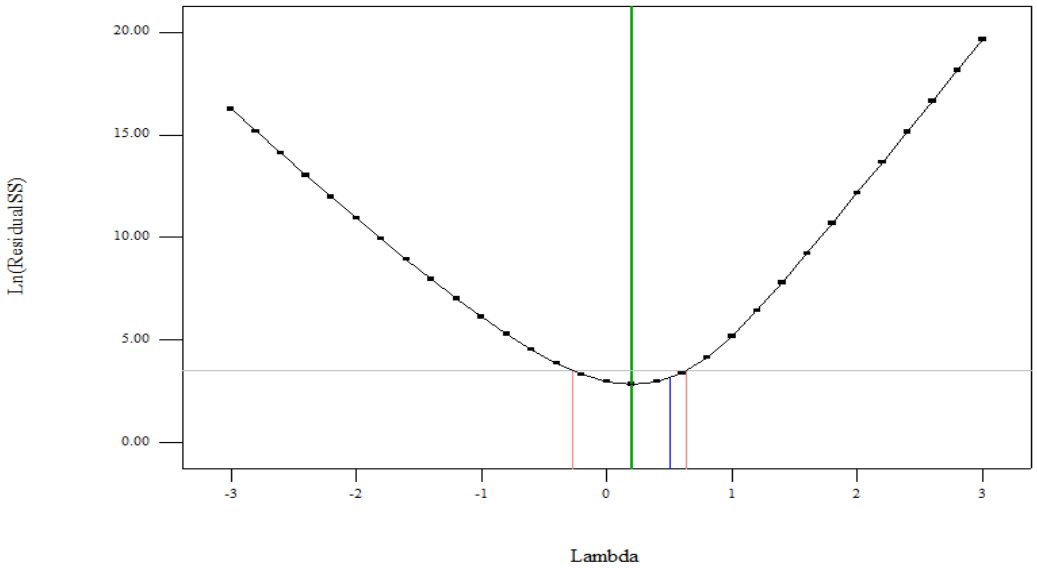

Figure 43 Box-Cox plot for evaluating the need for response transformation

Perturbation plot (Figure 44) compares the relative effects of all factors on the response by choosing a specific point (usually the midpoint) in the design space. Steeper slope or curvature indicates a higher sensitivity of the response to that factor, while flat line indicates an insensitivity. Figure 44 shows that all the investigated factors have significant curvature and hence, have significant impact on the Cd remedial efficiency. This corroborates the results obtained from the ANOVA in Table 25, where the curvature terms were highly significant at 0.05 p-value. In this case, any two of the factors can be used to form the axes of the 3D response surface and contour plots presented in Figure 45. The contours presents points of constant Cd remedial efficiency. These plots indicate that the factor levels successfully bracket the maximum Cd remedial efficiency, hence, optimal operating conditions can be found using the numerical optimization technique.

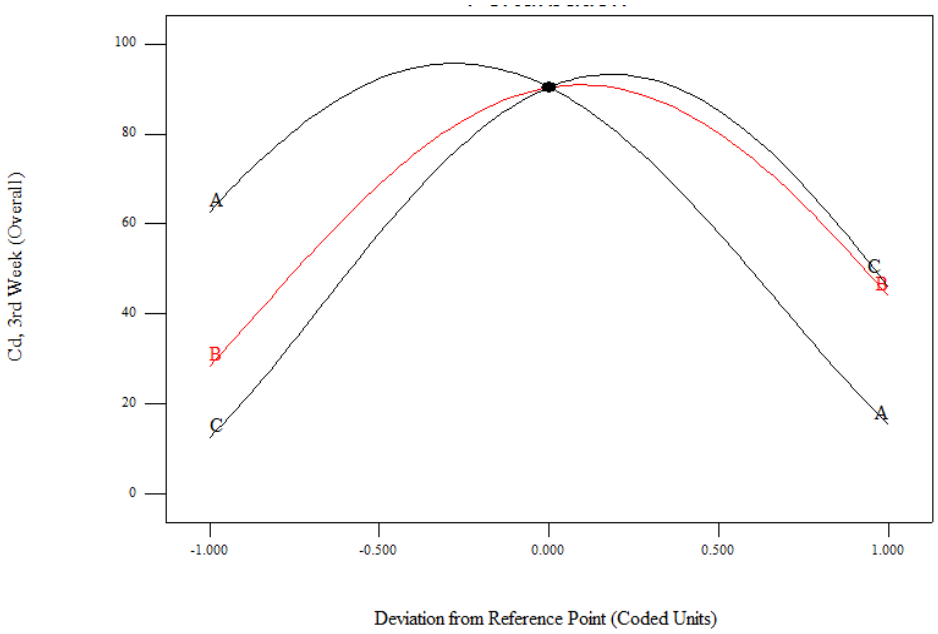

Figure 44 Perturbation plot showing the relative influence of factors on Cd remedial efficiency

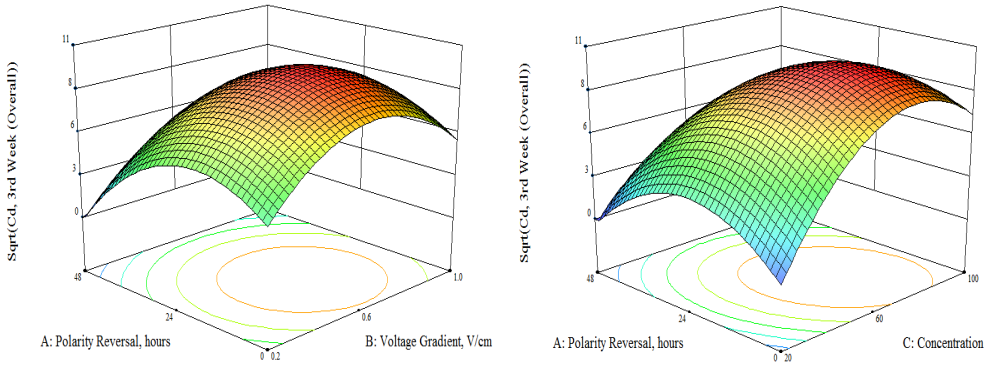

(a) (b)

Figure 45 3D response surface and contour plots showing the variation of Cd remedial efficiency relative to the factors: (a) Factors - polarity reversal and voltage gradient, (b) Factors - polarity reversal and concentration

The dominant transport mechanisms during electrokinetic remediation of low permeability soil has been identified as electromigration (EM) and electroosmosis (EO) [194]. At high ionic concentration, EM is the dominant transport mechanism of ionic species, while EO dominates at lower concentrations [194, 203]. EM and EO both depend on the applied voltage gradient and significantly affect the contaminant

remedial efficiency as shown in Figure 45(a). Polarity reversal affects the extent of ionic species migration in one direction before reaching the adsorption chambers, thus playing a significant role in subsequent removal of contaminants from the contaminated soil chamber.

7.3 Experimental Model Validation

Having run some important checks and dignostics on the developed model to evaluate its quality and ability to predict 'unseen' test results outside those used for model development, a different experimental test was run at voltage gradient of 1 V/cm, initial contaminant concentration of 62 mg/kg and without polarity reversal (Table 27). Results of the model validation presented in Table 27 reveals good prediction ability of the contaminant remedial efficiency with the percentage error in prediction ranging from 1 to 33. Models are meant to provide approximations as in this case and to help one move in the proper direction, but exact predictions do not form part of the model functions. Soil pH after the test was also predicted correctly. Similar modeling criteria for Cd were used in developing models for other contaminants and responses whose influential factors, adequate precision, raw and adjusted R^2 values are given in Table 28.

Table 27 Experimental validation of the developed model using voltage gradient = 1V/cm; average concentration = 62.02 mg/kg; polarity reversal rate = 0 hr

	Experimental results	Model predictions	% error
Cd remedial efficiency (3rd week), %	34.4	28.00	18.60
Zn remedial efficiency (3rd week), %	26.8	19.55	27.06
Pb remedial efficiency (2nd week), %	55.8	47.17	15.46
Cu remedial efficiency (3rd week), %	41	27.31	33.39
Cr remedial efficiency (3rd week), %	75.9	73.49	3.17
Hg remedial efficiency (3rd week), %	92.49	93.43	1.02
pH remedial efficiency (3rd week), %	12.3	12.76	3.75

7.4 Optimal Conditions for Cd Removal Using Numerical Optimization

Following adequate evaluation and experimental validation of the developed model for Cd remedial efficiency in addition to the established significance and effects of the investigated factors on the response, finding optimal conditions for effective Cd removal comes next. The hierarchical optimization scenarios presented in Table 22 were meant to investigate any synergistic or antagonistic characteristics that may result from the simultaneous optimization of several responses using the desirability function. Case 1 contains the simplest scenario of maximizing only Cd remedial efficiency, while additional goals were gradually and systematically introduced in the subsequent Cases.

Table 28 Information on the influential factors and R2 values of other responses

Response	Sequence of influential factors	Transformation	Adequate precision	R^2	Adjusted R^2
Zn, %	A > C > B	Square root	10	0.9070	0.8373
Pb, %	A > B > C	None	23	0.9954	0.9786
Cu, %	C > B > A	Square root	15	0.9725	0.9449
Cr, %	C > B > A	Square root	12	0.9335	0.8966
Hg, %	C > A > B	Natural Log	21	0.9949	0.9640
Phenol, %	B > C > A	None	-	1.0000	1.0000
TPH, %	C > A > B	None	10	0.9464	0.8749
Energy consumption, $kWhr/m^3$	B > C > A	Natural Log	33	0.9862	0.9807
Electrical current, A	B > C > A	Square root	23	0.9556	0.9435
Electroosmotic volume, mL	B > A > C	Square root	12	0.8560	0.8319
Flushed pore volume, #	B > A > C	Square root	11	0.8768	0.8275
Electroosmotic conductivity, $cm^2/s/V$	B > A > C	Square root	6	0.7383	0.6336
Anolyte refill rate, #	B > C > A	Square root	9	0.8167	0.7148
Catholyte refill rate, #	B > C = A	Square root	18	0.9684	0.9369
Anolyte replacement rate, #	B > C > A	None	17	0.9507	0.9232
Catholyte replacement rate, #	B > C > A	None	8	0.6956	0.6125
Soil electrical conductivity, dS/m	C > B > A	None	13	0.8466	0.7852
Soil pH	B > C > A	None	10	0.7725	0.7105

Optimal conditions required to achieve effective Cd removal together with their associated Desirability values are presented in Table 29. The table reveals that adding more responses led to decreased overall Desirability except for energy consumption which has led to a slight increase in the overall desirability, probably due to synergism. The more practical the optimization proceeds by including all the investigated responses, the less the value of the overall Desirability. Case 8 contains all the responses monitored during the tests that are eligible for optimization whose individual Desirability values are depicted in Figure 5.11. For this case, overall Desirability of 0.608 was attained at the following optimal condition: voltage gradient = 0.47 V/cm; polarity reversal rate = 19.77 hr; initial contaminant concentration = 65.44 mg/kg. Figure 5.12 presents a 3D graphical representation of the variation of Desirability relative to the influential factors.

7.5 Conclusion

In this study, the effects of voltage gradient, initial contaminant concentration and polarity reversal rate on the effective removal of Cd ions from a multiple contaminated natural saline-sodic soil were experimentally studied using the Box-Behnken Design of experiment and mathematically modeled and numerically optimized using Response Surface Methodology. The saline-sodic nature of the soil imparts some operational constraints that necessitated the need for elaborate investigations into the factors and responses for finding optimal operating conditions that will reduce the cost of the integrated electrokinetics-adsorption remediation of the contaminated soil. More than 90 % Cd remedial efficiency was achieved from the tests because of significant formation and subsequent migration of hydroxocomplexes from the contaminated chamber to the GAC chambers where they become adsorbed and immobile.

Table 29 Factor levels and corresponding response and Desirability values for all scenarios

Scenarios	Optimization results						
	A (hr)	B (V/cm)	C (mg/kg)	Energy consumed, kWhr/m^3	Optimized Cd removal efficiency, %	Overall Desirability, D	Remarks
Case 1	18.63	0.6	69.71	-	100	1.00	Optimize Cd removal only (factors in range)
Case 2	14.35	0.48	82.16	-	80	0.74	Optimize Cd removal + factors
Case 3	14.41	0.44	81.62	1017.35	75	0.784	Optimize Cd removal + energy + factors
Case 4	15.14	0.34	75.51	481.21	60	0.712	Optimize Cd removal + energy + factors + W/I assigned
Case 5	15.14	0.34	75.48	480.498	60	0.712	Optimize Cd removal + energy + factors + W/I* assigned + other contaminants (in range)
Case 6	16.12	0.41	65.9	853.9	78	0.624	Optimize Cd removal + energy + factors + W/I assigned + other contaminants (maximize)
Case 7	16.65	0.44	64.85	1049.13	83	0.617	Optimize all contaminants removals + energy + factors + W/I assigned
Case 8	19.77	0.47	65.44	1263.63	86	0.608	Optimize all responses + factors + W/I assigned

* W = *Weight,* I = *importance*

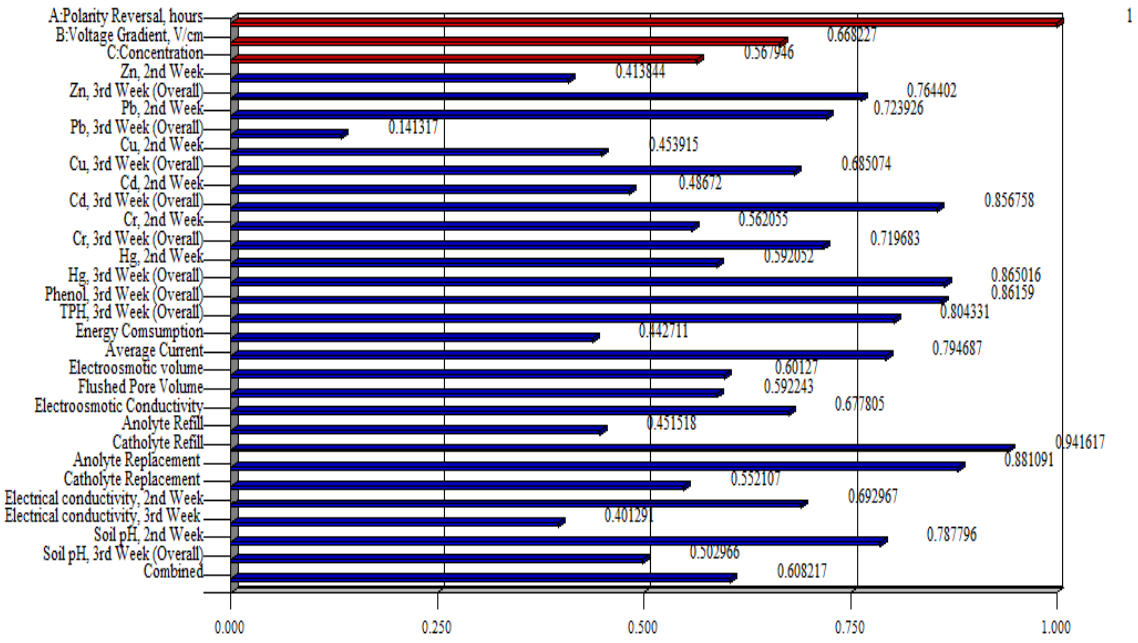

Figure 5.11 Overall and individual response Desirability values

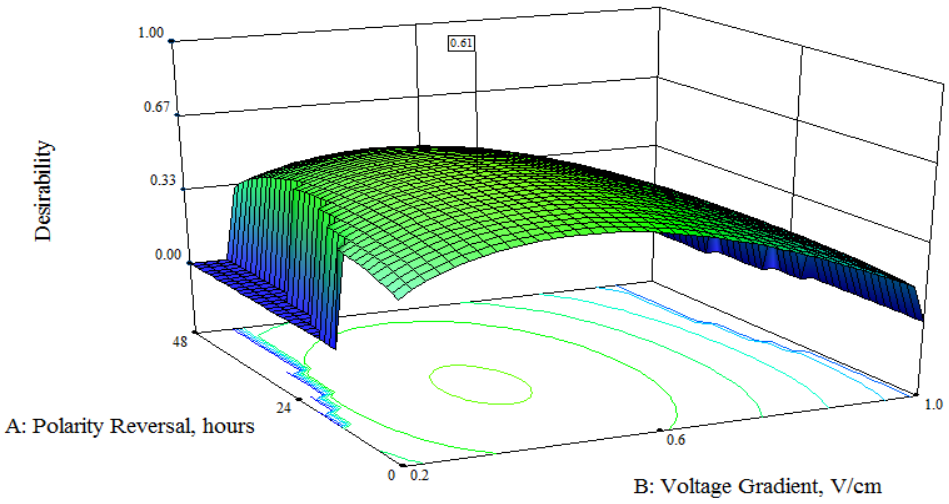

Figure 5.12 3D Overall Desirability variation relative to factors

Using the RSM technique, a mathematical model was developed using quadratic function for the prediction of the effective removal of Cd ions from natural saline-sodic soil that was contaminated with Cd, Cr, Cu, Zn, Pb, Hg, kerosene and phenol. Following effective

preliminary design evaluation, mathematical model development and running some diagnostic tests, experimental model validation was undertaken. A model prediction of 28 % Cd remedial efficiency was experimentally found to be 34 % after running the test for 3 weeks. The developed empirical model is limited to the derived results obtained from saline-sodic soil, hence, generalization and use of the model for different soil types and different operating conditions outside those investigated may lead to incorrect estimation of the responses. The results presented also revealed the influence of the factors on the target response using perturbation, 3D response surface and contour plots. For all the responses considered in this study, voltage gradient had the highest influence, followed by initial contaminant concentration and then polarity reversal rate. Eight (8) hierarchical optimization scenarios were planned and simulated using the Desirability function. The following optimal conditions were necessary to obtain overall Desirability of 0.608 and optimized Cd remedial efficiency of 86 % at 1263.63 kWhr/m^3 energy expenditure: voltage gradient = 0.47 V/cm; polarity reversal rate = 19.77 hr; initial contaminant concentration = 65.44 mg/kg.

CHAPTER 8

APPLICATION OF BOX-BEHNKEN DESIGN TO INTEGRATED ELECTROKINETICS-ADSORPTION TECHNIQUE FOR MERCURY REMOVAL FROM SALINE-SODIC SOIL

8.1 Introduction

Coal combustion, mercury and gold mining activities and several other industrial activities have led to increase in the mercury concentration in soil [204]. Environmental contamination caused by uncontrolled release of mercury is a serious problem worldwide [204-206]. Mercury polluted soil becomes a threat to the environment because in addition to the damage inflicted to the environment; mercury also poses serious risks to human health [206]. Mercury can readily be taken up by the plants and be accumulated in the human body through the food chain [204]. Hence due to its toxicity, mobility, and long residence time in the atmosphere, mercury is regarded as one of the "priority hazardous substances" by the USA Agency for Toxic Substances and Disease Registry [207]. Many efforts led to development of remediation technologies such as stabilization/solidification, immobilization, vitrification, soil washing, soil flushing,

bioventing, electrokinetics and sand thermal desorption that could be used to reduce or to manage mercury contamination in soil [204, 205, 208, 209].

Electrokinetic remediation (EKR) is considered as suitable alternative for removal of mercury from low permeability soils [209]. EKR consists of the controlled application of low intensity direct voltage or current via appropriate electrodes directly inserted into the soil. The applied electric field induces the migration and subsequent removal of charged ions via three main mechanisms: electroosmosis, electromigration and electrophoresis [65, 209]. During electroremediation process of mercury and other heavy metals contaminated soils, due to the combined effects of electromigration and electroosmosis, the movement of cationic species in soil matrix towards cathode is enhanced whereas the movement of anionic species towards anode is reduced [175]. In general, the electromigration rate is at least one order of magnitude greater than the electroosmotic flow, and hence electromigration generally dominates mass transport during electrokinetics treatment [210]. However, one of the difficulties of EKR of mercury contaminated soils is the low solubility of mercury in most natural soils [211]. Saline-sodic soils (usually found in arid and semiarid regions) possess high electrical conductivity (> 4 dS/m) which prevents the application of appropriate voltage gradient in an electrokinetic study owing to current limitations [12]. Moreover, considering that these soils are highly alkaline (pH > 8.2) with exchangeable sodium percentage at levels greater than 15 [212, 213], these extreme soil characteristics pose great difficulty in having such soils remediated from mixed contaminants using electrokinetics-based technique [214]. Presence of co-contaminants will further complicate effective remediation of Hg due to competitive environment created as well as the inducible

synergistic or antagonistic effects on EK removal of mercury [18, 20, 215]. Li et al [20] found that it was more difficult to achieve great simultaneous removal of hydrophobic organic compounds and heavy metal in soil by electrokinetics treatment at pilot scale. In addition, the solubility and hydrophobicity differences between the different types of co-pollutants in soil indicate the complexity of electrokinetics of mixed polluted-contaminated soils. In order to overcome challenges of electrokinetics, a number of strategies were suggested for enhancing the performance of electrokinetics which involves integrating electrokinetics with other remediation techniques (i.e., hybrid techniques) for improved efficacy [14, 34, 53, 216, 217].

Hybrid electro-remediation called Lasagna^{TM} is a technique that incorporates several treatment zones (e.g. adsorption, immobilization, degradation) filled with appropriate materials (adsorbents, catalytic agents, microbes, oxidants, buffers, etc.), and transports contaminants from the soil into the treatment zones, thereby possessing high potential to considerably increase the removal efficiency [13, 57]. In fact, Lasagna^{TM} technology showed great potential in remediation of soils polluted with trichloroethylene and p-nitrophenol both at large and small scales [12, 14, 53, 218]. However, in using absorption chamber in processes like Lasagna^{TM}, commercially activated carbon is expensive, which may limit its use in field-scale remediation. Therefore, from economic point of view and for cost-effectiveness, the need to develop low-cost, easily available adsorbents cannot be overemphasized. Ma et al [34] coupled electrokinetics technology with adsorption using a new-type cheap bamboo charcoal adsorbent for simultaneous removal of 2,4-dichlorophenol (2,4-DCP) and Cd from a sandy loam. After 10.5 days of continuous operation under different experimental conditions, they observed 40.13-75.97% and

24.98-54.92% removal of Cd 2,4-DCP, respectively. They concluded that, electrokinetics technique combined with adsorption using activated bamboo charcoal is a promising technology for cost-effective remediation of soils contaminated with organic compounds and heavy metals.

In this study, mercury removal efficiency and energy consumption for mercury removal in a heavily contaminated saline-sodic clay soil matrix using hybrid electrokinetics-adsorption (HEKA) technique were investigated and optimized by employing Response Surface Methodology (RSM). The activated carbon used in this study was produced from cheap and readily available local date palm pits. The contaminated clay was obtained by spiking natural saline-sodic clay material with several heavy metals and organic compounds that included phenol and kerosene. Experiments were designed according to BBD and the data obtained were used to develop models which were analyzed for statistical significance and used for determining optimal conditions for mercury removal using HEKA.

8.2 Results and Discussion

As provided in Table 30, the fifteen (15) experimental runs were carried out by different combinations of the independent variable as per the BBD in order to study the single and interaction effects of the variables on the studied responses. Also, Table 30 presents data for the studied responses obtained from the experimental analyses.

8.2.1 Mercury Removal Efficiency in the HEKA Cell

From the results presented in Table 30, it is obvious that in the central replicated runs (5, 8 and 13), the performance of the HEKA cell in terms of Hg removals were much more

effective than in the other runs. The highest amount of Hg removals of up to 99% occurred after 14 days, while in almost all other runs, the rate of the Hg removal diminished gradually or did not change significantly after 14 days of operation. This excellent removal of mercury observed from the tested saline-sodic clay soil after 21 days of operation with HEKA cell was attributed to the introduced GAC chamber. In order to verify the contribution of the GAC during the treatment process, additional experiments was conducted using electrokinetic cell only operated at voltage gradient of 0.6 V/cm without polarity reversal for the removal of 100 mg Hg per kg soil i.e. under the same operating conditions as in run order 7 in Table 30. The removal efficiency obtained was 71.75 and 26.8 % with and without GAC, respectively. This clearly indicated that higher Hg removal was associated with the hybrid cell. It has been well established that activated carbon has excellent adsorption capacity for heavy metals [34, 219, 220]. By comparing these two cell types under the same experimental conditions, it could be inferred that the produced GAC is a promising adsorbent that can be used for improving the electroremediation of soils cocontaminated with mercury. During all the electrokinetic tests performed in this study, Hg was never detected in the unspiked soil chambers lying between the GAC and the electrode chambers, indicating that the migration of Hg was mainly intercepted by the presence of the activated carbon. These observation show that electrokinetics coupled with adsorption using locally produced GAC from date palm pits has great potential for the remediation of Hg-contaminated soils.

Table 30 Box-Behken Experimental Design and Data for Mercury Removal

Design order	Run order	Variables levels			Hg removal (Y_1) %	EC* (Y_2) $kWh.m^{-3}mg^{-1}$
		A	*B*	*C*		
1	5	24	0.6	60	98.67	50.69
2	8	24	0.6	60	97.78	51.22
3	13	24	0.6	60	99.03	50.46
4	6	0	0.2	60	79.77	4.26
5	9	48	0.2	60	81.77	2.57
6	1	0	1	60	90.87	268.96
7	2	48	1	60	77.46	276.85
8	11	0	0.6	20	27.09	629.20
9	10	48	0.6	20	45.42	423.38
10	7	0	0.6	100	71.75	23.15
11	3	48	0.6	100	79.49	41.05
12	12	24	0.2	20	70.62	9.63
13	4	24	1	20	71.98	758.89
14	5	24	0.2	100	60.75	2.40
15	8	24	1	100	83.69	118.35

*E_C = Energy Consumption measured as $kWh.m^{-3}mg^{-1}$ = kWh per m^3 of treated soil per mg of mercury removed

8.2.2 Effect of Variation of Soil pH

Soil pH as vital factor influencing speciation of contaminants controls the transport processes of contaminants in the soil. Water electrolysis at electrodes during electrokinetics causes decrease in soil pH near the anode and increase near the cathode depending on the soil buffering capacity. High pH value enhances metal hydroxides to precipitate in soil close to cathode, decreasing soil conductivity. However, low pH value may decrease and reverse the soil zeta potential leading to reduced electroosmotic flow rate, and thus limiting electrokinetics of contaminants [34]. Heavy metals and organics removal in soil is greatly influence by pH, as such keeping pH value suitable and stable in electrode chamber is of great importance [34]. Figure 46 shows the temporal variation of pH for thirteen (13) experimental runs (i.e., including only one of the three (3)

replicated central runs).The initial pH indicates the spiked soil pH before treatment begins. The rapid electrochemical decomposition of water at the electrodes (for 0.6 and 1 V/cm) has necessitated conditioning the anode and cathode chambers with H^+ and OH^- neutralizing chemicals using 2 N NaOH and 1 N HNO_3 respectively. These processing fluids were monitored every 8 hours because of the soil electrical conductivity (high salinity) which allows the passage high current in the soil with consequent rapid degradation of the processing fluids. From Figure 46, the minimum pH value of 8 was recorded which may be far off the point of zero charge (PZC). It may be suggested that the soil zeta potential was not reversed which may lead to the reversal of the electroosmotic flow. The observed unidirectional nature of the electroosmotic flow also supports this assertion.

Barrow and Cox [221] and Yin et al [222] reported that the maximum mercury adsorption occurred at acidic pH, and at higher pH values (basic pH) the adsorption decreased significantly. Thus, increased Hg availability in the soil is expected at such basic pH shown in Figure 46. In all runs, the final pH is always higher than the initial pH indicating high acid buffering capacity of soil due to the presence of calcite minerals.

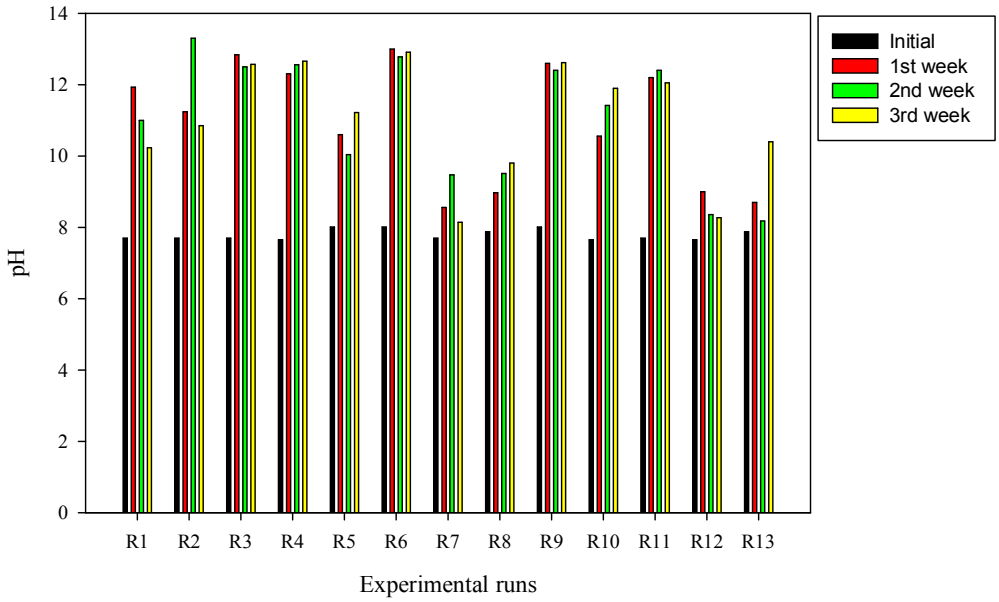

Figure 46 Initial and weekly variations of soil pH for the Box-Behken Design Runs

Adsorption of mercury in clay soils has been attributed to speciation of mercury and the spatial variability of organic matter in the soil [222, 223]. At a higher pH, the surface potential becomes more negative resulting in decrease in HgOH with a corresponding increase of $Hg(OH)_2$ which readily desorbs. Moreover, the dissolution of organic matter occurs at higher pH values, and this reduced organic adsorption sites in the soil and enhanced Hg complexation with soluble organic ligands possibly contributed to high removal efficiency of Hg in the saline-sodic soil used in this study [223]. Beside the contribution of the adsorption chamber introduced within the HEKA cell, the fact that the clay used in this study possessing low organic content (2.59%) and, under all experimental conditions, the pH drastically rose to the basic region, explain the reason behind the good removal of mercury. Additionally, this high removal efficiency of up to 99 % may also be attributed to the presence of excess Cl^- under aerobic conditions and

subsequent formation and migration of the mercury complex $HgCl_4^{2-}$ according to equation 8.1 [172].

$$O_2 + 2Hg + 8Cl^- + 2H_2O \rightarrow 2HgCl_4^{2-} + 4OH^- \quad (8.1)$$

8.2.3 Mercury Speciation

Visual MINTEQ version 3.0 [112] was used to model the Hg speciation before and after the experiment using its dissolved concentration, pH, temperature and ionic strength. The speciation result suggests the relative concentrations of the hydroxo-complexes present- $Hg(OH)_2$, Hg^{+2}, Hg_2OH^{+3} , $Hg_3(OH)_3^{+3}$ and $HgOH^+$- as presented in Table 31. The species having the highest initial % of total Hg concentration and removal efficiency is $Hg(OH)_{2(aq)}$ which suggests that precipitated mercury hydroxides can redissolve at high alkaline pH values encountered in this study. The formation of complexes with OH^- anions that have increased pore fluid solubility may be attributed to the redissolution of $Hg(OH)_2$ and its subsequent high removal efficiency [188].

Table 31 Mercury Speciation During HEKA Treatment

Hg species	Concentration, mol/L	Concentration, mol/L	Removal efficiency %
$Hg(OH)_2$	1.51×10^{-4}	1.49×10^{-04}	98.67
Hg^{+2}	2.85×10^{-14}	8.34×10^{-21}	2.93×10^{-05}
Hg_2OH^{+3}	4.24×10^{-23}	6.31×10^{-33}	1.49×10^{-08}
$Hg_3(OH)_3^{+3}$	6.28×10^{-24}	1.31×10^{-33}	2.09×10^{-08}
$HgOH^+$	9.52×10^{-10}	5.19×10^{-13}	10^{-02}

8.2.4 RSM Modeling and Numerical Optimization

Data obtained (Table 30) were fitted into equation 3.10 to obtain equations 8.2 and 8.3 in terms of the coded factors for mercury removal efficiency (Y_1) and specific energy consumption for removal of mercury (Y_2) as suggested by the Design Expert software,

respectively. Qualities of the developed models were further improved by dropping insignificant interaction effects that dwindles the respective response prediction accuracy. While the best fitted model for the mercury was reduced cubic model (Y_1), reduced quadratic model (Y_2) was found be best fitted model for the energy consumption. These reduced models show only the parameters and/or their interactions effects that have significant effects on the respective responses. For instance, for the Y_1, all the main effects A, B and C and two squared terms A^2 and $C^2$and cubic terms A^2C and AC^2were the significant model terms, as such were included in the model. Whereas all other terms not included in the reduced model, were insignificant. Moreover, positive and negative coefficients in the response functions indicate synergistic and antagonistic effect between the independent variables and the responses, respectively. Also, the relative contribution of any given factor or interaction in any of the models is directly proportional to the value of its coefficient.

$$Y_1 = 98.71 - 2.85A + 3.89B + 0.46C \quad -3.85AB - 2.65AC + 5.40BC - 16.1A^2 - 26.81C^2 + 19.22A^2C + 9.37AC^2 \qquad (8.2)$$

$$Y_2 = 100.72 - 22.71A + 175.52B - 204.52C - 158.33BC + 156.28C^2 \qquad (8.3)$$

Qualities of the developed models are indicated by the coefficient of regression R^2. As the closer the R^2 value to unity, the higher the model's quality. Hence, the obtained values of R^2 of 0.992 and 0.923 for Y_1 and Y_2, are high, indicating good models prediction abilities. This could be inferred from the experimental versus models' predictions plots provided in Figure 47-I and 47-II for mercury removal and energy consumption, respectively. The Design Expert software also provided the analysis of

variance (ANOVA) for the parameters of the regression models. All the sources of variations of the models' *F*-values determined from ANOVA indicated that the models are statistically significant at 5% significant level (i.e. at probability values $p < 0.05$). This also further supports the fact that equations 8.2 and 8.3 can adequately predict the experimental results with high degree of accuracy. Similarly, the respective values for all the different sources of the models' variations established at either 5% or 10% significant level (i.e., $p < 0.05$ or $p < 0.1$) suggest that all the investigated parameters are significant models terms (Table 32). In addition, the adequate precision values (i.e., measure of signal to noise ratio) for the models provided in Table 32 imply adequate signals (> 4 is desirable) signifying suitability for navigating the design space for drawing credible conclusions. The dependencies of Y_1 and Y_2 on polarity reversal interval (A), voltage gradient (B) and initial Hg concentration (C) are depicted in surface and contour plots presented in Figures 48 - 50.

I

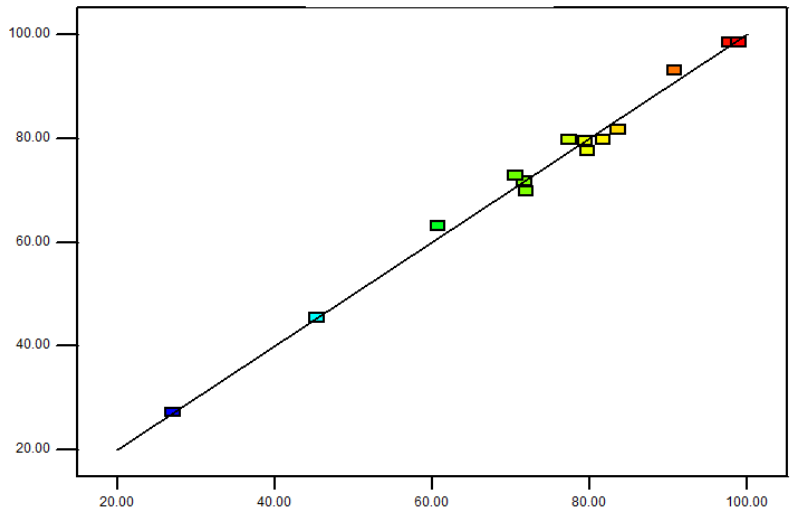

II

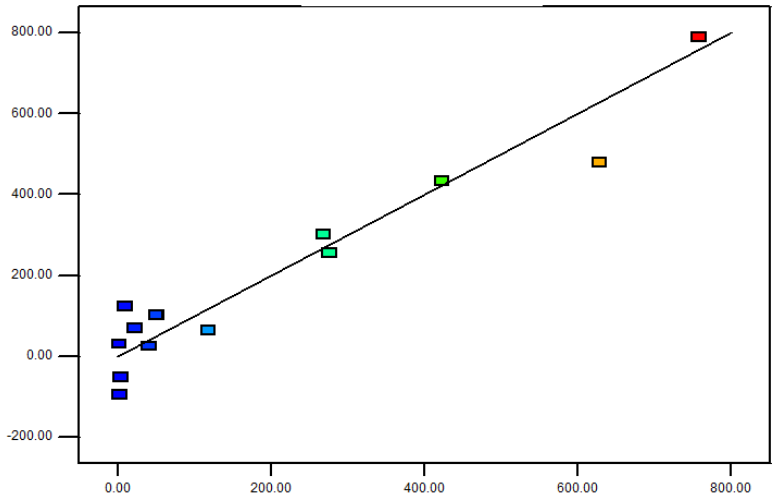

Figure 47 Model's Predicted vs Actual for (I) Mercury Removal Efficiency and (II) Specific Energy Consumption for Mercury Removal

Table 32 Reduced Models ANOVA for Hg Removal and Energy Consumption

I: ANOVA for Hg Removal Reduced Cubic Model (Y_1) R^2= 0.993; Adequate Precision= 22.098					
Source	Sum of Squares		Mean Square	F -Value	*p*-value*
Model	6807.12	10	680.71	123.13	< 0.0001*
A	32.55	1	32.55	5.89	0.0457*
B	120.82	1	120.82	21.85	0.0023*
C	0.85	1	0.85	0.15	0.7072
AB	59.37	1	59.37	10.74	0.0135*
AC	28.04	1	28.04	5.07	0.0590**
BC	116.42	1	116.42	21.06	0.0025*
A^2	1140.49	1	1140.49	206.29	< 0.0001*
C^2	3161.97	1	3161.97	571.94	< 0.0001*
A^2C	739.01	1	739.01	133.67	< 0.0001*
AC^2	175.59	1	175.59	31.76	0.0008*
II:ANOVA for Energy Consumption Reduced Quadratic Model (Y_2) R^2= 0.923; Adequate Precision = 15.860					
Model	769535.9	5	153907.2	21.43951	0.0001*
A	4127.542	1	4127.542	0.574973	0.4677
B	246468.8	1	246468.8	34.33349	0.0002*
C	334621.4	1	334621.4	46.61329	0.0001*
BC	100271.1	1	100271.1	13.96792	0.0046*
C^2	84047	1	84047	11.70788	0.0076*

*Significance was established at $p < 0.05$; **Significance was established at $p < 0.1$

Response Surface plots and their corresponding contour maps (Figure 47) for the modeled responses were constructed to assess, visualize and further understand the influence of the independent variables on the responses in a more detailed perspective. Considering the main (e.g., linear) effects only, the coefficients of the independent variables in Y_1 and Y_2 were mainly positive except for polarity reversal interval (A) and C which is negative in both models and in Y_2, respectively. Moreover, initial Hg concentration has less significant effect on mercury removal, while the energy consumption was insignificantly influenced by the polarity reversal interval. This is evident in the coefficients in Y_1 and Y_2 as well as the respective *p*-values. The *p*-values in Table 32, the 3-D plots for removal efficiency as well as the main effect plots as illustrated in Figures 48 - 50, respectively, show that all the three independent variables as either single (main), squared term or by their interactions to the have contributed to the Hg removal. However, the stronger degree of curvature due interactive variations between factors A and C is portrayed in the upward plateau shape depicting Hg removal increases with increase in polarity reversal reaching highest value in the region around central point (i.e., 24 hours polarity reversal interval and 0.6 V/cm and concentration of 60 mg/kg). Thereafter, the Hg removal efficiency decreases with increase in A and C. In fact, this visual point is supported by the data obtained from run order 5, 6 and 13, where the removals were close to 100%. This clearly indicated that as per as Hg removal is concerned only (i.e., while ignoring energy consumption), the best optimal condition for Hg removal is attainable within the central point. These non-linear behaviors of polarity reversal interval and initial mercury concentration is clearly indicated by the substantial contributions of the higher interactive effects of these two parameters (Table 32-I). In the

case of energy consumption, polarity reversal interval has no significant effect under all circumstance (both linear and interactive) as presented in Table 32-II and depicted in Figures 48 and 50. Meanwhile, the dependency of the energy consumption on both voltage gradient and initial Hg concentration as depicted also in Figures 48 and 50, shows that both the main and interactive effects are simultaneously significant while curvature is not well pronounced and is mainly attributed to initial Hg concentration.

Based on the F and *p*-values, presented in the ANOVA (Table 31), voltage gradient (B) was the most significant variables (i.e., high F-values and low *p*-values) on both models. Obviously, when voltage gradient increases, the electroosmotic flow as well as electromigration is expected to increase due to increase in induced electrical field, and hence, more of the Hg will be removed from the soil. Similarly, higher voltage gradient invariably imply more energy exerted across the cell, and hence higher energy consumption is dissipated in the process. Also higher concentration would lead to better utilization of the supplied energy. It could be deduced from the forgone analysis that the overall relative contributions of the main effects on the mercury removal follows the order; voltage gradient > concentration > polarity reversal interval. This implies that, when using HEKA technique for removal of mercury from heavily contaminated soils, high voltage gradient and more frequently reversing the polarity are expected to result in higher mercury removal especially when the mercury concentration in soil is high. Higher energy consumption is as a result of higher induced voltage gradient and lower initial Hg concentration. The lowest energy consumption of 2.4 $kWh.m^{-3}mg^{-1}$ was observed to be attributed with Hg removal of 60.75% (run 5), while 50.46 $kWh.m^{-3}mg^{-1}$ was needed to achieve the best removal of 99.03% (run 13).

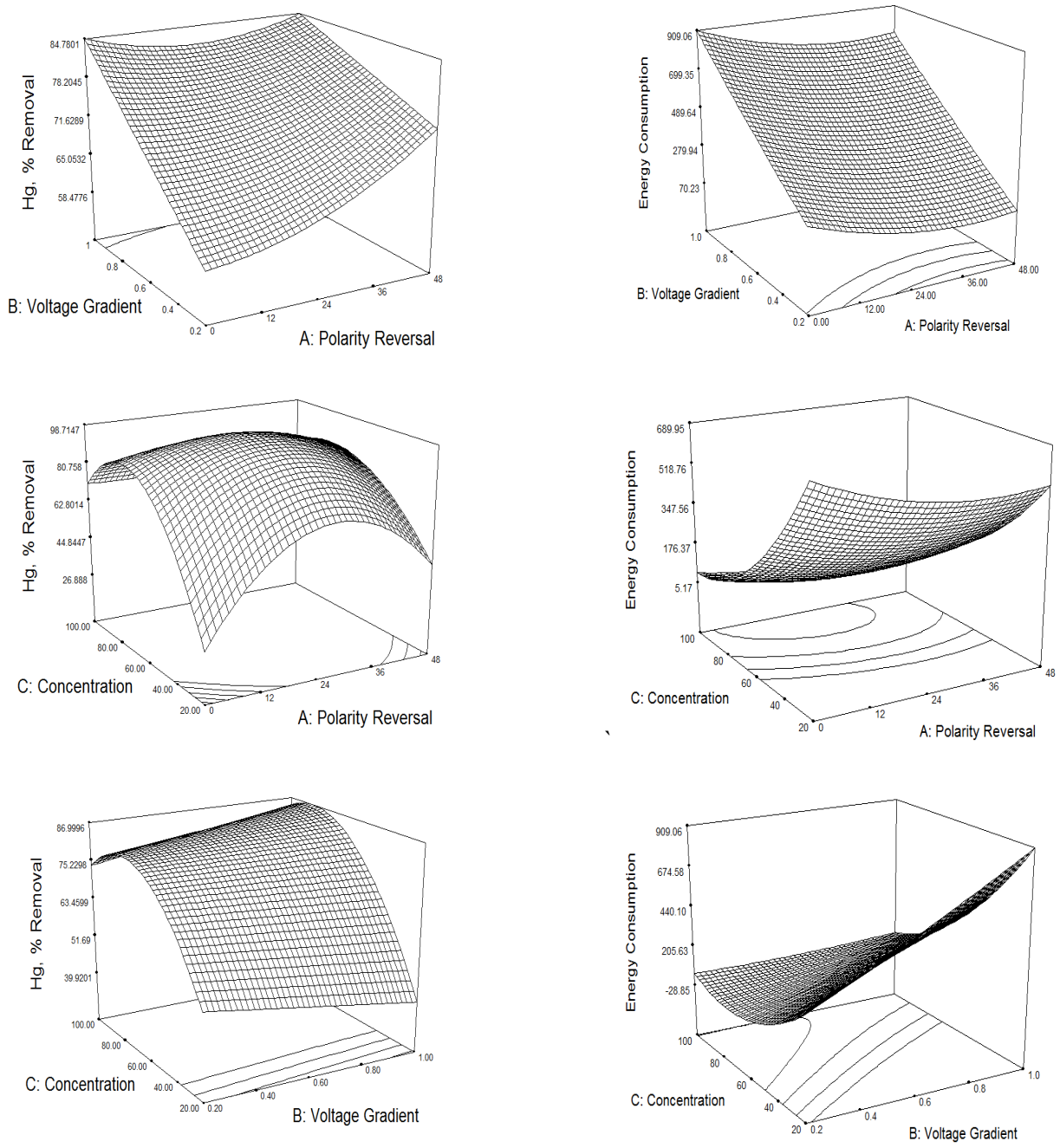

I **II**

Figure 48 3D response surface and contour plots for combined effect of Polarity reversal interval, applied voltage gradient and initial heavy metals concentration in soil on (I) Mercury Removal and (II) Energy consumed for Hg removal

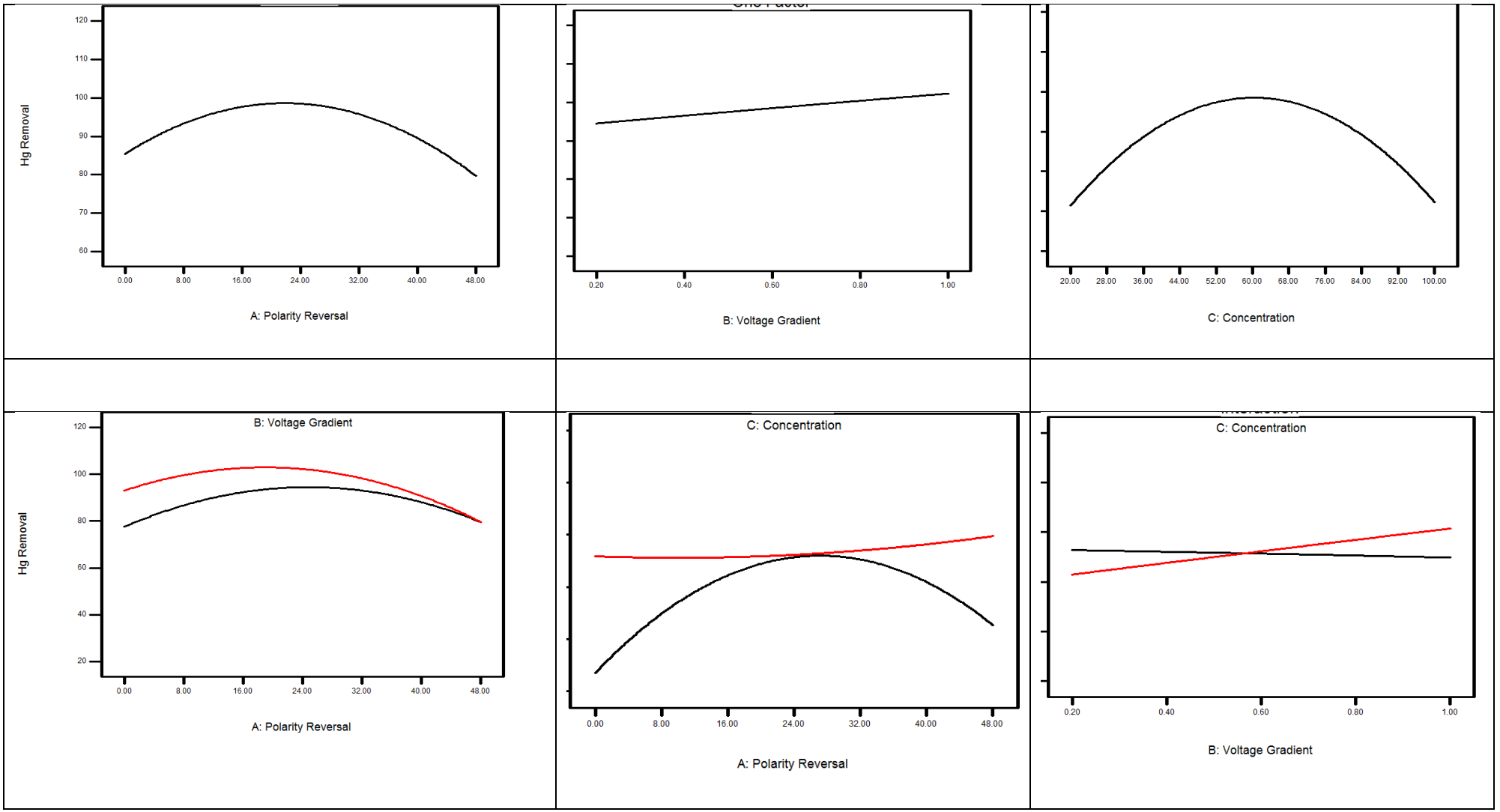

Figure 49 Main and interactive effects of independent variables on Hg removal efficiency

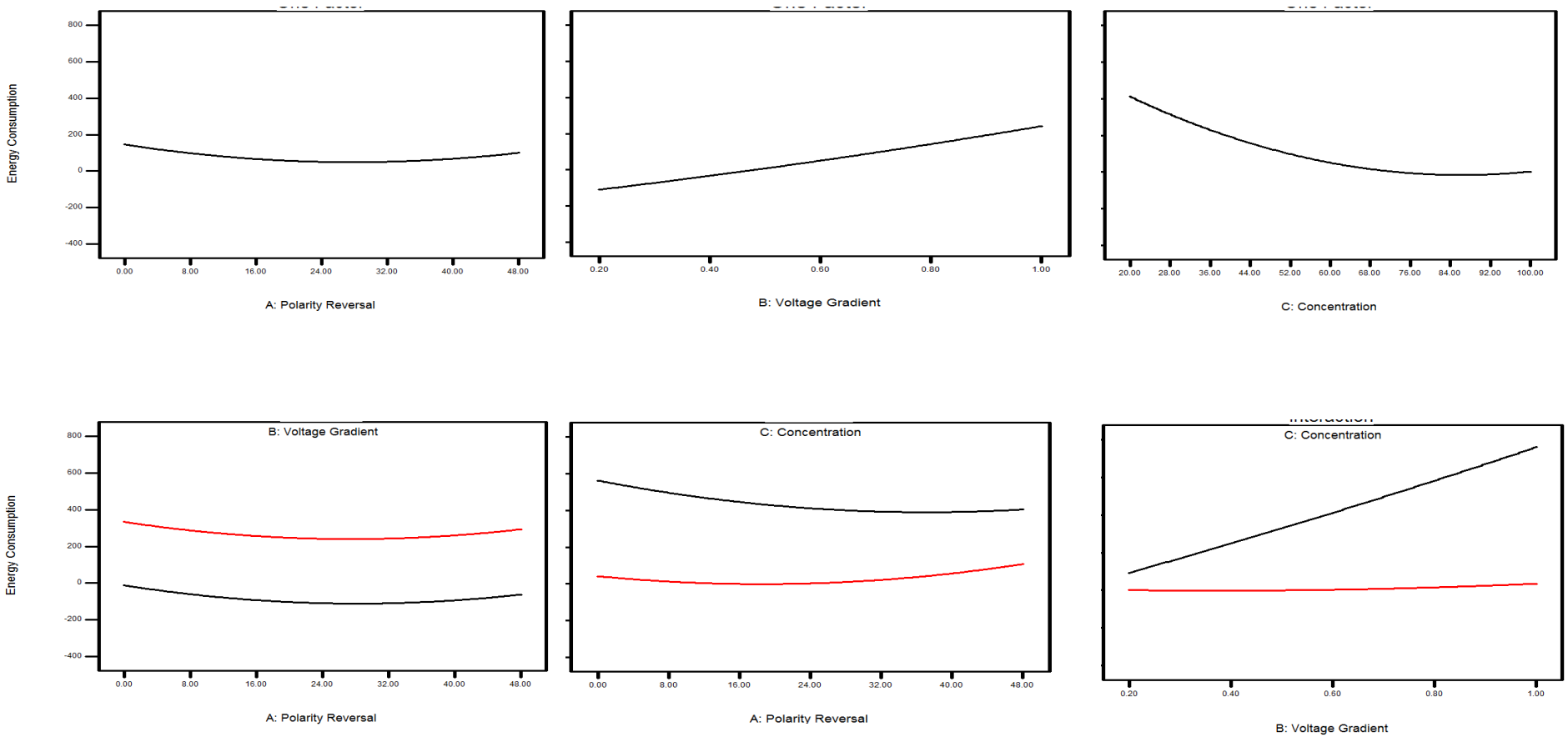

Figure 50 Main and interactive effects of independent variables on energy consumption

As polarity reversal changed migration direction of charged contaminants repeatedly and thus could increase the energy consumption at the expense of increased removal efficiency in comparison with unidirectional operation. Hence, when reversing the polarity, it is possible that portion of the mercury carried by electromigration and/or electroosmosis did not reach treatment zone in the activated carbon chamber before the polarity changed, and then they would move towards the opposite directions, leading to higher power consumption while achieving lower removal efficiency. Therefore, an optimal reversal interval should be adopted for the purpose of cost-effectiveness.

8.3 Optimal Conditions for Mercury Removal

Design-Expert software was also employed for the numerical optimization of Hg removal. The optimization was performed to get the best set of experimental conditions that can ensure complete Hg removal at minimal energy consumption. The coordinates of the optimal points were calculated through equating the first derivatives of the reduced models to zero (equation 8.2) in conjunction with set of convergent criteria [224]. The criteria composed of set of goals based on desired constraints for the parameters of interest. The criteria also weighted the individual parameters with numerical values ranging between 1 to 5 according to their relative priorities and/or importance in contributing towards attaining the desired overall targeted goals. As Desirability is one of the mathematical methods for computing optimum values [120], numerical solutions with Desirability ranging from 0.90, the best, to 0.88 the worst were obtained suggesting the region of interest for optimality aimed at maximizing Hg removal at reduced energy consumption was found to be 24 hours polarity reversal interval, 0.2 V/cm voltage gradient and 100 mg/kg initial mercury concentration. This optimum operating condition

yielded near complete removal of mercury (99.5%) at reduced energy consumption of 50.1 $kWh.m^{-3}mg^{-1}$ within the defined experimental region studied. This shows great economic superiority to remedy saline-sodic clay soils contaminated by Hg. Hence, with the RSM optimization point prediction using BBD, good removal of mercury (near zero residual Hg in the treated soil) was achieved with reduced requirements for energy consumption.

8.4 Validation of the RSM Models

For the developed models' validations, additional experiment was run also for three weeks resident time at operating conditions without polarity reversal, 1 V/cm voltage gradient and 86 mg/kg initial mercury concentration which does not belong to any of the experimental design runs. The results for the experimental validation and the models' point predictions are provided in the Table 33. For mercury removal efficiency, the model's prediction of removal efficiency of 95.83 % is quite close to the value obtained experimentally i.e., 92.49 %, indicating a good model's prediction (model's % error of 0.0348 %). In contrast, for the energy consumption, the model significantly overestimated the experimental value. It could be attributed to the fact that the Y_2 model's prediction to the lower (i.e., lower R^2 value) as well as the validation run experimental conditions falls within the region where the EC is likely to be overestimated.

Table 33 Experimental Validation of the developed models for Mercury and Energy Consumption model using voltage gradient = 1 V/cm; average concentration = 86 mg/kg; polarity reversal rate = 0 hr

	Models prediction	Experimental validation
Energy Consumption, $kWh.m^{-3}mg^{-1}$	159.044	51.826
Initial concentration, mg/kg	86	86
Final concentration after 3 weeks, mg/kg	4.51	6.46
Removal efficiency	95.87	92.49

8.5 Conclusion

In the present study, uniform electrokinetics remediation combined with adsorption on locally produced activated carbon for the removal of Hg ions in sodic-saline soil contaminated with several pollutants was investigated using a multivariate statistical technique via employing RSM technique. Fifteen (15) experiments each with resident time of three (3) weeks were conducted at different initial mercury concentration (20-100 mg/kg), polarity reversal interval (0-48 hours) and voltage gradient (0.2-1 V/cm) according to Box-Behnken Design (BBD). The main target responses were mercury removal efficiency and energy consumed for mercury removal which were both collectively taken into account in RSM optimization. Respectively, the responses fitted reduced cubic (R^2 = 0.993) and quadratic models (R^2 = 0.923) with the overall relative contributions of the investigated parameters on the responses following the order: voltage gradient > initial Hg concentration > polarity reversal interval based on analysis of variance (ANOVA). The optimal conditions obtained with Desirability of 90% aimed at maximizing Hg removal at reduced energy consumption was 24 hours polarity reversal interval, 0.2 V/cm voltage gradient and 100 mg/kg initial mercury concentration. This optimum operating condition yielded near complete removal of mercury (99.5%) at reduced energy consumption of 50.1 $kWh.m^{-3}mg^{-1}$. Experimental validation of the models indicated that mercury removal could be predicted with high degree of accuracy (0.0368% error). The results presented in this work have demonstrated the applicability of RSM using BBD to hybrid electrokinetic and adsorption using GAC for the removal of mercury in heavily contaminated saline-sodic clay soils. It also shows that RSM is an economical way of obtaining sufficient information with the least requirement of

experimental runs. Also, it suggests that HEKA technology could be utilized effectively for removal of mercury from contaminated clays under extreme soil and contamination conditions. To further understand the potentials of the technology, studying the effects of non-uniform electric fields as well as explore the overall efficacy of simultaneous removal of several pollutants in soil matrixes is recommended.

CHAPTER 9

EFFECTS OF VOLTAGE GRADIENT AND CONCENTRATION ON SOIL ELECTRICAL CONDUCTIVITY

9.1 Introduction

Sparks (2003) posited that electrical conductivity (EC) is the best index for the assessment of soil salinity. Unfortunately, most works on electrokinetic remediation failed to at least report the soil electrical conductivity, let alone, monitor its variation. Electrical conductivity greatly influences electrokinetic remediation, because it determines the amount of current flowing through the soil. EC is simultaneously influenced by many soil properties, viz; water content, soluble salts, grain size, humus, temperature, texture and cation exchange capacity (CEC) [193].

In this study, an integrated in situ remediation technique which couples electrokinetics with adsorption, using locally produced granular activated carbon (GAC) from date palm pits in the treatment zones that are installed directly to bracket the contaminated soils at bench-scale is investigated. Natural saline-sodic clay soil sampled from Al-Hassa Oasis, Saudi Arabia spiked with contaminant mixture (kerosene, phenol, Cr, Cd, Cu, Zn, Pb and Hg) was used in this study to investigate the effects of voltage gradient, initial

contaminant concentration and polarity reversal rate on the soil electrical conductivity using RSM. Optimal conditions (factor levels) required to minimize the soil electrical conductivity were also obtained using numerical optimization.

9.2 Results and Discussions

9.2.1 Mathematical Modeling Using Response Surface Methodology (RSM)

Table 34 presents the different combinations of the factors (independent variables) based on BBD that will enable the generation of 3D response surface and contour plots. These plots depict the relative influence of the factors on electrical conductivity for proper visualization and evaluation. The weekly results of the electrical conductivity measurements are also contained in the table.

Table 34 Weekly results of electrical conductivity based on Box-Behnken Design

Run order	Polarity reversal, A	Voltage gradient, B	Concentration, C	Electrical conductivity dS/m		
				1st Week	2nd Week	3rd Week
1	24	0.6	60	42.2	74.5	150.1
2	0	0.2	60	48.72	176.7	117.3
3	0	0.6	20	102.6	82.93	105.5
4	48	0.6	20	64.4	191.3	147.7
5	24	0.6	60	37.98	67.05	135.09
6	48	0.2	60	12.85	37.8	94.75
7	24	0.6	60	46.42	81.95	165.11
8	48	1	60	84.9	90.12	221.9
9	24	1	20	138.8	103.2	129.1
10	24	0.2	20	7.14	16.88	51.98
11	24	0.2	100	39.11	36.39	37.3
12	0	1	60	83.78	76.8	193.9
13	0	0.6	100	40.8	48.82	25.64
14	48	0.6	100	55.23	62.77	124.1
15	24	1	100	59.74	86.98	91.93

The data in Table 7.1 were fitted to quadratic, reduced cubic and reduced quadratic models for the 1st (equation 9.1), 2nd (equation 9.2) and 3rd (equation 9.3) weeks EC measurement respectively. These equations (in terms of coded factors) contain only effects or terms that are significant based on 5 % significant level (from analysis of variance). All insignificant terms have been dropped, except where hierarchy is violated. Good model prediction abilities may be inferred using coefficient of determination, R^2 and lack of fit tests [70]. Equation 9.2 has the best R^2, followed by equation 9.1 and 9.3. Lack of fit for all the models is insignificant.

$$Y_1 = 4.22 - 7.31A + 32.43B - 14.76C + 9.25AB + 13.16AC - 27.76BC + 9.96A^2 + 5.4B^2 + 13.6C^2 \quad (9.1)$$

(R^2 = 0.9766, quadratic model)

$$Y_2 = 70.64 + 30.58A + 34.23B + 0.82C + 38.06AB - 23.6AC - 8.93BC + 28.71A^2 - 6.89B^2 - 46.12A^2B - 41.48A^2C - 61.97AB^2 \quad (9.2)$$

(R^2 = 0.9919, reduced cubic model)

$$Y_3 = 15.402 + 18.26A + 41.94B - 19.416C - 6.487C^2 \quad (9.3)$$

(R^2 = 0.8466, reduced quadratic model)

Where Y_1 = electrical conductivity (dS/m), 1st week; Y_2 = electrical conductivity (dS/m), 1st week; Y_3 = electrical conductivity (dS/m), 1st week; A = polarity reversal, hr; B = voltage gradient, V/cm; C = concentration, mg/kg.

The perturbation plot is useful in comparing the relative effects of all factors on the response using a particular point in the design space (midpoint), with steeper slope or curvature in a factor signifying higher sensitivity of response to that factor. From Figure 51(a) and (c), voltage gradient (B) and concentration (C) have the steepest slope and curvature, hence, have greatest impact on the response. These influential factors became the best choice for the axes of the 3D response surface and contour plots as presented in Figure 51(b) and (d). Initial contaminant concentration affects the EC directly by increasing the available soluble ions in the soil, thereby enhancing its electrical conduction. The dependence of EC on factors such as soluble salts, water content and temperature that directly affect the electrical current makes voltage gradient influential on the EC as shown in Figure 51(a) and (c).

9.2.2 Numerical Optimization Using Desirability Function

Numerical optimization module in Design-Expert® software searches for a combination of factor levels that simultaneously satisfy the goals placed on the operating parameters (factors and responses). These goals are then combined into an overall Desirability function which ranges from 0 (i.e. outside of the limits) to 1 (i.e. at the goal). The program utilizes numerical optimization algorithms to find a point(s) that maximizes the Desirability function, not to clinch a Desirability value of 1 but to find a good set of conditions that will meet all the set goals for each factor and response. Simply put, Desirability is one of the mathematical methods for computing optimum values [120]. Overall Desirability of 0.64 was obtained after minimizing the weekly EC (Table 35).

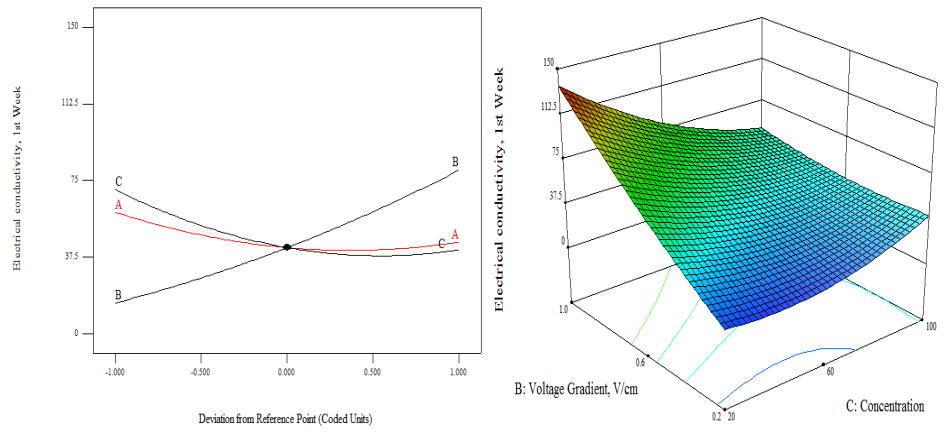

(a) (b)

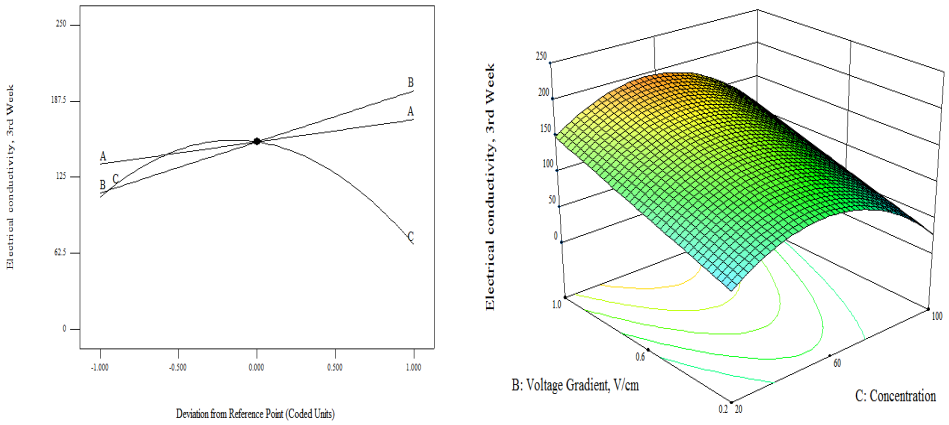

(c) (d)

Figure 51 Perturbation plots showing the relative significance of factors on electrical conductivity (left). 3D response surface and contour plots showing the relative influence of factors on electrical conductivity (Right): (a) and (b) - 1st week; (c) and (d) – 3rd week

Table 35 Results of numerical optimization of factors and responses using Desirability

Item	Value
Polarity reversal, hours	21.61
Voltage gradient, V/cm	0.51
Concentration, mg/kg	76.02
1st Week electrical conductivity, dS/m	34.59
2nd Week electrical conductivity, dS/m	63.20
3rd Week electrical conductivity, dS/m	124.88
Desirability	0.64

The optimization results presented in Table 35 suggest a steady increase in the EC with time. Similar trend is also discernible from most of the experimental runs in Table 34. The saline-sodic nature of the soil necessitates the use of processing fluids to continuously neutralize the rapidly generated H^+ and OH^- ions at the anode and cathode respectively. These fluids were monitored every 8 hours and replaced as they deteriorated. HNO_3 and NaOH are strong acid and base respectively, and dissociate completely according to the following reactions.

$$HNO_3(l) \rightarrow H^+(aq) + NO_3^-(aq) \tag{9.4}$$

$$NaOH(aq) \rightarrow Na^+(aq) + OH^-(aq) \tag{9.5}$$

As a result of the electrochemical decomposition of water, OH^- and H^+ ions are produced at the cathode and anode respectively as shown in equations 9.6 and 9.7.

$$4H_2O(l) + 4e^- \rightarrow H_2(g) + 4OH^-(aq) \tag{9.6}$$

$$2H_2O(l) \rightarrow O_2(g) + 4H^+(aq) + 4e^- \tag{9.7}$$

The electrochemically generated H^+ and OH^- ions due to water electrolysis at the anode and cathode respectively are neutralized to form water molecules (equation 9.8) as a

result of the OH^- and H^+ ions produced from the dissociation of the catholyte and anolyte respectively as shown in equations 9.5 and 9.4.

$$H^+(aq) + OH^-(aq) \rightarrow H_2O(l) \quad (9.8)$$

The oxygen and hydrogen gases generated may be vented out, while some amount may go into the soil and alter the redox chemistry. Na^+ and NO_3^- ions migrate into the soil to the opposite electrodes thereby increasing the electrical conductivity as the treatment process progresses. A sustained and variable electroosmotic flow was observed due to the migration of the Na^+ ions which could enhance the migration of the double layer complexes toward the cathode, while nitrate ions could be involved in complex formation with the cations.

Since the processing fluids are finite in volume and the electrochemical decompositon of water at the electrodes is continuous, then, a time will be reached when all the ions in the processing fluids have been exhausted. Consequently, rise and fall in catholyte pH and anolyte pH respectively are expected before the replacement of the processing fluids. At this juncture, OH^- ions generated at the cathode according to equation 9.6 migrate into soil toward the anode. In this migration process, soil pH rises and metal hydroxides are formed which could precipitate and reduce the electrical conductivity and increase current consumption near the cathode. At the same time, soluble hydroxocomplexes are formed with the cations due to complexing property of the hydroxyl ions. On the other, hydrogen ions generated at the anode (equation 9.7) migrate toward the cathode. This process may lead to soil protonation or desorption of indigeneous and spiked heavy metals, hence increase the electrical conductivity. Given the presence of carbonates in the soil minerals, the developing acid front may be buffered by the carbonate minerals,

thereby hindering any fall in the soil pH. From the forgoing discussion, it is clear that, there will be an increase in the soil electrical conductivity as the integrated electrokinetics-adsorption remediation progresses. In addition, the electroosmotic flow will undoubtedly vary spatially and temporally as it also depends on the soil zeta potential, pore fluid viscosity and permitivity.

9.3 Conclusion

The results presented have highlighted and elucidated the extent of the influence of voltage gradient and concentration on electrical conductivity using mathematical models and numerical optimization. The empirical models developed in this study may be used for preliminary estimation of soil electrical conductivity; however, actual soil under study should be tested for verification. The models are limited to the derived results obtained for saline-sodic soil, hence, generalization and use of these models for different soil types and operating conditions may lead to incorrect estimation of the electrical conductivity. From the perturbation plot, the following sequence of relative influence of the operating parameters on EC can be inferred: concentration > voltage gradient > polarity reversal. Hence lower voltage gradient may lead to lower electrical current, temperature, energy consumption and consequently lower electrical conductivity. On the other hand, high electrical conductivity was found to allow high electrical current through the soil and eventual rise in the cost of operating the remediation process.

CHAPTER 10

EFFECTS OF VOLTAGE GRADIENT ON THE PROCESSING FLUIDS DURING INTEGRATED ELECTROKINETICS-ADSORPTION REMEDIATION

10.1 Introduction

The rapid electrochemical decomposition of the electrolyte at the electrodes and subsequent generation of H^+ and OH^- ions at the anode and cathode respectively has necessitated the need to condition the anode and cathode chambers with H^+ and OH^- neutralizing chemicals. Saline-sodic soils have electrical conductivity greater than 4 dS/m and pH greater than 8.2. Hence, the exchangeable sodium percentage is usually greater than 15 [36, 225]. Lukman et al. [188] have demonstrated that processing fluids are rapidly degraded as a result of the soil nature which leads to excessive soil heating, reduction in the soil moisture content, high energy and process fluid consumption, and in some cases, higher percentage removal of contaminants. Ultimately, these consequences may lead to eventual rise in the cost of operating the remediation process if proper investigation on the rate of replacement or refill of processing fluids is not carried out. While numerous previous investigations concentrated on the optimization of the concentration of the processing fluids (popularly referred to as anolyte and catholyte) [47, 65, 190] using the Response Surface Methodology (RSM) or the traditional one-factor-at-

a-time (OFAT) - the present study was aimed at investigating the simultaneous effects of voltage gradient, initial contaminant concentration and polarity reversal on the rate of replacement or refill of processing fluids (anolyte and catholyte). This study was carried out experimentally based on Box-Behnken Design of experiment and subsequent generation of mathematical models and optimization using RSM and numerical optimization approaches followed.

10.2 Results and Discussions

The saline-sodic nature of the soil necessitates the use of processing fluids to continuously neutralize the rapidly generated H^+ and OH^- ions at the anode and cathode respectively. These fluids were monitored every 8 hours and replaced as they degraded. HNO_3 and NaOH are strong acid and base respectively, and dissociate completely according to the following reactions.

$$HNO_3(l) \rightarrow H^+(aq) + NO_3^-(aq) \quad (10.1)$$

$$NaOH(aq) \rightarrow Na^+(aq) + OH^-(aq) \quad (10.2)$$

Because of the electrochemical decomposition of water, OH^- and H^+ ions are produced at the cathode and anode respectively as shown in equations (10.3) and (10.4).

$$4H_2O(l) + 4e^- \rightarrow H_2(g) + 4OH^-(aq) \quad (10.3)$$

$$2H_2O(l) \rightarrow O_2(g) + 4H^+(aq) + 4e^- \quad (10.4)$$

The electrochemically generated H^+ and OH^- ions due to water electrolysis at the anode and cathode respectively are neutralized to form water molecules (equation 10.5) because

of the OH^- and H^+ ions produced from the dissociation of the catholyte and anolyte respectively as shown in equations 10.2 and 10.1.

$$H^+(aq) + OH^-(aq) \rightarrow H_2O(l) \qquad (10.5)$$

The oxygen and hydrogen gases generated may be vented out, while some amount may go into the soil and alter the redox chemistry [187]. Na^+ and NO_3^- ions migrate into the soil to the opposite electrodes thereby increasing the electrical conductivity as the treatment process progresses. A sustained and variable electroosmotic flow was observed due to the migration of the Na^+ ions, which could have enhanced the migration of the double layer complexes toward the cathode, while nitrate ions could have been involved in complex formation with the cations [167]. This electroosmotic flow will lead to decreasing volume of the anolyte and increasing volume of the catholyte over time. Hence, refilling the anolyte is necessary even if it has not degraded completely. In addition, since the processing fluids are finite in volume and the electrochemical decomposition of water at the electrodes is continuous, then, a time will be reached when all the ions in the processing fluids have been exhausted. Consequently, rise and fall in catholyte pH and anolyte pH respectively are expected before the complete replacement of the processing fluids. Now, OH^- ions generated at the cathode according to equation 8.3 migrate into soil toward the anode. In this migration process, soil pH rises and metal hydroxides are formed which could precipitate and reduce the electrical conductivity and increase current consumption near the cathode [5]. At the same time, soluble hydroxocomplexes are formed with the cations due to complexing property of the hydroxyl ions [65, 188]. On the other hand, hydrogen ions generated at the anode (equation 10.4) migrate toward the cathode. This process may lead to soil protonation or

desorption of indigenous and spiked heavy metals, hence increasing the electrical conductivity [166]. Given the presence of calcite in the soil minerals, the developing acid front may be buffered by the carbonate mineral, thereby hindering any fall in the soil pH. From the forgoing discussion, it is clear that, there will be an increase in the soil electrical conductivity as the integrated electrokinetics-adsorption remediation progresses. In addition, the electroosmotic flow will undoubtedly vary spatially and temporally as it also depends on the soil zeta potential, pore fluid viscosity and permittivity [175].

10.2.1 Mathematical Modeling Using Response Surface Methodology (RSM)

Table 36 presents the different combinations of the factors (independent variables) based on BBD that will enable the generation of 3D response surface and contour plots. These plots are necessary for the depiction of the relative influence of factors on the processing fluids for proper visualization and evaluation. It is evident from Table 8.1, that the rate of anolyte refill is usually greater than or equal to its corresponding rate of anolyte replacement for a given run (except for Runs 9-11, 14).

Continuous electroosmotic flow emanating from the anode to the cathode is responsible for the volume reduction of the anolyte prior to its subsequent degradation as the electrochemical decomposition of water continues. The saline-sodic nature of the clay led to rapid degradation of the conditioning fluids which necessitated the use of 2 N NaOH solution as anolyte; a value that is higher than the usual concentration used by previous researchers [47, 65, 226]. Consequently, anolyte volume reduces which leads to refill, without commensurate degradation in pH that would lead to replacement.

Table 36 Processing fluids replacement and refill rate results based on Box-Behnken Design

Run order	Polarity reversal, A	Voltage gradient, B	Concentration, C	Processing fluids refill/replacement rates, #			
				(a) Anolyte refill rate	(b) Catholyte refill rate	(c) Anolyte replacement rate	(d) Catholyte replacement rate
1	24	0.6	60	47	1	7	50
2	0	0.2	60	3	0	1	6
3	0	0.6	20	40	0	11	51
4	48	0.6	20	37	6	13	42
5	24	0.6	60	42	1	6	45
6	48	0.2	60	0	0	0	4
7	24	0.6	60	52	1	8	55
8	48	1	60	33	0	24	54
9	24	1	20	12	0	32	42
10	24	0.2	20	3	0	5	5
11	24	0.2	100	2	0	5	7
12	0	1	60	29	0	28	57
13	0	0.6	100	9	16	9	16
14	48	0.6	100	6	0	20	26
15	24	1	100	14	0	29	44

However, low voltage gradient of 0.2 V/cm (Runs 2, 6, 10-11) produced an extremely low electroosmotic flow rate (Figure 52) so that the rate of refill is extremely low (Runs 2, 10-11), or even zero (Run 6).

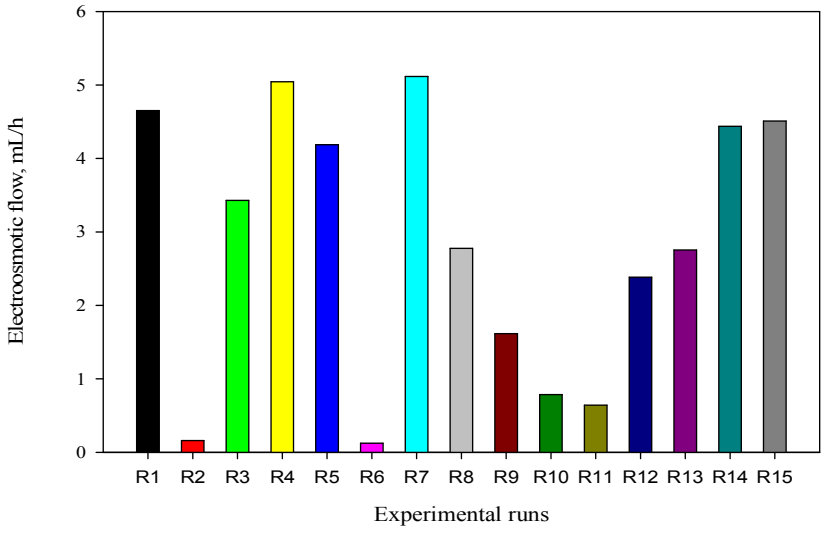

Figure 52 Average electroosmotic flow rates for the 15 experimental runs

On the other hand, the sustained electroosmotic flow led to an increase in the volume of the catholyte and rapid degradation necessitating much more frequent replacement than refill (Table 36). The few times that refill was carried out may be attributed to evaporation of the catholyte and leaks detected during the tests. Electroosmotic flow from the anode to the cathode in addition to the higher concentration of the anolyte compared to the catholyte led to higher rates of catholyte replacement. The data in Table 36 (last four columns) were fitted to reduced quadratic models for the anolyte refill rate (equation 10.6), catholyte refill rate (equation 10.7), anolyte replacement rate (equation 10.8) and catholyte replacement rate (equation 10.9).

Coded model equations:

$$\text{Sqrt (Anolyte refill rate)} = 6.31 - 0.27 * A + 1.68 * B - 0.87 * C - 2.69 * B^2 - 1.44 * C^2 \quad (10.6)$$

$$\text{Sqrt (Catholyte refill rate)} = 1 - 0.19 * A + 0.19 * C - 1.61 * A * C + 0.31 * A^2 - 1.31 * B^2 + 0.31 * C^2 \quad (10.7)$$

$$\text{Anolyte replacement rate} = 7.54 + A + 12.75 * B + 0.25 * C + 5.31 * B^2 + 5.31 * C^2 \quad (10.8)$$

$$\text{Catholyte replacement rate} = 46.77 - 0.50 * A + 21.88 * B - 5.88 * C - 14.10 * B^2 - 10.60 * C^2 \quad (10.9)$$

Where A = polarity reversal, hr; B = voltage gradient, V/cm; C = concentration, mg/kg.

These equations (in terms of coded factors) contain only effects or terms that are significant based on 5 % significant level whose analysis of variance (ANOVA) are

provided in Table 37. All insignificant terms have been dropped, except where hierarchy is violated or marginal significance exists.

Table 37 Significant levels of models, lack of fit and individual model terms at 5 % ($p < 0.05$)

Response	Significance of model and model terms								
	Model	Lack of fit	A	B	C	A^2	B^2	C^2	AC
Anolyte refill rate, #	0.0039	0.0655	0.5533	0.0040	0.0778	-	0.0024	0.0527	-
Catholyte refill rate, #	< 0.0001	-	0.1036	1.0000	0.1036	0.0846	< 0.0001	0.0846	< 0.0001
Anolyte replacement rate, #	< 0.0001	0.0868	0.3620	< 0.0001	0.8157	-	0.0070	0.0070	-
Catholyte replacement rate, #	0.0007	0.2238	0.8775	< 0.0001	0.0954	-	0.0139	0.0478	-

Anderson and Whitcomb [70] have defined coefficient of determination (R^2) as a measure of the amount of variation around the mean prediction explained by the model. This statistic may be used to assess model prediction abilities together with the lack of fit statistic. However, raw R^2 has been reported to be biased [70], because it can be increased by increasing the number of terms in the model irrespective of the significance of these additional terms. Adjusted R^2 gives more accurate, less biased and better goodness-of-fit measure than raw R^2. Adequate precision measures the signal to noise ratio and a value greater or equal to 4 is required to indicate adequate signal. Mathematical analyses of these statistics are treated by Anderson and Whitcomb [70]. Anolyte replacement rate is the most important of the responses, and has a high adequate precision (17) and good adjusted R^2 value of 0.9232 (Table 38). Nonetheless, high values of R^2 are essential for modeling the experimental design space, while in identification of significant factors, R^2 value does not matter, for significant factors will remain significant [70].

Table 38 Salient characteristics of the developed models

Response	Sequence of influential factors	Response Transformation	Adequate precision	R^2	Adjusted R^2
(a) Anolyte refill rate, #	B > C > A	Square root	9	0.8167	0.7148
(b) Catholyte refill rate, #	B > C = A	Square root	18	0.9684	0.9369
(c) Anolyte replacement rate, #	B > C > A	None	17	0.9507	0.9232
(d) Catholyte replacement rate, #	B > C > A	None	11	0.8787	0.8113

Perturbation plots were used to obtain the sequence of the influential factors presented in Table 38. These plots, presented in Figure 53, have been used to compare relative effects of all factors on the response by choosing a particular point in the design, usually the midpoint. Steeper slope or curvature indicates higher sensitivity of the response to that factor, while flat line indicates insensitivity. It is evident from Figure 53 that voltage gradient (B) and concentration (C) have the steepest slope and curvature, hence, have greatest impact on the responses (Figure 54). These influential factors became the best choice for the axes of the 3D response surface and contour plots as presented in Figure 54. Voltage gradient determines the amount of current flow into the soil, which in turn, controls the rate of the electrochemical decomposition of the electrolyte and its subsequent degradation. Hence, it is not by accident, that it emerged as the most influential factor.

Figures 54(a), (c) and (d) depict that increasing the voltage gradient will lead to an increase in the rates of anolyte refill and replacement and catholyte replacement. However, increasing the voltage gradient beyond 0.6 V/cm, led to a decrease in the rate of catholyte refill as shown in Figure 54(b). Because, within this range of the voltage gradient, the catholyte becomes completely degraded (turned alkaline) and complete

replacement is necessary. Catholyte pH value of about 13 was persistently recorded for all tests having 1 V/cm.

10.2.2 Desirability Function for Numerical Optimization

Numerical optimization module in Design-Expert® software searches for a combination of factor levels that simultaneously satisfy the goals placed on the operating parameters (factors and responses). These goals are then combined into an overall Desirability function which ranges from 0 (i.e. outside of the limits) to 1 (i.e. at the goal) using a geometeric mean. The overall Desirability value measures the overall success in simultaneous optimization of multiple responses [120]. The program utilizes numerical optimization algorithms to find a point(s) that maximizes the Desirability function, not to clinch a Desirability value of 1 but to find a good set of conditions that will meet all the set goals for each factor and response. Tables 39 and 40 present the optimization plan for each scenario and optimal conditions respectively.

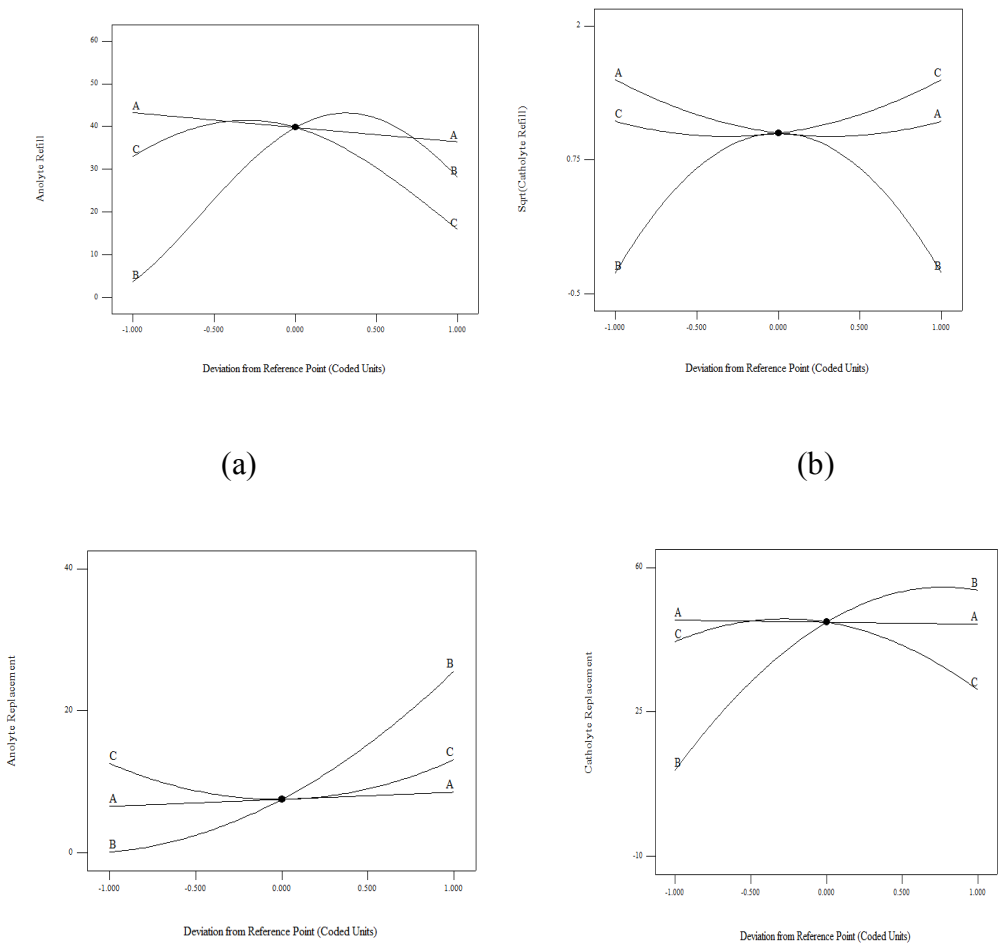

Figure 53 Perturbation plots showing the relative influence of factors on rate of processing fluids refill and replacement: (a) anolyte refill rate; (b) catholyte refill rate; (c) Anolyte replacement rate; (d) catholyte replacement rate

Case 1 contains the simplest scenario of minimizing the replacement of the processing fluids. Additional goals were gradually introduced in the subsequent cases to systematically analyze any synergistic or antagonistic characteristics that may result from the simultaneous optimization of several responses. Desirability results from Table 40 reveals how adding more responses led to decreased overall Desirability.

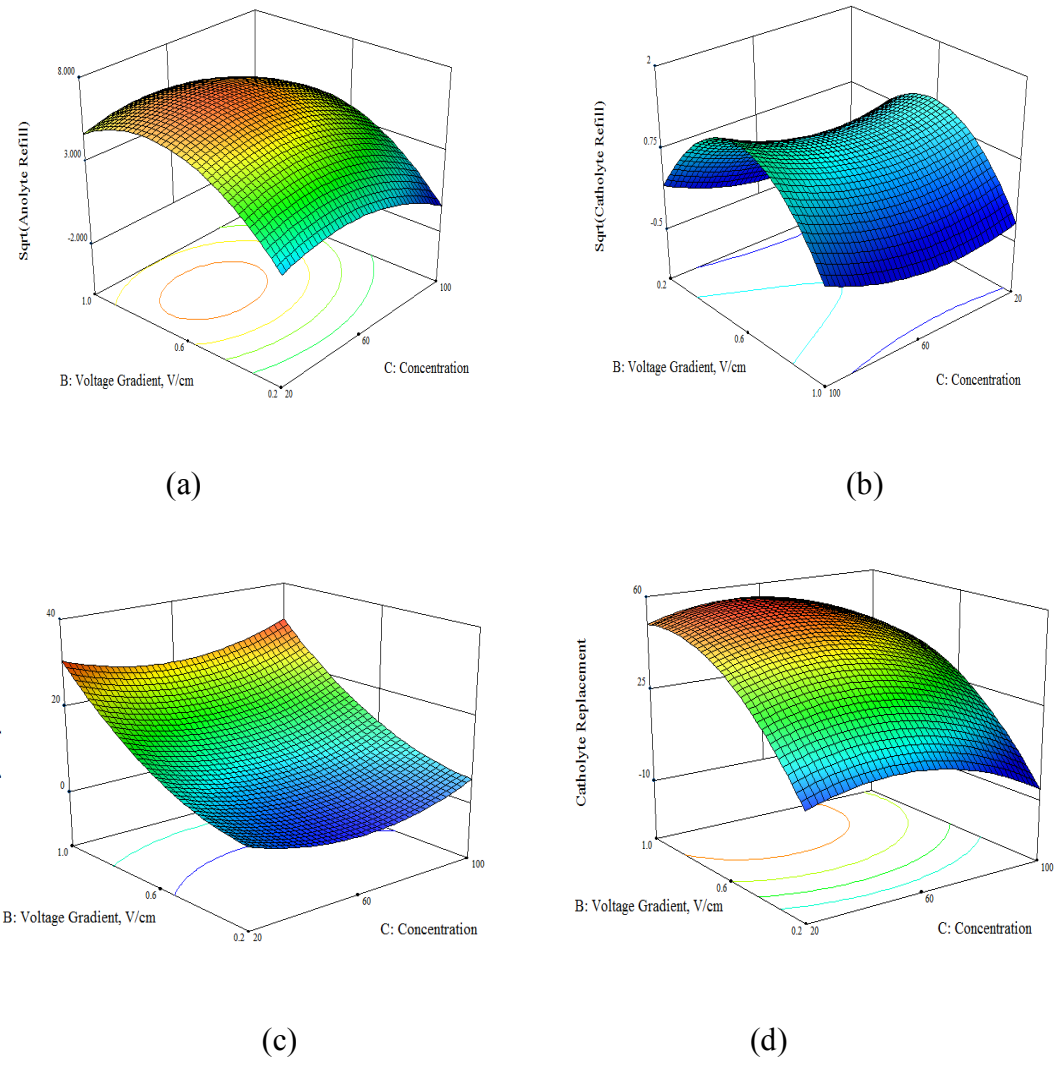

Figure 54 3D response surface and contour plots showing the variation of the rate of processing fluids refill and replacement relative to the influential factors: (a) anolyte refill rate; (b) catholyte refill rate; (c) Anolyte replacement rate; (d) catholyte replacement rate

Case 6 contains all the responses monitored during the tests that are eligible for optimization whose individual Desirability values are depicted in Figure 55. For this case, overall Desirability of 0.61 was attained at optimal voltage gradient of 0.34 V/cm. Figure 56 presents a 3D graphical representation of the variation of Desirability relative to the influential factors.

Table 39 Optimization plan for different scenarios

Scenarios	Optimization parameters & goals						
	Replacement of fluids	Refill of fluids	Factors, A, B, C	Other contaminants*	Other responses**	Weight	Importance
Case 1	minimize	-	in range	-	-	default - 1	default - 3
Case 2	minimize	-	A-in range; B-min; C-max	-	-	default - 1	default - 3
Case 3	minimize	minimize	A-in range; B-min; C-max	-	-	default - 1	default - 3
Case 4	minimize	minimize	A-in range; B-min; C-max	maximize	optimize***	default - 1	default - 3
Case 5	minimize	minimize	A-in range; B-min; C-max	maximize	optimize***	3	5

*Zn, Pb, Cu, Cr, Phenol, TPH (2nd & 3rd week)

**Average current, electroosmotic volume (EOV), flushed pore volume (PV), electroosmotic conductivity (K_e), anolyte refill, catholyte refill, anolyte replacement, catholyte replacement, electrical conductivity (2nd & 3rd weeks), soil pH (2nd & 3rd weeks)

***Maximize: Contaminant removal efficiencies, EOV, PV, K_e - Minimize: electrical conductivity, soil pH

Table 40 Optimized factor levels and corresponding response and Desirability values for all scenarios

Scenarios	Optimization results								
	A (hr)	B (V/cm)	C (mg/kg)	Anolyte replacement	Catholyte replacement	Anolyte refill	Catholyte refill	Overall Desirability, D	Remarks
Case 1	0	0.2	83.91	1.1	4.0	-	-	0.98	Optimize replacement of processing fluids only (factors in range)
Case 2	0	0.2	87.38	1.8	2.3	-	-	0.95	Optimize replacement of processing fluids + factors
Case 3	12.98	0.2	90.69	3.0	0.3	0.3	0.6	0.96	Optimize replacement & refill of processing fluids + factors
Case 4	20.76	0.49	66.93	4.4	38.1	29.7	1.0	0.71	Optimize replacement & refill of processing fluids + factors + all responses
Case 5	20.92	0.34	67.87	1.6	24.6	14.7	0.3	0.61	Optimize replacement & refill of processing fluids (*Weight* & *Importance* assigned) + factors + all responses

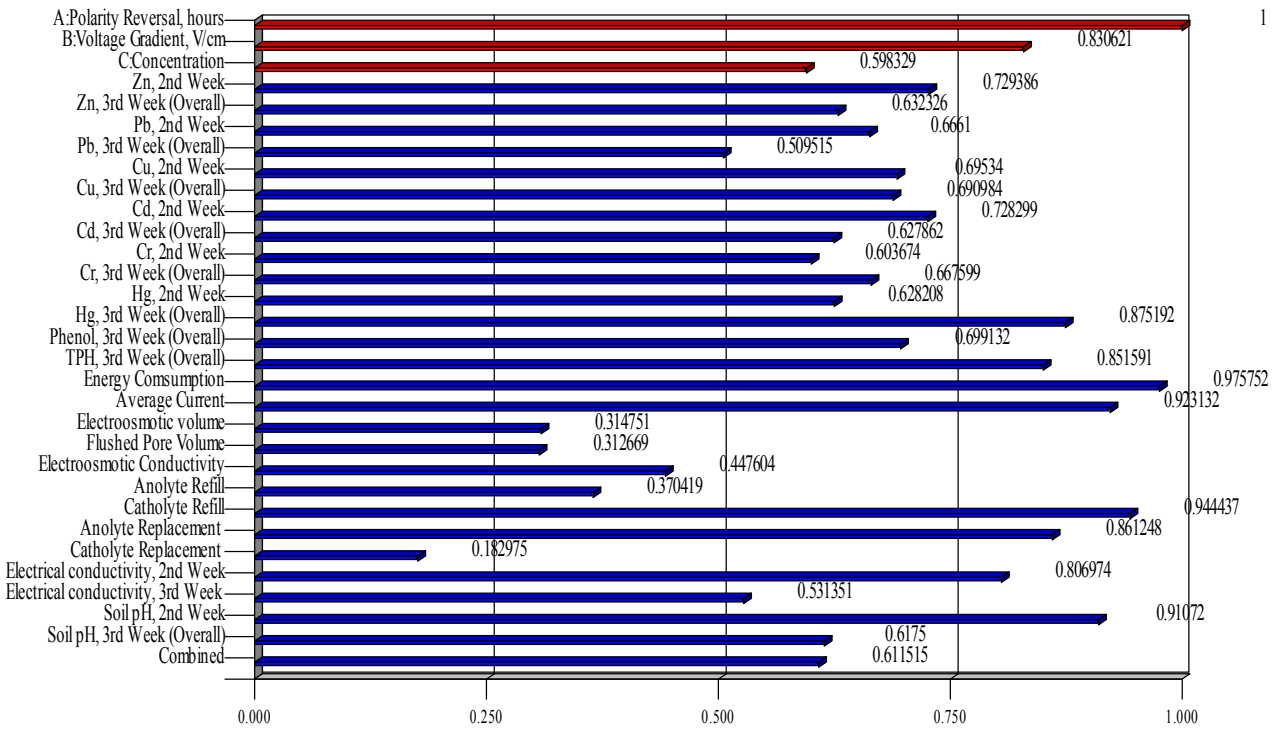

Figure 55 Overall and individual response Desirability values

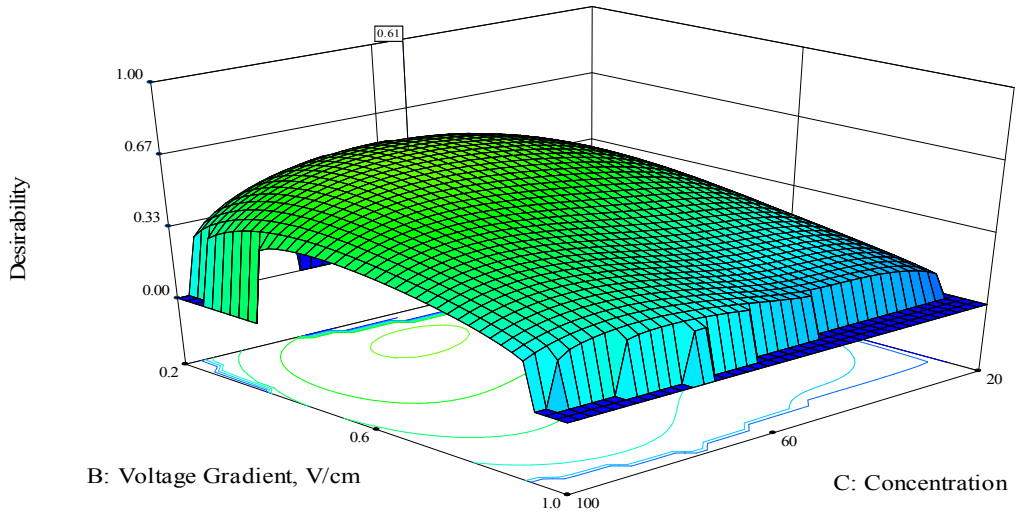

Figure 56 3D Variation of overall Desirability relative to the influential factors

10.3 Conclusion

In this study, the effects of voltage gradient, initial contaminant concentration and polarity reversal on the rate of the replacement or refill of processing fluids (anolyte and catholyte) were experimentally studied based on Box-Behnken Design of experiment and mathematically modeled using Response Surface Methodology. The saline-sodic nature of the soil necessitated the use of conditioning fluids whose operational intricacies need elaborate investigations to achieve an optimal operating cost of the integrated electrokinetics-adsorption remediation of contaminated soil. Using the RSM technique, mathematical models were developed using quadratic functions for the prediction of the rate of refill or replacement of these conditioning fluids. The results presented also highlighted the extent of the influence of voltage gradient and concentration on the target response using perturbation plots, mathematical models and numerical optimization. Desirability function was successfully applied for the optimization of five (5) different scenarios. After simultaneous optimization of all the investigated responses, a Desirability value of 0.61 was obtained at an optimal voltage gradient of 0.34 V/cm. Under this condition, the rate of replacement of the anolyte was approximately 2 as against the maximum rate of 32 that was encountered during the tests. The empirical models developed in this study may be used for preliminary estimation of the target responses; however, actual soil under study should be tested for verification. The models are also limited to the derived results obtained for saline-sodic soil, hence, generalization and use of these models for different soil types and different operating conditions may lead to incorrect estimation of the target responses. From the perturbation plots, sequence of relative influence of the operating parameters on the target responses is as follows:

voltage gradient > concentration > polarity reversal. Hence, lower voltage gradient obtained from the numerical optimization results may lead to lower electrical current, temperature, energy consumption and consequently lower electrical conductivity and eventual reduction in the cost of operating the remediation process.

CHAPTER 11

CONCLUSIONS AND RECOMMENDATIONS

11.1 Summary

In this research, three sets of tests were conducted, namely, set 1, set 2 and set 3, to study the potential of remediating saline-sodic soil that was spiked with contaminant mixture (Cr, Cu, Cd, Pb, Zn, Hg, phenol and kerosene) using integrated electrokinetics-adsorption remediation (IEKAR).

In set 1, the soil physico-chemical characteristics determined include: pH, moisture content, soil organic matter, electrical conductivity, specific surface area, pore volume, pore size, mineralogy and elemental analysis. Adsorption and desorption behaviors selectivity sequences of Cd, Cr, Cu, Pb and Zn ions onto the clay minerals were investigated in single and multi-component scenarios at different pH values (2, 4, 6, 8, 10 and 12).

The potential of coupling electrokinetics and adsorption using locally produced granular activated carbon from date palm pits for the remediation of the saline-sodic soil was investigated in set 2. The soil was spiked with Cr, Cd, Cu, Zn, Pb, Hg, phenol, kerosene, at given concentrations and three bench-scale tests were run for a period of 21 days. Two of the experiments had GAC chambers bracketing the contaminated soil chamber and were operated at voltage gradients of 0.6 V/cm and 1 V/cm. The third one utilized only electrokinetics at a voltage gradient of 0.6 V/cm.

In set 3, fifteen (15) bench-scale experiments, each having a 21-day run time, were designed and performed to investigate the migration and distribution of the contaminant mixture using the IEKAR and to understand the operating variables' effects on some key factors and responses. Box-Behnken Design (BBD) was chosen for the experimental design because of its advantages over central composite design (CCD) and 3-level factorial design when dealing with only three factors. The investigated variables (called factors in RSM) are the voltage gradient, initial contaminant concentration and polarity reversal rate. These variables were selected based on their known influence on contaminant remedial efficiency and were coded and varied at three levels simultaneously to investigate their interaction effects on the 41 responses monitored. RSM, incorporated into Design-Expert® 8.0, was used in mathematical modeling, numerical optimization and interpretation of the results. Geochemical modeling and ionic speciation were carried out using Visual MINTEQ 3.0.

11.2 Conclusions

The adsorption selectivity sequences obtained using the coefficient of distribution for the single and multi-component scenarios are Cr > Pb > Cu > Cd > Zn and Cr > Cu > Pb > Cd > Zn respectively. Desorption study has revealed a selectivity sequence of Cr < Cd < Cu < Pb < Zn with the highest percentage desorption occurring at pH = 12, due to the formation of soluble hydroxocomplexes. Ionic size or activity, first hydrolysis constant, soil type and pH of the system have been identified as the general factors that influence selectivity sequence of heavy metals. The main focus of this investigation was not on the adsorbed or precipitated species, but rather, on the mobile or dissolved species that can be

removed via electromigration or electroosmotic flow during electrokinetic remediation. Hence, heavy metal precipitation at high pH values were not of any concern.

The soil salinity and sodicity, which provided large amount of dissolved salts and minerals in the pore fluid for sustained high electrical conduction, were responsible for the extremely high electric current flow which led to excessive soil heating, high energy and process fluid consumption, high electroosmotic volume, dissolution and corrosion of anodic electrodes and DC voltage clips and in some cases, higher contaminant remedial efficiency. However, it has been shown that high voltage gradient (1 V/cm) or passage of high electric current does not necessarily yield high remedial efficiency. Despite the high selectivity of trivalent Cr exhibited by the clay soil, the alkaline pH maintained for most of the experimental duration has led to the formation of anionic hydroxocomplexes which were removed via electromigration.

Significant contaminant migration from the contaminated chamber to the GAC chamber was recorded which led to high remedial efficiencies for tests involving 60 mg/kg initial contaminant concentration, whereas extremely low or no removal was recorded for all tests involving 20 mg/kg. Hence, initial contaminant concentration significantly influences the remedial efficiency of heavy metals. Optimum range of Polarity reversal rate has been found to be 18 - 24 hr. Values outside this range could lead to increased energy expenditure at the expense of higher remedial efficiency.

Conditioning of electrolyte pH at the electrodes enhanced the migration of double layer complexes leading to increased electroosmotic flow. It has been found that the complexing capacity of the OH^- ions and HNO_3 is sufficient for effective heavy metal

complexation, so that use of an external complexant or chelant may not be necessary. In addition, a good understanding of the geochemical processes is a prerequisite to obtaining good remedial efficiency. Passage of electric current and variations in the pore fluid chemistry led to soil mineral dissolution and alteration via biotransformation. Dissolution of the clay minerals, indigenous soil salts and changes in the soil characteristics affected the soil specific surface area, pore volume and size and mineralogy.

Using the RSM technique, many mathematical models were developed using quadratic functions for effective prediction of contaminants remedial efficiencies and obtaining optimal factor levels. Following effective preliminary design evaluation, mathematical model development and running model diagnostic tests, experimental model validation was successfully undertaken. The models are limited to the derived results obtained from the saline-sodic soil, hence, generalization and use of the model for different soil types and different operating conditions outside those investigated may lead to incorrect estimation of the responses. Synergistic or antagonistic effects arising from simultaneously optimizing multiple factors and responses have been revealed using the hierarchical optimization scenarios which utilized the Desirability function.

From the experimental results and analysis of the interaction effects of the factors on the responses, voltage gradient has the highest influence, followed by initial contaminant concentration and then polarity reversal rate. Conclusively, application of RSM using BBD to IEKAR is an economical way of obtaining sufficient information with the least experimental runs.

11.3 Contributions of the Research

Although several investigations were carried out on a high buffering capacity soil called glacial till, none of them focused on saline-sodic soil which has an extremely high EC and is dominant in arid and semi-arid regions. Operating condition peculiarities (such as high current processing fluids refill or replacement rate), in addition to factor interaction effects that are specific to the soil were extensively investigated using mathematical modeling and numerical optimization. This will enrich the literature of soil remediation using electrokinetic technique. The research has exposed many areas of potential investigations.

This is the first research that used BBD for experimental design of EKR - two previous investigators used CCD and optimal design. Hence, it is the third paper that utilized RSM for EKR of soils and the only one that clearly demonstrated the mathematical modeling and numerical optimization concepts as they affect remediation of saline-sodic soils contaminated with mixed pollutants. It is the first study that clearly validated the predicted model results experimentally using different factor levels from those used for the model development. In addition, the study is novel in addressing synergistic and antagonistic effects arising from simultaneous optimization of multiple factors and responses for effective soil remediation. These contributions can be clearly seen in the articles that evolved from the research. Eleven (11) articles were extracted from this research so far, seven (7) in journals and four (4) in conference proceedings.

11.4 Recommendations for Future Research

In the course of carrying out this research, some areas that are outside the scope of the present study have been identified and are thus, recommended for future research. These areas are detailed below:

a) The soil salinity and sodicity, which provided large amount of dissolved salts and minerals in the pore fluid for high electrical conduction, were responsible for the extremely high electric current flow when using values of 0.6 and 1 V/cm. This led to the dissolution and corrosion of the supposed inert graphite anodic electrodes and DC voltage clips. It is believed that these dissolution and corrosion products could affect the contaminants remedial efficiencies, hence, it is recommended that different electrode materials such as platinum, graphite coated with diamond, titanium and titanium coated electrodes should be investigated under varying operating conditions. Depending on their stability and how they affect the remedial efficiency, the best electrode material can be chosen for the EKR of the saline-sodic soil.

b) During one of the tests, bentonite, which is an expansive soil that consists of 100 % montmorillonite, was used for four (4) days. The operational difficulties encountered were an extremely high electroosmotic conduction in addition to the expansive nature of the soil. This necessitated shutting down the test. Thereafter, a different soil that did not contain montmorillonite was used for the EKR for twenty one (21) days under the same factor levels as the bentonite test. The former test was found to achieve far higher contaminants remedial efficiencies than the latter test, which suggested that the amount of montmorillonite affected

the remedial efficiency. It is recommended that different amount of montmorillonite be investigated so that a clearer understanding on the extent of this effect is obtained vis-à-vis the extremely high surface area of montmorillonite for adsorption.

c) Although, it has been postulated that the complexing capacity of the OH^- ions and HNO_3 is sufficient for effective heavy metal complexation, it is recommended that the effects of other complexing or chelating agents on the remedial efficiencies of heavy metals in saline-sodic soil be investigated.

d) Use of RSM optimization to investigate how non-uniform electric field, pulse and continuous current affect the EKR of saline-sodic soil will also help in optimizing the remedial efficiency.

e) Given the contrasting high mobility, low sorptive capacity and remedial efficiency for trivalent Cr during the IEKAR, investigation of redox conditions that may ensue due to presence of Fe, SOM, Mn and electrode reactions (generating oxygen and hydrogen) vis-à-vis Cr oxidation or reduction is recommended.

f) Many researchers have used different soil to water ratio (1:1, 1:2, 1:5, 1:10), agitation times and methods (stirring, shaking, centrifuging) in trying to maximize the measurement of soil EC, which is an important parameter in classifying soil salinity. OFAT optimization technique was employed, which underestimates the true optimum value. Use of RSM optimization to investigate how these factors simultaneously interact to produce the optimum soil EC value is recommended.

g) Synergistic coupling of RSM and artificial neural network (ANN) will lead to a higher accuracy in model predictions and result analysis. Although ANN cannot produce a model equation as in RSM, it represents the nonlinearities better than the RSM does, and has superior accuracy over RSM in data learning and prediction by working in a similar way as the human brain does. Using RSM and ANN for EKR studies will greatly improve the modeling and optimization analysis.

h) The optimal operating conditions obtained in this research could be utilized for pilot scale implementation of the IEKAR. It will help in the scaling-up process, from bench-scale to pilot-scale, and will facilitate in investigating scaling effects.

REFERENCES

[1] J.I. Chang, C.-C. Lin, A study of storage tank accidents, Journal of Loss Prevention in the Process Industries, 19 (1), 51-59, (2006).

[2] S.V. Ho, C.J. Athmer, P.W. Sheridan, A.P. Shapiro, Scale-up aspects of the lasagna™ process for in situ soil decontamination, J. Hazard. Mater., 55 (1–3), 39-60, (1997).

[3] L. Casagrande, Electro-osmotic stabilization of soils, Boston Society Civil Engineers Journal, 39 (1), 51-83, (1952).

[4] A.P. Shapiro, P. Renaud, R.F. Probstein, Preliminary studies on the removal of chemical species from saturated porous media by electroosmosis, Physicochemical Hydrodynamics, 11 (5/6), 785 - 802, (1989).

[5] J. Hamed, Y. Acar, R. Gale, Pb(ii) removal from kaolinite by electrokinetics, Journal of Geotechnical Engineering, 117 (2), 241-271, (1991).

[6] Y. Acar, H. Li, R. Gale, Phenol removal from kaolinite by electrokinetics, Journal of Geotechnical Engineering, 118 (11), 1837-1852, (1992).

[7] C. Bruell, B. Segall, M. Walsh, Electroosomotic removal of gasoline hydrocarbons and tce from clay, Journal of Environmental Engineering, 118 (1), 68-83, (1992).

[8] B. Segall, C. Bruell, Electroosmotic contaminant-removal processes, Journal of Environmental Engineering, 118 (1), 84-100, (1992).

[9] Y.B. Acar, A.N. Alshawabkeh, Principles of electrokinetic remediation, Environmental Science & Technology, 27 (13), 2638-2647, (1993).

[10] R. Lageman, Electroreclamation. Applications in the netherlands, Environmental Science & Technology, 27 (13), 2648-2650, (1993).

[11] A.P. Shapiro, R.F. Probstein, Removal of contaminants from saturated clay by electroosmosis, Environmental Science & Technology, 27 (2), 283-291, (1993).

[12] C.J. Athmer, S.V. Ho, Field studies: Organic-contaminated soil remediation with lasagna technology, in: K.R. Reddy, C. Cameselle (Eds.) Electrochemical remediation technologies for polluted soils, sediments and groundwater, John Wiley & Sons, Inc., 2009, pp. 625-646.

[13] S.V. Ho, P.W. Sheridan, C.J. Athmer, M.A. Heitkamp, J.M. Brackin, D. Weber, P.H. Brodsky, Integrated in situ soil remediation technology: The lasagna process, Environmental Science & Technology, 29 (10), 2528-2534, (1995).

[14] S.V. Ho, C. Athmer, P.W. Sheridan, B.M. Hughes, R. Orth, D. McKenzie, P.H. Brodsky, A.M. Shapiro, T.M. Sivavec, J. Salvo, D. Schultz, R. Landis, R. Griffith, S. Shoemaker, The lasagna technology for in situ soil remediation. 2. Large field test, Environmental Science & Technology, 33 (7), 1092-1099, (1999).

[15] S.V. Ho, B.M. Hughes, P.H. Brodsky, J.S. Merz, L.P. Egley, Advancing the use of an innovative cleanup technology: Case study of lasagna™, Remediation Journal, 9 (3), 103-116, (1999).

[16] USEPA, Lasagna public-private partnership, United States Environmental Protection Agency, EPA542-F-97-012a, (1997).

[17] D. Huang, Q. Xu, J. Cheng, X. Lu, H. Zhang, Electrokinetic remediation and its combined technologies for removal of organic pollutants from contaminated soils, International Journal of Electrochemical Science, 7 (1), 4528-4544, (2012).

[18] K. Maturi, K.R. Reddy, Simultaneous removal of organic compounds and heavy metals from soils by electrokinetic remediation with a modified cyclodextrin, Chemosphere, 63 (6), 1022-1031, (2006).

[19] K.R. Reddy, P.R. Ala, S. Sharma, S.N. Kumar, Enhanced electrokinetic remediation of contaminated manufactured gas plant soil, Engineering Geology, 85 (1–2), 132-146, (2006).

[20] T. Li, S. Yuan, J. Wan, L. Lin, H. Long, X. Wu, X. Lu, Pilot-scale electrokinetic movement of hcb and zn in real contaminated sediments enhanced with hydroxypropyl-β-cyclodextrin, Chemosphere, 76 (9), 1226-1232, (2009).

[21] M. Elektorowicz, Electrokinetic remediation of mixed metals and organic contaminants, in: Electrochemical remediation technologies for polluted soils, sediments and groundwater, John Wiley & Sons, Inc., 2009, pp. 315-331.

[22] K.R. Reddy, Integrated electrokinetic remediation technologies: Opportunities and challenges, 6th Symposium on Electrokinetic Remediation, EREM Vigo, Spain, 12-15th June, (2007).

[23] M. Elektorowicz, R. Chifrina, B. Konyukhov, Behaviour of tension - active compounds used to clean up of contaminated manufactured gas plant sites, Land Contamination & Reclamation, 3 (4), 2 - 4, (1995).

[24] M. Elektorowicz, M. Hakimipour, Electrical fi eld applied to the simultaneous removal of organic and inorganic contaminants from clayey soil 18th Eastern Research Symposium on Water Quality, October 18, Montreal, Canada : CAWQ ((2001).

[25] M. Elektorowicz, M. Hakimipour, Practical consideration for electrokinetic remediation of contaminated soil, CSCE 8th Environmental and Sustainable Engineering Specialty Conference and Offshore Engineering, June 4 - 7, Moncton, Canada : CSCE , pp. 689 - 698, (2003).

[26] M. Elektorowicz, M. Hakimipour, Electrokinetic soil remediation method for mixed contaminated soil, 6th Conference on Civil Engineering,, May 5 - 7, Isfahan, Iran, (2003).

[27] K.R. Reddy, S.N. Kumar, Electrokinetic remediation of organic silty sand contaminated with heavy metals and pahs at a mgp site, Soil and Sediment Contamination: An International Journal, 11 (3), 426-426, (2002).

[28] A.P. Khodadoust, K.R. Reddy, K. Maturi, Removal of nickel and phenanthrene from kaolin soil using different extractants, Environmental Engineering Science, 21 (6), 691-704, (2004).

[29] K.R. Reddy, K. Maturi, Enhanced electrokinetic remediation of mixed heavy metal

and organic contaminants in low permeability soils, 16th International Conference on Soil

Mechanics and Geotechnical Engineering, September 12 - 16, Osaka, Japan. Rotterdam, the Netherlands : Millpress Science Publishers, pp. 2429 - 2432, (2005).

[30] K. Reddy, K. Maturi, C. Cameselle, Sequential electrokinetic remediation of mixed contaminants in low permeability soils, Journal of Environmental Engineering, 135 (10), 989-998, (2009).

[31] K. Maturi, K.R. Reddy, Cosolvent - enhanced desorption and transport of organic and metal contaminants in soils during electrokinetic remediation, Water, Air, Soil Pollut., 189 (1 - 4), 199 - 211, (2008).

[32] K.R. Reddy, P.R. Ala, Electrokinetic remediation of contaminated dredged sediment, Journal of ASTM International 3(6), 254 - 267, (2006).

[33] K.R. Reddy, M.R. Karri, Effect of oxidant dosage on integrated electrochemical remediation of contaminant mixtures in soils, Journal of Environmental Science and Health Part A, 43 (8), 881 - 893, (2008).

[34] J.W. Ma, F.Y. Wang, Z.H. Huang, H. Wang, Simultaneous removal of 2,4-dichlorophenol and cd from soils by electrokinetic remediation combined with activated bamboo charcoal, J. Hazard. Mater., 176 (1–3), 715-720, (2010).

[35] D.L. Sparks, Environmental soil chemistry, Second Edition ed., Academic Press, 2003.

[36] I.P. Abrol, J.S.P. Yadav, F.I. Massoud, Salt-affected soils and their management, Food and Agriculture Organization of the United Nations, FAO SOILS BULLETIN 39, 1988.

[37] J.W. Ma, H. Wang, Q. Luo, Movement-adsorption and its mechanism of cd in soil under combining effects of electrokinetics and a new type of bamboo charcoal (in chinese), Chinese Journal of Environmental Science, 28 (8), 1829 - 1834, (2007).

[38] J.W. Ma, H. Wang, R.R. Li, Removal of cadmium in kaolin by electrokinetics-bamboo charcoal adsorption (in chinese) Environmental Chemistry, 26 (5), 634 - 637, (2007).

[39] M.A. Al-Zahrani, S.T. Nesaratnam, M.H. Essa, Preparation of phosphoric acid-activated carbon using palm date pits: Physio-chemical and adsorptive properties, The journal of the institution of engineers, Singapore, 46 (2), 24-41, (2005).

[40] M.H. Essa, M.A. Al-Zahrani, Date pits as potential raw materials for the production of activated carbons in saudi arabia, International Journal of Applied Environmental Sciences, 4 (1), 47-58, (2009).

[41] M.H. Essa, M.A. Al-Zahrani, S. Nesaratnam, A step towards national reliance using locally produced activated carbon from dates, Third Saudi Technical Conference and Exhibition (STCEX-3), Riyadh, Saudi Arabia, (2004).

[42] M.H. Essa, M.A. Al-Zahrani, T.N. Suresh, Optimization of activated carbon production from date pits International Journal of Environmental Engineering, 5 (3), 325-338, (2013).

[43] M.S. Vohra, M.A. Al-Zahrani, M.H. Essa, M.M. Rahman, Synthetic industrial wastewater treatment using gac produced from date palm tree branches, in: A.S. Al-Dhuwaihi (Ed.) 8th International Conference and Exhibition on Chemistry in Industry (CHEMINDIX 2010), Gulf International Convention Center, Gulf Hotel, Kingdom of Bahrain, 2010.

[44] R.H. Myers, D.C. Montgomery, Response surface methodology: Process and product optimization using designed experiments, Wiley & Sons, second edition, New York, (2001).

[45] J. Lee, L. Ye, W.O. Landen Jr, R.R. Eitenmiller, Optimization of an extraction procedure for the quantification of vitamin e in tomato and broccoli using response surface methodology, Journal of Food Composition and Analysis, 13 (1), 45-57, (2000).

[46] V.V. Guaracho, N.M.S. Kaminari, M.J.J.S. Ponte, H.A. Ponte, Central composite experimental design applied to removal of lead and nickel from sand, J. Hazard. Mater., 172 (2–3), 1087-1092, (2009).

[47] D.J.R. Bongay, R.L. Ngo, Electroremediation of cu-contaminated soil, World Academy of Science, Engineering and Technology 61 (768 - 773, (2012).

[48] P.H. Brodsky, S.V. Ho, In situ remediation of contaminated soils, U.S. Patent 5,398,756, (1995).

[49] S.V. Ho, P.H. Brodsky, In-situ remediation of contaminated heterogeneous soils, U.S. Patent 5,476,992, (1995).

[50] J.M. Odom, Lab-scale development of microbial degradation process, Monsanto Topical Report for Task #6, (1996).

[51] F.F. Reuss, Sur un nouveleffet de l'electricitéglavanique, Mém. Soc. Impériale Nat., Moscou2, 327-337), (1809).

[52] H.A. Abramson, Electrokinetic phenomena and their application to biology and medicine, ACS Monograph Series, Chemical Catalog, New York, (1934).

[53] S.V. Ho, C. Athmer, P.W. Sheridan, B.M. Hughes, R. Orth, D. McKenzie, P.H. Brodsky, A. Shapiro, R. Thornton, J. Salvo, D. Schultz, R. Landis, R. Griffith, S. Shoemaker, The lasagna technology for in situ soil remediation. 1. Small field test, Environmental Science & Technology, 33 (7), 1086-1091, (1999).

[54] A.T. Yeung, Milestone developments, myths, and future directions of electrokinetic remediation, Sep. Purif. Technol., 79 (2), 124-132, (2011).

[55] B.A. A.N. Puri, Reclamation of alkali soils by electrodialysis, Soil science, 42 (23-27, (1936).

[56] B.D. Swift, J.J. Tarantino, Application of the lasagna™ soil remediation technology at the doe paducah gaseous diffusion plant, WM'03 Conference, February 23-27, 2003, Tucson, AZ, (2003).

[57] J. Virkutyte, M. Sillanpää, P. Latostenmaa, Electrokinetic soil remediation — critical overview, Sci. Total Environ., 289 (1–3), 97-121, (2002).

[58] S.-J. Kim, J.-Y. Park, Y.-J. Lee, J.-Y. Lee, J.-W. Yang, Application of a new electrolyte circulation method for the ex situ electrokinetic bioremediation of a laboratory-prepared pentadecane contaminated kaolinite, J. Hazard. Mater., 118 (1–3), 171-176, (2005).

[59] J.-Y. Park, H.-H. Lee, S.-J. Kim, Y.-J. Lee, J.-W. Yang, Surfactant-enhanced electrokinetic removal of phenanthrene from kaolinite, J. Hazard. Mater., 140 (1–2), 230-236, (2007).

[60] S.-S. Kim, S.-J. Han, Y.-S. Cho, Electrokinetic remediation strategy considering ground strate: A review, Geosciences Journal, 6 (1), 57-75, (2002).

[61] J.P. Zelina, J.F. Rusling, Electrochemical remediation of soils, Encyclopedia of Environmental Pollution and Cleanup, 11 (532-539, (1999).

[62] G. Sposito, The surface chemistry of soils, Oxford University Press, New York, (1984).

[63] G. Sposito, On points of zero charge, Environmental Science & Technology, 32 (19), 2815-2819, (1998).

[64] A. Yeung, C. Hsu, Electrokinetic remediation of cadmium-contaminated clay, Journal of Environmental Engineering, 131 (2), 298-304, (2005).

[65] A.T. Yeung, Y.-Y. Gu, A review on techniques to enhance electrochemical remediation of contaminated soils, J. Hazard. Mater., 195 (0), 11-29, (2011).

[66] J.-H. Choi, S. Maruthamuthu, H.-G. Lee, T.-H. Ha, J.-H. Bae, Electrochemical studies on the performance of ss316l electrode in electrokinetics, Metals and Materials International, 15 (5), 771-781, (2009).

[67] A.P. Shapiro, Electrokinetic modeling, Monsanto Topical Report for Tasks No. 2 - 4 (1996).

[68] R.H. Myers, D.C. Montgomery, C.M. Anderson-Cook, Response surface methodology: Process and product optimization using designed experiments, Wiley, 2009.

[69] M.A. Bezerra, R.E. Santelli, E.P. Oliveira, L.S. Villar, L.A. Escaleira, Response surface methodology (rsm) as a tool for optimization in analytical chemistry, Talanta, 76 (5), 965-977, (2008).

[70] M.J. Anderson, P.J. Whitcomb, Rsm simplified: Opitimizing processes using response surface methods for design of experiments, Productivity Press, 2005.

[71] G.E. Box, J.S. Hunter, Multi-factor experimental designs for exploring response surfaces, The Annals of Mathematical Statistics, 28 (1), 195-241, (1957).

[72] R. Ortega, Analytical methods for heavy metals in the environment: Quantitative determination, speciation, and microscopic analysis, in: B. Sarkar (Ed.) Heavy metals in the environment, Marcel Dekker, 2002.

[73] USEPA, Method 7000b - flame atomic absorption spectrophotometry, United States Environmental Protection Agency, (2007).

[74] USEPA, Method 7473 - mercury in solids and solutions by thermal decomposition, amalgamation, and atomic absorption spectrophotometry, United States Environmental Protection Agency, (2007).

[75] USEPA, Method 8015b - nonhalogenated organics using gc/fid, United States Environmental Protection Agency, (1996).

[76] W. Weisman, Analysis of petroleum hydrocarbons in environmental media - volume 1, Total Petroleum Hydrocarbon Criteria Working Group Series, USA, (1998).

[77] E.B. Woodruff, H.B. Lammers, T.F. Lammers, Steam-plant operation, Seventh Edition, McGraw-Hill, New York, (1998).

[78] T.L. Potter, Analysis of petroleum contaminated soil and water, In P. T. Kostecki, E. Calabrese, and H. Inyang (eds.), 11th Annual Conference on Contaminated Soils: Analytical Workshop Report, University of Massachusetts, Amherst, U.S.A., October 1996, (1996).

[79] D.Y. Chang, I. Lopez, S.G. Yocklovich, Determination of kerosene and #2 diesel in soil by purge and trap vs. Extraction procedure, Journal of Soil Contamination, 1 (3), 239-251, (1992).

[80] P. Paíga, L. Mendes, J. Albergaria, C. Delerue-Matos, Determination of total petroleum hydrocarbons in soil from different locations using infrared spectrophotometry and gas chromatography, Chemical Papers, 66 (8), 711-721, (2012).

[81] Z. Wang, M.F. Fingas, Development of oil hydrocarbon fingerprinting and identification techniques, Marine Pollution Bulletin, 47 (9–12), 423-452, (2003).

[82] Z. Wang, M. Fingas, Developments in the analysis of petroleum hydrocarbons in oils, petroleum products and oil-spill-related environmental samples by gas chromatography, J. Chromatogr. A, 774 (1–2), 51-78, (1997).

[83] I. Eide, K. Zahlsen, A novel method for chemical fingerprinting of oil and petroleum products based on electrospray mass spectrometry and chemometrics, Energy & Fuels, 19 (3), 964-967, (2005).

[84] P.S. Daling, L.-G. Faksness, A.B. Hansen, S.A. Stout, Improved and standardized methodology for oil spill fingerprinting, Environmental Forensics, 3 (3–4), 263-278, (2002).

[85] API, Methods for determination of petroleum hydrocarbons in soil, American Petroleum Institute, Washington DC, USA, (1992).

[86] API, Interlaboratory study of three methods for analyzing petroleum hydrocarbons in soils, American Petroleum Institute, Publication Number 4599), Washington DC, USA, (1994).

[87] USEPA, Method 418.1 - test method for evaluating total recoverable petroleum hydrocarbons (spectrophotometric, infrared), United States Environmental Protection Agency (1978).

[88] USEPA, Method 8440 - total recoverable petroleum hydrocarbon by infrared spectrophotometry, United States Environmental Protection Agency, (1996).

[89] USEPA, Method 9071b - n-hexane extractable material (hem) for sludge, sediment, and solid samples, United States Environmental Protection Agency, (1998).

[90] ASTM, Comparison of waterborne petroleum oils by infrared spectroscopy - d 3414, Annual book of ASTM standards, American Society for Testing and Materials, Philadelphia, PA, USA, (1997).

[91] ASTM, Oil and grease and petroleum hydrocarbons in water - d 3921, Annual book of ASTM standards, American Society for Testing and Materials, Philadelphia, PA, USA, (1997).

[92] USEPA, Method 9074 - turbidimetric screening method for total recoverable petroleum hydrocarbons in soil, United States Environmental Protection Agency, (1996).

[93] K.A. Burns, Analytical methods used in oil spill studies, Marine Pollution Bulletin, 26 (2), 68-72, (1993).

[94] ASTM, Comparison of waterborne petroleum oils by fluorescence analysis - d 3650, In Annual book of ASTM standards, American Society for Testing and Materials Philadelphia, PA, USA, (1997).

[95] S. Wang, G. Guo, Z. Yan, G. Lu, Q. Wang, F. Li, The development of a method for the qualitative and quantitative determination of petroleum hydrocarbon components using thin-layer chromatography with flame ionization detection, J. Chromatogr. A, 1217 (3), 368-374, (2010).

[96] M.M. Krahn, G.M. Ylitalo, J. Buzitis, S.-L. Chan, U. Varanasi, Rapid high-performance liquid chromatographic methods that screen for aromatic compounds in environmental samples, J. Chromatogr. A, 642 (1–2), 15-32, (1993).

[97] M.M. Krahn, J.E. Stein, Peer reviewed: Assessing exposure of marine biota and habitats to petroleum compounds, Anal. Chem., 70 (5), 186A-192A, (1998).

[98] ASTM, Determination of the aromatic content and polynuclear aromatic content of diesel fuels and aviation turbine fuels by supercritical fluid chromatography - d 5186-96, Annual book of ASTM standards, American Society for Testing and Materials, Philadelphia, PA, USA, (1997).

[99] C.G. Schreier, W.J. Walker, J. Burns, R. Wilkenfeld, Total organic carbon as a screening method for petroleum hydrocarbons, Chemosphere, 39 (3), 503-510, (1999).

[100] Z. Wang, M. Fingas, D.S. Page, Oil spill identification, J. Chromatogr. A, 843 (1–2), 369-411, (1999).

[101] Z. Ge, C.W. Brown, J.J. Alberts, Infrared fiber optic sensor for petroleum, Environmental Science & Technology, 29 (4), 878-882, (1995).

[102] G. Xie, M.J. Barcelona, J. Fang, Quantification and interpretation of total petroleum hydrocarbons in sediment samples by a gc/ms method and comparison with epa 418.1 and a rapid field method, Anal. Chem., 71 (9), 1899-1904, (1999).

[103] K.C. Swallow, N.S. Shifrin, P.J. Doherty, Hazardous organic compound analysis, Environmental Science & Technology, 22 (2), 136-142, (1988).

[104] USEPA, Method 8270d - semivolatile organic compounds by gas chromatography/mass spectrometry (gc/ms) United States Environmental Protection Agency, (2007).

[105] F. Nadim, S. Liu, G.E. Hoag, J. Chen, R.J. Carley, P. Zack, A comparison of spectrophotometric and gas chromatographic measurements of heavy petroleum products in soil samples, Water, Air, & Soil Pollution, 134 (1), 97-109, (2002).

[106] K. Bielicka-Daszkiewicz, M. Hadzicka, A. Voelkel, Optimization of spe/gc/hplc analytical procedure for determination of phenol, quinones, and carboxylic acids in water samples, ISRN Chromatography, 2012 (7, (2012).

[107] USEPA, Method 3050b: Acid digestion of sediments, sludges, and soils, U.S. Environmental Protection Agency, (1996).

[108] ASTM, Annual book of standards: Soil and rock 04.08, , West Conshohocken, PA, (2004).

[109] T.D. Martin, Creed, J.T., Brockhoff, C.A., , Sample preparation procedure for spectrochemcial determination of total recoverable elements: Method 200.2, in, U.S. Environmental Protection Agency Report, EMMC Version, USA, 1994.

[110] T.D. Martin, C.A. Brockhoff, J.T. Creed, Determination of metals and trace elements in water and wastes by inductively coupled plasma-atomic emission spectrometry: Method 200.7, U.S. Environmental Protection Agency Report, Revision 4.4, EMMC Version, USA, (1994).

[111] J.T. Creed, C.A. Brockhoff, T.D. Martin, Determination of trace elements in waters and wastes by inductively coupled plasma - mass spectrometry: Method

200.8, U.S. Environmental Protection Agency Report, Revision 5.4, EMMC Version, USA, (1994).

[112] J.P. Gustafsso., Visual minteq ver. 3.0. , Available at http://www2.lwr.kth.se/English/OurSoftware/vminteq/index.htm [Verified 7 July 2011]. (2010).

[113] EPA, Method 3050b - acid digestion of sediments, sludges, and soils, United States Environmental Protection Agency, (1996).

[114] Perkin-Elmer, Sms 100 - mercury analyzer, PerkinElmer, Inc., 940 Winter Street, Waltham, MA 02451 USA, (2009).

[115] USEPA, Method 3450c - soxhlet extraction, United States Environmental Protection Agency, (1996).

[116] USEPA, Method 3545: Pressurized fluid extraction (pfe), United States Environmental Protection Agency, (1996).

[117] Dionex, Ase® 200 accelerated solvent extractor operator's manual, Document No. 031149, Revision 04, (1999).

[118] USEPA, Method 8000c - determinative chromatographic separations, United States Environmental Protection Agency, (2003).

[119] Start-Ease, Design-expert®: Version 8 software for window, in, Start-Ease, Inc., 2021 E. Hennepin Avenue, Suite 480, Minneapolis, MN 55413-2726, 2011.

[120] D. Derringer, R. Suich, Simultaneous optimization of several response variables, Journal of Quality Technology, 12 (4), 214–219, (1980).

[121] WHO, Guidelines for drinking-water quality, in, 1984.

[122] R. Han, Zou, L., Zhao, X., Xu, Y., Xu, F., Li, Y., Wang, Y.,, Characterization and properties of iron oxide-coated zeolite as adsorbent for removal of copper (ii) from solution in fixed bed column, Chem. Eng. J., 149 (1 - 3), 123 – 131, (2009).

[123] M.F. Leitzmann, Stampfer, M.J., Wu, K., Colditz, G.A., Willett, W.C., Giovannucci, E.L.,, Zinc supplement use and risk of prostate cancer, JNCI Journal of the National Cancer Institute, 95 (13), 1004, (2003).

[124] A.I. Alabdula'aly, Khan, M.A.,, Chemical composition of bottled water in saudi arabia, Environ. Monit. Assess., 54 (2), 173-189, (1999).

[125] R.C. Bansal, M. Goyal, Activated carbon adsorption, Taylor & Francis, 2005.

[126] D.B. Adie, Olarinoye, N.O., Oke, I.A., Ismail, A., Lukman, S., Otun, J.A., , Removal of lead ions from aqueous solutions using powdered corn cobs, Can. J. Chem. Eng., 88 (2), 241 - 255, (2010).

[127] I.A. Oke, S. Lukman, O.A. Obijode, N.B. Omodara, E.A. Adekanbi, M.A. Asani, Removal of pb2+ from aqueous solutions using a common household waste (used batteries): Kinetics models, in: Innovative technologies for socio-economic transformation in developing countries, Conference centre and guest houses ltd, Obafemi Awolowo University, Ile-Ife, Nigeria, 2011, pp. 153-163.

[128] N.O. Olarinoye, Lukman, S., Otun, J.A., Adie, D.B., Oke, I.A., Igboro, S.B., Fasuyi-Enang, O.T., Ismail, A.,, Multi-component adsorption equilibria of pb2+ and cd2+ onto powdered corn cobs (pcc), in: K. Demadis (Ed.) Water treatment processes, Nova Science Publishers, USA, 2011.

[129] A. Ismail, D.B. Adie, I.A. Oke, J.A. Otun, N.O. Olarinoye, S. Lukman, C.A. Okuofu, Adsorption kinetics of cadmium ions onto powdered corn cobs, Can. J. Chem. Eng., 87 (6), 896-909, (2009).

[130] C.M. Futalan, Kan, C.-C., Dalida, M.L., Hsien, K.-J., Pascua, C., Wan, M.-W.,, Comparative and competitive adsorption of copper, lead, and nickel using chitosan immobilized on bentonite, Carbohydr. Polym., 83 (2), 528-536, (2011).

[131] E.F. Covelo, F.A. Vega, M.L. Andrade, Competitive sorption and desorption of heavy metals by individual soil components, J. Hazard. Mater., 140 (1–2), 308-315, (2007).

[132] M. Eloussaief, I. Jarraya, M. Benzina, Adsorption of copper ions on two clays from tunisia: Ph and temperature effects, Applied Clay Science, 46 (4), 409-413, (2009).

[133] S. Gier, W.D. Johns, Heavy metal-adsorption on micas and clay minerals studied by x-ray photoelectron spectroscopy, Applied Clay Science, 16 (5–6), 289-299, (2000).

[134] J. Hizal, Apak, R.,, Modeling of copper(ii) and lead(ii) adsorption on kaolinite-based clay minerals individually and in the presence of humic acid, Journal of Colloid and Interface Science, 295 (1), 1-13, (2006).

[135] R. Ishii, Y. Imai, M. Wada, T. Ebina, T. Hanaoka, F. Mizukami, Adsorption and desorption behaviors of flavor molecules into a microporous pillared clay mineral and the application to flavor capsule composites, Applied Clay Science, 33 (2), 99-108, (2006).

[136] M.-Q. Jiang, X.-Y. Jin, X.-Q. Lu, Z.-L. Chen, Adsorption of pb(ii), cd(ii), ni(ii) and cu(ii) onto natural kaolinite clay, Desalination, 252 (1–3), 33-39, (2010).

[137] P. Liu, Polymer modified clay minerals: A review, Applied Clay Science, 38 (1–2), 64-76, (2007).

[138] P. Liu, L. Zhang, Adsorption of dyes from aqueous solutions or suspensions with clay nano-adsorbents, Sep. Purif. Technol., 58 (1), 32-39, (2007).

[139] S.H.S.S. Ahmad, Competitive adsorption of 90sr on soil sediments, pure clay phases and feldspar minerals, Appl. Radiat. Isot., 46 (5), 287-292, (1995).

[140] J. Vejsada, D. Hradil, Z. Řanda, E. Jelínek, K. Štulík, Adsorption of cesium on czech smectite-rich clays—a comparative study, Applied Clay Science, 30 (1), 53-66, (2005).

[141] W.J. Walker, C.S. Cronan, H.H. Patterson, A kinetic study of aluminum adsorption by aluminosilicate clay minerals, Geochim. Cosmochim. Acta, 52 (1), 55-62, (1988).

[142] C.-J. Wang, Z. Li, W.-T. Jiang, Adsorption of ciprofloxacin on 2:1 dioctahedral clay minerals, Applied Clay Science, 53 (4), 723-728, (2011).

[143] S. Bekkouche, S. Baup, M. Bouhelassa, S. Molina-Boisseau, C. Petrier, Competitive adsorption of phenol and heavy metal ions onto titanium dioxide (dugussa p25), Desalination and Water Treatment, 37 (1 - 3), 364 - 372, (2012).

[144] P. Srivastava, B. Singh, M. Angove, Competitive adsorption behavior of heavy metals on kaolinite, J. Colloid Interface Sci., 290 (1), 28-38, (2005).

[145] F.J. Stevenson, Humus chemistry: Genesis, composition, reactions, John Wiley & Sons, New York, 1982.

[146] R.B. Grisso, M. Alley, D. Holshouser, W. Thomason, Soil electrical conductivity: Publication 442-508, in, Virginia Cooperative Extension, Communications and Marketing, College of Agriculture and Life Sciences, Virginia Polytechnic Institute and State University, USA, 2009.

[147] L.N. Reddi, H.I. Inyang, Geoenvironmental engineering: Principles and applications, 1st ed., CRC Press, 2000.

[148] C.P. Huang, Ostovic, F.B.,, Removal of cadmium(ii) by activated carbon adsorption, Environmental Engineering, ASCE, 104 (5), 863-878, (1978).

[149] M.A. Ferro-García, Rivera-Utrilla, J., Rodríguez-Gordillo, J., Bautista-Toledo, I.,, Adsorption of zinc, cadmium, and copper on activated carbons obtained from agricultural by-products, Carbon, 26 (3), 363-373, (1988).

[150] M.M. Benjamin, Leckie, J.O.,, Multiple-site adsorption of cd, cu, zn, and pb on amorphous iron oxyhydroxide, J. Colloid Interface Sci., 79 (1), 209-221, (1981).

[151] C.C. Biddappa, M. Chino, K. Kumazawa, Adsorption, desorption, potential and selective distribution of heavy metals in selected soils of japan, Journal of Environmental Science Health B, 156 (511–528, (1981).

[152] N. Kannan, Vanangamudi, A.,, A study on the removal of chromium (vl) by adsorption on lignite coal, Indian Journal of Environmental Protection, 11 (4), 241 - 245, (1991).

[153] C.P. Huang, Wu, M.H.,, Chromium removal by carbon adsorption, Journal of Water Pollution Control Federation, 47 (10), 2437 - 2446, (1975).

[154] C.P. Huang, Wu, M.H., The removal of chromium(vi) from dilute aqueous solution by activated carbon, Water Res., 11 (8), 673-679, (1977).

[155] M.A. Khan, Khattak, Y.I.,, Adsorption of copper from copper sulfate solution on carbon black “spheron 9”—ii, Carbon, 30 (7), 957-960, (1992).

[156] M.A. Khan, Khattak, Y.I.,, Adsorption of copper from copper sulfate solution on carbon black spheron-9, J. Chem. Soc. Pak., 12 (3), (1990).

[157] M. Goyal, Rattan, V.K., Aggarwal, D., Bansal, R.C.,, Removal of copper from aqueous solutions by adsorption on activated carbons, Colloids and Surfaces A: Physicochemical and Engineering Aspects, 190 (3), 229-238, (2001).

[158] M.O. Corapcioglu, Huang, C.P.,, The adsorption of heavy metals onto hydrous activated carbon, Water Res., 21 (9), 1031-1044, (1987).

[159] B.E. Reed, Jamil, M., Thomas, B., , Effect of ph, empty bed contact time and hydraulic loading rate on lead removal by granular activated carbon columns, Water Environmental Research, 68 (877–882, (1996).

[160] E.A. Forbes, Posner, A.M., Quirk, J.P., , The specific adsorption of divalent cd, co, cu, pb and zn on goethite, Journal of Soil Science, 27 (154 - 166), (1976).

[161] E.F. Covelo, Vega, F.A., Andrade, M.L.,, Simultaneous sorption and desorption of cd, cr, cu, ni, pb, and zn in acid soils: I. Selectivity sequences, J. Hazard. Mater., 147 (3), 852-861, (2007).

[162] K. Reddy, C. Cameselle, P. Ala, Integrated electrokinetic-soil flushing to remove mixed organic and metal contaminants, J. Appl. Electrochem., 40 (6), 1269-1279, (2010).

[163] K. Reddy, Special issue on contaminant mixtures: Fate, transport, and remediation, Journal of Hazardous, Toxic, and Radioactive Waste, 15 (3), 128-129, (2011).

[164] S. Lukman, M.H. Essa, N.D. Mu’azu, A. Bukhari, C. Basheer, Adsorption and desorption of heavy metals onto natural clay material: Influence of initial ph, Journal of Environmental Science and Technology 6 (1), 1 - 15, (2013).

[165] R.N. Yong, M. Nakano, R. Pusch, Environmental soil properties and behaviour, CRC Press, 2012.

[166] K.R. Reddy, U.S. Parupudi, S.N. Devulapalli, C.Y. Xu, Effects of soil composition on the removal of chromium by electrokinetics, J. Hazard. Mater., 55 (1–3), 135-158, (1997).

[167] S. Chinthamreddy, K.R. Reddy, Oxidation and mobility of trivalent chromium in manganese-enriched clays during electrokinetic remediation, Journal of Soil Contamination, 8 (2), 197-216, (1999).

[168] K.R. Reddy, S. Chinthamreddy, Effects of initial form of chromium on electrokinetic remediation in clays, Advances in Environmental Research, 7 (2), 353-365, (2003).

[169] Y.B. Acar, R.J. Gale, A.N. Alshawabkeh, R.E. Marks, S. Puppala, M. Bricka, R. Parker, Electrokinetic remediation: Basics and technology status, J. Hazard. Mater., 40 (2), 117-137, (1995).

[170] B. Beverskog, I. Puigdomenech, Revised pourbaix diagrams for zinc at 25–300 °c, Corros. Sci., 39 (1), 107-114, (1997).

[171] L.M. Ottosen, H.K. Hansen, P.E. Jensen, Electrokinetic removal of heavy metals, in: Electrochemical remediation technologies for polluted soils, sediments and groundwater, John Wiley & Sons, Inc., 2009, pp. 95-126.

[172] H.K. Hansen, L.M. Ottosen, B.K. Kliem, A. Villumsen, Electrodialytic remediation of soils polluted with cu, cr, hg, pb and zn, Journal of Chemical Technology & Biotechnology, 70 (1), 67-73, (1997).

[173] E.R. Weiner, Applications of environmental aquatic chemistry: A practical guide, Taylor & Francis Group, 2008.

[174] I. Ravina, D. Zaslavsky, Non-linear electrokinetic phenomena i: Review of literature, Soil Science, 106 (1), 60-66, (1968).

[175] A.T. Yeung, Geochemical processes affecting electrochemical remediation, in: Electrochemical remediation technologies for polluted soils, sediments and groundwater, John Wiley & Sons, Inc., 2009, pp. 65-94.

[176] S. Chinthamreddy, K.R. Reddy, Geochemistry of chromium during electrokinetic remediation, in: Proceedings of the 4th International Symposium on Environmental Geotechnology and Global Sustainable Development, Boston (Danvers), Massachusetts, 1998.

[177] K.R. Reddy, U.S. Parupudi, Removal of chromium, nickel and cadmium from clays by in-situ electrokinetic remediation, Soil and Sediment Contamination, 6 (4), 391-407, (1997).

[178] K. Reddy, T. Cutright, Nutrient amendment for the bioremediation of a chromium-contaminated soil by electrokinetics, Energy Sources, 25 (9), 931-943, (2003).

[179] L. Hopkinson, A. Cundy, D. Faulkner, A. Hansen, R. Pollock, Electrokinetic stabilization of chromium (vi)-contaminated soils, Electrochemical Remediation Technologies for Polluted Soils, Sediments and Groundwater, 179-193, (2009).

[180] D.B. Gent, R.M. Bricka, A.N. Alshawabkeh, S.L. Larson, G. Fabian, S. Granade, Bench-and field-scale evaluation of chromium and cadmium extraction by electrokinetics, J. Hazard. Mater., 110 (1), 53-62, (2004).

[181] P.R. Buchireddy, R.M. Bricka, D.B. Gent, Electrokinetic remediation of wood preservative contaminated soil containing copper, chromium, and arsenic, J. Hazard. Mater., 162 (1), 490-497, (2009).

[182] C.D. Palmer, P.R. Wittbrodt, Processes affecting the remediation of chromium-contaminated sites, Environ. Health Perspect., 92 (25, (1991).

[183] P.-M. Huang, M.-K. Wang, C.-Y. Chiu, Soil mineral–organic matter–microbe interactions: Impacts on biogeochemical processes and biodiversity in soils, Pedobiologia, 49 (6), 609-635, (2005).

[184] M. Pazos, A. Plaza, M. Martín, M. Lobo, The impact of electrokinetic treatment on a loamy-sand soil properties, Chem. Eng. J., 183 (231-237, (2012).

[185] S.-H. Kim, H.-Y. Han, Y.-J. Lee, C.W. Kim, J.-W. Yang, Effect of electrokinetic remediation on indigenous microbial activity and community within diesel contaminated soil, Sci. Total Environ., 408 (16), 3162-3168, (2010).

[186] Q.-Y. Wang, D.-M. Zhou, L. Cang, T.-R. Sun, Application of bioassays to evaluate a copper contaminated soil before and after a pilot-scale electrokinetic remediation, Environ. Pollut., 157 (2), 410-416, (2009).

[187] A.Z. Al-Hamdan, K.R. Reddy, Transient behavior of heavy metals in soils during electrokinetic remediation, Chemosphere, 71 (5), 860-871, (2008).

[188] S. Lukman, M.H. Essa, N.D. Mu'azu, A. Bukhari, Coupled electrokinetics-adsorption technique for simultaneous removal of heavy metals and organics from saline-sodic soil, Scientific World Journal 2013 (1-9, (2013).

[189] K.R. Reddy, S. Chinthamreddy, Enhanced electrokinetic remediation of heavy metals in glacial till soils using different electrolyte solutions, Journal of Environmental Engineering, 130 (4), 442-455, (2004).

[190] A. Alok, R.P. Tiwari, R.P. Singh, Effect of ph of anolyte in electrokinetic remediation of cadmium contaminated soil, International Journal of Engineering Research & Technology (IJERT), 1 (10), 1 - 11, (2012).

[191] L.M. Vane, G.M. Zang, Effect of aqueous phase properties on clay particle zeta potential and electro-osmotic permeability: Implications for electro-kinetic soil remediation processes, J. Hazard. Mater., 55 (1), 1-22, (1997).

[192] K. Beddiar, T. Fen-Chong, A. Dupas, Y. Berthaud, P. Dangla, Role of ph in electro-osmosis: Experimental study on nacl–water saturated kaolinite, Transport in Porous media, 61 (1), 93-107, (2005).

[193] F.E. Asimakopoulou, I.F. Gonos, I.A. Stathopulos, Methodologies for determination of soil ionization gradient, Journal of Electrostatics, 70 (5), 457-461, (2012).

[194] S. Pamukcu, Electrochemical transport and transformations, Electrochemical Remediation Technologies for Polluted Soils, Sediments and Groundwater, John Wiley & Sons, New York, 29-65, (2009).

[195] K.R. Reddy, R.E. Saichek, K. Maturi, P. Ala, Effects of soil moisture and heavy metal concentrations on electrokinetic remediation, Indian Geotechnical Journal, 32 (2), 258-288, (2002).

[196] R.J. Hunter, M. James, Charge reversal of kaolinite by hydrolyzable metal ions: An electroacoustic study, Clays Clay Miner., 40 (6), 644-649, (1992).

[197] J.M. Dzenitis, Steady state and limiting current in electroremediation of soil, J. Electrochem. Soc., 144 (4), 1317-1322, (1997).

[198] K.R. Reddy, M.R. Karri, Effect of voltage gradient on integrated electrochemical remediation of contaminant mixtures, Land Contamination & Reclamation, 14 (3), 685-698, (2006).

[199] M. Pourbaix, Atlas of electrochemical equilibria in aqueous solutions, (1974).

[200] J.K. Mitchell, Fundamentals of soil behavior, Wiley, 1993.

[201] K.R. Reddy, S. Danda, R.E. Saichek, Complicating factors of using ethylenediamine tetraacetic acid to enhance electrokinetic remediation of multiple heavy metals in clayey soils, Journal of environmental engineering, 130 (11), 1357-1366, (2004).

[202] G.E. Box, D.R. Cox, An analysis of transformations, Journal of the Royal Statistical Society. Series B (Methodological), 211-252, (1964).

[203] K.R. Reddy, C. Cameselle, Overview of electrochemical remediation technologies, Electrochemical Remediation Technologies for Polluted Soils, Sediments and Groundwater, 1-28, (2009).

[204] J. Wang, X. Feng, C.W.N. Anderson, Y. Xing, L. Shang, Remediation of mercury contaminated sites – a review, Journal of Hazardous Materials, 221–222 (0), 1-18, (2012).

[205] C.N. Mulligan, R.N. Yong, B.F. Gibbs, Remediation technologies for metal-contaminated soils and groundwater: An evaluation, Engineering Geology Geoenvironmental Engineering, 60 (1-4), 193-207, (2001).

[206] P. Li, X.B. Feng, G.L. Qiu, L.H. Shang, Z.G. Li, Mercury pollution in asia: A review of the contaminated sites, Journal of Hazardous Materials, 168 (2–3), 591-601, (2009).

[207] Agency for toxic substances and disease registry (atsdr): Priority list of hazardous substances (2011), in, Atlanta, USA, http://www.atsdr.cdc.gov/

[208] C.N. Mulligan, R.N. Yong, B.F. Gibbs, An evaluation of technologies for the heavy metal remediation of dredged sediments, Journal of Hazardous Materials, 85 (1-2), 145-163, (2001).

[209] J. Virkutyte, M. Sillanpää, P. Latostenmaa, Electrokinetic soil remediation -- critical overview, The Science of The Total Environment, 289 (1-3), 97-121, (2002).

[210] Q. Luo, X. Zhang, H. Wang, Y. Qian, Mobilization of phenol and dichlorophenol in unsaturated soils by non-uniform electrokinetics, Chemosphere, 59 (9), 1289-1298, (2005).

[211] Z. Shen, J. Zhang, L. Qu, Z. Dong, S. Zheng, W. Wang, A modified ek method with an i−/i2 lixiviant assisted and approaching cathodes to remedy mercury contaminated field soils, Environmental geology, 57 (6), 1399-1407, (2009).

[212] D.L. Sparks, Sorption phenomena on soils, in: Environmental soil chemistry (second edition), Academic Press, Burlington, 2003, pp. 133-186.

[213] I.P. Abrol, J.S.P. Yadav, F.I. Massoud, Salt-affected soils and their management, in: Food and Agriculture Organization of the United Nations, FAO SOILS BULLETIN, 1988.

[214] N.D. Muazu, S. Lukman, H.M. Essa, A.S. Mohammad, Challenges in the electrokinetic remediation of natural saudi arabian soil for agriculture: Effect of salinity and sodicity, in: J. Royal Commission for Jubail, Saudi Arabia (Ed.) Celebration for the World Environment Day (WED13) Symposium, 2013.

[215] K.R. Reddy, P.R. Ala, S. Sharma, S.N. Kumar, Enhanced electrokinetic remediation of contaminated manufactured gas plant soil, Engineering Geology

Geoenvironmental Engineering, 85 (1-2), 132-146, (2006).

[216] T.D. Pham, R.A. Shrestha, J. Virkutyte, M. Sillanpää, Combined ultrasonication and electrokinetic remediation for persistent organic removal from contaminated kaolin, Electrochimica Acta, 54 (5), 1403-1407, (2009).

[217] Q. Luo, H. Wang, X. Zhang, X. Fan, Y. Qian, In situ bioelectrokinetic remediation of phenol-contaminated soil by use of an electrode matrix and a rotational operation mode, Chemosphere, 64 (3), 415-422, (2006).

[218] S.V. Ho, C.J. Athmer, P.W. Sheridan, A.P. Shapiro, Scale-up aspects of the lasagna(tm) process for in situ soil decontamination, Journal of Hazardous Materials

Electrochemical Decontamination of Soil and Water, 55 (1-3), 39-60, (1997).

[219] C.B. Roop, G. Meenakshi, Activated carbon adsorption applications, in: Activated Carbon Adsorption, Taylor & Francis, 2005.

[220] T.G. Chuah, A. Jumasiah, I. Azni, S. Katayon, S.Y. Thomas Choong, Rice husk as a potentially low-cost biosorbent for heavy metal and dye removal: An overview, Desalination, 175 (3), 305-316, (2005).

[221] N.J. Barrow, V.C. Cox, The effects of ph and chloride concentration on mercury sorption. Ii. By a soil, Journal of Soil Science, 43 (2), 305-312, (1992).

[222] Y. Yin, H.E. Allen, Y. Li, C.P. Huang, P.F. Sanders, Adsorption of mercury(ii) by soil: Effects of ph, chloride, and organic matter, J. Environ. Qual., 25 (4), 837-844, (1996).

[223] K.R. Reddy, C. Chaparro, R.E. Saichek, Removal of mercury from clayey soils using electrokinetics, Journal of Environmental Science and Health, Part A, 38 (2), 307-338, (2003).

[224] M.A. Bezerra, R.E. Santell, E.P. Oliveira, L.S. Villar, L.A. Escaleira, Response surface methodology (rsm) as a tool for optimization in analytical chemistry, Talanta, 76 (965–977, (2008).

[225] V.P. Evangelou, Environmental soil and water chemistry: Principles and applications, Wiley, 1998.

[226] C. Cameselle, K.R. Reddy, Development and enhancement of electro-osmotic flow for the removal of contaminants from soils, Electrochim. Acta, 86 (0), 10-22, (2012).

Vitae

Name :Salihu Lukman

Nationality :Nigerian

Date of Birth :2/20/1980

Email :salihulukman@yahoo.com

Address :King Fahd University of Petroleum and Minerals, P.O. Box # 8632, Dhahran 31261, Tel: +966-860-2197

Academic Background :B.Eng. Water Resources and Environmental Engineering, Ahmadu Bello University (ABU), Nigeria (2004); M.Sc. Water Resources and Environmental Engineering, ABU, Nigeria (2009)